







DIELECTRIC PROPERTIES OF NON-NEWTONIAN LIQUIDS

PART I: Measurements of the Dielectric Constant of Solutions  
of Macromolecules Under Shear

PART II: Dielectric Dispersion Studies of Polyvinyl Acetate  
in Toluene

A Thesis

by

Boris Lionel Funt, B.Sc., M.Sc.

Submitted to the Faculty of Graduate  
Studies and Research in partial ful-  
filment of the requirements for the  
degree of Doctor of Philosophy.

McGill University

April 1949

## ACKNOWLEDGEMENTS

It is a pleasure for the author to record his appreciation to Dr. S. G. Mason for his helpful advice, resourceful suggestions and constant interest.

The author is likewise deeply indebted to Dr. O. Maass who acted as director and overseer for this work.

Thanks are also due to Mr. G. B. Gunn for his cooperation and advice in various phases of this work.

Acknowledgement is made to the National Research Council for a Studentship in 1947-48 and a Fellowship in 1948-49, and to the Defence Research Board for financial assistance for parts of this work.

## TABLE OF CONTENTS

GENERAL INTRODUCTION . . . . .	1
THEORETICAL INTRODUCTION	
Dielectric Theory . . . . .	5
Effect of Temperature and Rate of Shear on Dipole Orientation . . . . .	9
Dielectric Dispersion. . . . .	17
Dielectric Relaxation as a Chemical Kinetic Process. . . . .	21
Viscosity and Streaming Birefringence of Asymmetric Particles . . . . .	25
Aluminum Soap - Benzene Systems . . . . .	28
Previous Work . . . . .	29
PART I - MEASUREMENTS OF THE DIELECTRIC CONSTANT OF SOLUTIONS OF MACROMOLECULES UNDER SHEAR	
EXPERIMENTAL	
Electrical Apparatus. . . . .	32
Rotating Condensers . . . . .	40
Materials . . . . .	45
Preparation of Samples. . . . .	47
Procedure . . . . .	49
RESULTS	
Aluminum Soaps. . . . .	50
High Polymers . . . . .	55
Carbon Black Suspensions. . . . .	64
DISCUSSION OF RESULTS	
Sources of Error. . . . .	67
Aluminum Soaps. . . . .	69
High Polymers . . . . .	71
Carbon Black Suspensions. . . . .	73

Table of Contents (cont'd.)

PART II - DIELECTRIC DISPERSION STUDIES OF POLYVINYL ACETATE  
IN TOLUENE

EXPERIMENTAL

Electrical Apparatus. . . . .	75
Dielectric Cell . . . . .	80
Analysis of Residual Impedances . . . . .	83
Materials . . . . .	92
RESULTS . . . . .	94
Dielectric Dispersion Data. . . . .	97
Densities and Refractive Indices of Samples . . . . .	109
DISCUSSION OF RESULTS	
Application of the Theory of Absolute Reaction Rates. . . . .	111
Size of the Rotating Unit . . . . .	114
Dipole Moment . . . . .	116
Distribution of Relaxation Times. . . . .	121
Conclusions . . . . .	124
CLAIMS TO ORIGINAL WORK AND CONTRIBUTIONS TO KNOWLEDGE . . . . .	126
BIBLIOGRAPHY . . . . .	128

## GENERAL INTRODUCTION

The behavior of asymmetric molecules subjected to external electrical and mechanical forces is of considerable interest. If the molecule is electrically asymmetric, it will tend to be oriented in an external electric field. The extent of this orientation can be determined experimentally by measuring the dielectric constant of the material. Substances having high dielectric constants are known to possess large permanent electric moments on the molecular scale. The molecules of such substances can therefore be considered as electrical dipoles, in which the centres of positive and negative charge are separated by finite distances. In the presence of an external electric field, these dipoles will tend to orient themselves in the direction of the field, although this tendency will be opposed by their random thermal motion.

In addition to electrical asymmetry we can consider geometrical asymmetry. A solution of long chain, cylindrically shaped molecules is normally isotropic. When such a system is subjected to a sufficiently high rate of shear an optical anisotropy is produced. Experimentally this can be observed in the phenomenon of streaming birefringence (1). The appearance of anisotropy under such conditions is believed to be due to an orientation of the cylindrical particles or long chain molecules along the stream lines in a velocity gradient.

The hydrodynamic principles governing this type of orientation have been extensively investigated for particles of idealized shapes in dilute solutions (2). The phenomenon of non-Newtonian viscosity is theoretically predicted for systems in which orientation in a velocity gradient occurs (3). A system is considered to be non-Newtonian when the apparent viscosity is a function of the rate of shear at which it is measured. Such behavior is very general for solutions of macromolecules and for most colloidal systems (4). Although it is unlikely that the orientation in a velocity gradient is the sole factor governing non-Newtonian behavior (5), it is one which can be analyzed experimentally. Several authors (6)(7) have recently reported simultaneous measurement of non-Newtonian viscosity and streaming birefringence, and a correlation between these phenomena has been attempted.

On the basis of such considerations it seemed interesting to investigate the behavior of long cylindrical polar molecules simultaneously subjected to an electric field and to flow at varying rates of shear. If the orientations under shear and in an electric field involved similar molecular units, the possibility existed that changes in dielectric constant could be observed, which could be related to the degree of orientation in a velocity gradient. Such an experimental technique was considered to be the electrical equivalent of the optical phenomenon of streaming birefringence. Changes in the dielectric constant of solutions of macromolecules in a velocity gradient were found to occur. The investigation of such

changes in dielectric constant is reported in Part I.

A theoretical analysis of data obtained from streaming birefringence measurements can be used to obtain a rotary diffusion constant (1). In principle this constant is directly related to the size and geometry of the rotating unit and to the viscosity of the medium.

For polar molecules the rotary diffusion constant can, in principle, be evaluated from high frequency measurements of the dielectric constant. At the appropriate high frequency, a region of anomalous dispersion is found in which the dipole polarization is markedly dependent on the frequency. Measurements of the two vector components of the dielectric constant in this region have been made in the present work and were used to evaluate a relaxation time, which, in principle, is directly related to the rotary diffusion constant. On this basis the size of the rotating unit was evaluated. The dipole moment per monomer unit was also found.

In Part II measurements performed on samples of polyvinyl acetate of three molecular weights at frequencies of 1, 3 and 10 Mc. are reported. Data are presented for solutions of various concentrations of these samples in toluene over the temperature range  $-80^{\circ}$  to  $60^{\circ}\text{C}$ .

By application of the theory of absolute reaction rates values of the free energy, enthalpy and entropy of dipole rotation have been evaluated. The bearing of these quantities on the nature of the dipole rotation involved has been considered. The data were also interpreted as indicating the existence of a distribution of

relaxation times, and a measure of the relative distribution was obtained.

## THEORETICAL INTRODUCTION

### Dielectric Theory

Let us consider the effect of an electric field on a molecule. Since the electrons and nuclei in an atom possess a certain degree of mobility it is reasonable to assume that a displacement of charges may occur, resulting in the formation of an electrical dipole. In addition to dipoles formed by deformations induced by the field in this way, asymmetric molecules may possess permanent dipoles in the absence of an external electric field.

We begin by considering the effect of a uniform field on molecules which do not possess such permanent dipoles. Let us focus our attention on a slab of dielectric in an electric field of strength  $F$  between two plates bearing charges  $+\sigma$  and  $-\sigma$  per unit area. The discussion is simplified if we consider a small spherical cavity enclosing a unit charge in the dielectric. This is illustrated in diagram 1, Fig. 1.

The force of this unit charge is  $D$ , the electric displacement which is related to the field by the general relation

$$D = F + 4\pi I$$

where  $I$  is the electric moment per unit volume. In Maxwell's formal theory the assumption is made that  $D = \epsilon E$  where  $\epsilon$  is the dielectric constant of the medium. Hence

$$(\epsilon - 1) F = 4\pi I \quad \underline{1}$$

We assume that an actual electric intensity  $\underline{S}$  acts on a given molecule and induces a moment  $\underline{m}$ . We denote the dipole moment

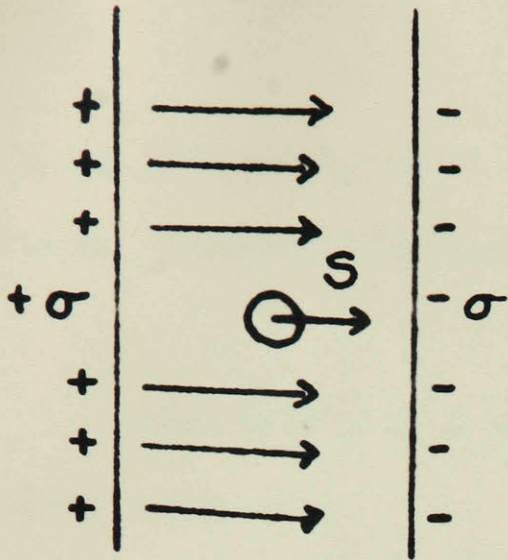


Diagram 1  
Clausius-Mosotti derivation

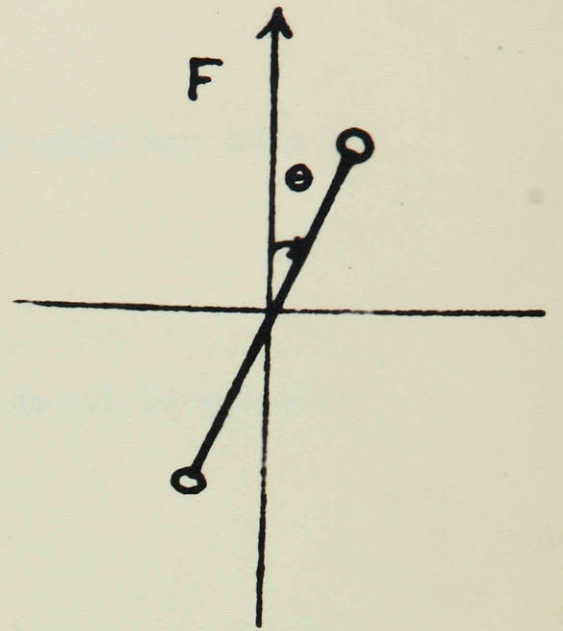


Diagram 2  
Orientation of a dipole

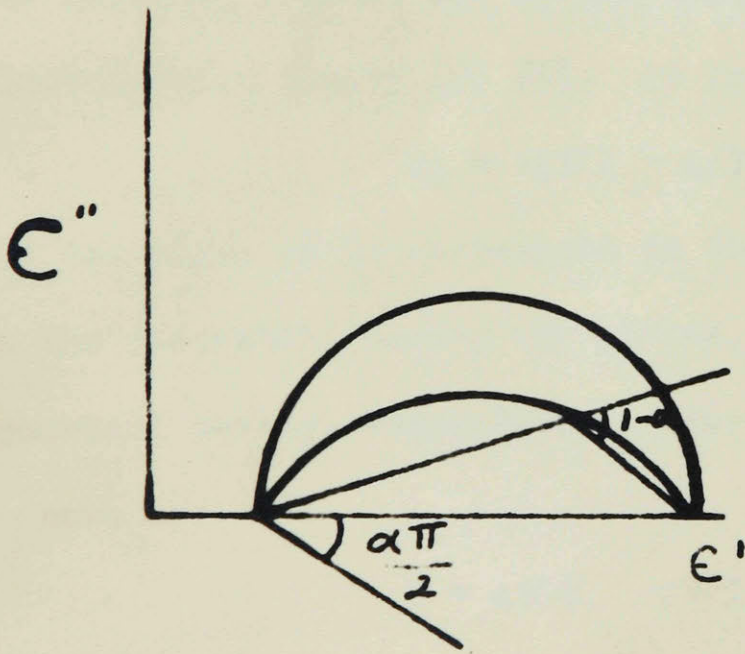


Diagram 3  
Cole and Cole plot

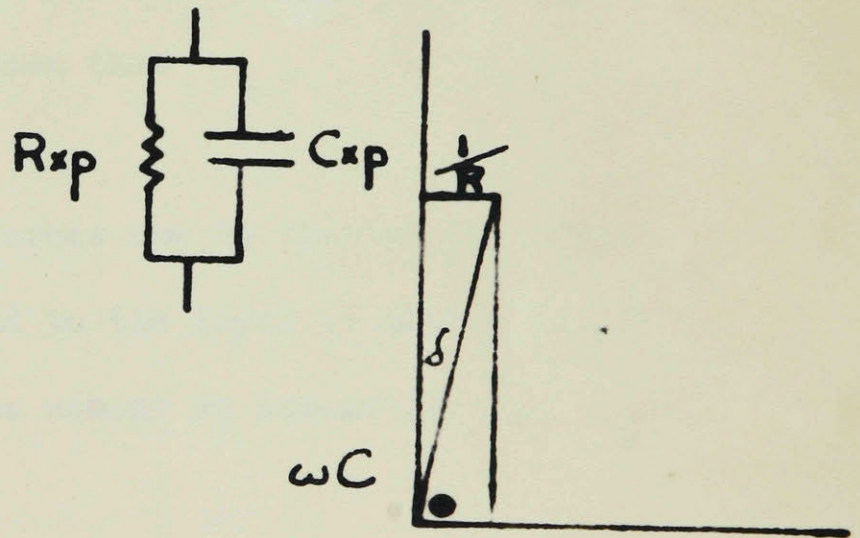


Diagram 4  
Equivalent circuit of a condenser

set up by unit field as  $\alpha$ , the polarizability, and consider this a constant. Therefore we can write

$$m = \alpha S$$

The intensity  $S$  may conveniently be considered to consist of three components

$$S = S_1 + S_2 + S_3$$

where  $S_1$  is the force due to the charge distribution on the plates,

$S_2$  is the force due to the dielectric outside the sphere,

$S_3$  is due to the material inside the small sphere.

The force  $S_1 = 4\pi\sigma$ , and  $S_2$  can readily be evaluated by classical electrostatic theory (8) (20). It is shown that

$$S_2 = -4\pi I - 4/3\pi I$$

The two parts of  $S_2$  correspond to the forces due to the induced charge on the dielectric facing the plates, and to the layer of charge on the spherical cavity, respectively. For the moment we assume  $S_3 = 0$ . Then, we have

$$S = 4\pi\sigma - 4\pi I + 4/3\pi I$$

and since  $D = 4\pi\sigma$

$$S = F + 4/3\pi I$$

but  $I = nm = n\alpha S = n\alpha(F + 4/3\pi I)$

where  $n$  is the number of dipoles/c.c.

From 1 we have

$$4\pi I = (\epsilon - 1) F$$

$$F(\epsilon - 1) = 4/3\pi n \alpha (3F + (\epsilon - 1)F)$$

or

$$\frac{\epsilon - 1}{\epsilon + 2} = 4/3 \pi n \alpha \quad \underline{2}$$

This is the equation first derived by Clausius and Mosotti (9). We can obtain a more convenient form by multiplying both sides by  $M/\rho$

$$\frac{\epsilon - 1}{\epsilon + 2} \frac{M}{\rho} = 4/3 \pi N \alpha - P \quad \underline{3}$$

where  $N$  is the Avogadro number,  $M$  the molecular weight,  $\rho$  the density, and  $P$  is termed the molar polarization. For systems of two components this relation can be put in the form

$$\frac{\epsilon - 1}{\epsilon + 2} \frac{M_1 f_1 + M_2 f_2}{\rho} = P_1 f_1 + P_2 f_2$$

where  $f_1, f_2$  are the mole fractions.

The assumptions involved limit the general validity of these equations. In neglecting the internal field  $S_3$  we adopted a procedure which is justifiable for gases and perhaps to non-associated liquids where the molecules can be considered totally independent of one another. For polar liquids, however, this derivation cannot be considered rigorous. Since the experimental work was performed with polar molecules the limitations of this equation should be noted.

This weakness in the Clausius-Mosotti equation has been the basis for intensive theoretical work in recent years. Onsager (10), Debye (11), Kirkwood (12)(13), Frank (14), Bauer and Massignon (15), Frohlich (16) and Fowler (17) have devoted their attention to this problem. It is generally accepted, however, that a satisfactory modification has not been found, and it was necessary to apply a semi-empirical correction to the present data which will be discussed at a future point.

Let us now consider the influence of permanent dipoles.

The total polarization  $P$  can be regarded as consisting of three parts

$$P = P_e + P_a + P_d$$

where  $P_e$  and  $P_a$  are the polarizations due to the electronic and atomic distortions, and  $P_d$  is the polarization due to the presence of permanent dipoles.

The contributions of these components can be assessed experimentally by performing measurements over a frequency spectrum. At optical frequencies only the contribution  $P_e$ , due to electric distortion, is effective. In this region the dielectric constant obeys the classical equation

$$\epsilon = n^2$$

The atomic polarization is present at frequencies below the infra-red region. Experimentally it is found to be approximately 5% of the electronic polarization (18). At audio and low radio frequencies the polarization due to permanent dipoles is also present. For polar molecules this represents the major contribution to the dielectric constant. It will be shown that, whereas the electronic and atomic polarizations are independent of temperature, dipole polarization is temperature dependent.

We now proceed to assess the effects of temperature, frequency and rate of shear on the dipole polarization.

#### Effect of Temperature and Rate of Shear on Dipole Orientation

(a) We start by considering the orientation of permanent dipoles in an electric field alone. Once the distribution function is known,

it is a simple matter (in principle) to compute the dielectric constant from the Clausius-Mosotti equation. In our treatment we will assume a simple one dimensional angular distribution rather than the two dimensional distribution considered by Debye.

Let

$F$  = strength of the field whose direction is along the  
Y axis of a frame of reference X Y.

$\mu$  = dipole moment

$\theta$  = angular displacement (measured counterclockwise) of  
positive end of dipole from the direction of the field,  
as illustrated in diagram 2, Fig. 1.

For simplicity we restrict our consideration to the case where all the axes of the dipoles are confined to the plane X-Y. The potential energy corresponding to  $\theta$  due to the electric field may be written

$$u(\theta) = -\mu F \cos \theta \quad 4$$

If we have a large assembly of dipoles without interaction, in statistical equilibrium, the fraction  $\rho(\theta)$  having orientations in the region  $\theta$ , and  $(\theta + d\theta)$  is given by the Boltzmann distribution law:

$$\rho(\theta) = A e^{\frac{-u(\theta)}{kT}} \quad 5$$

where  $k$  = Boltzmann constant,  $T$  = temperature and  $A$  = integration constant such that

$$\int_0^{2\pi} \rho(\theta) d\theta = 1 \quad 6$$

Thus we have

$$\rho(\theta) = A e^{\frac{+\mu F}{kT} \cos(\theta)} \quad 7$$

We are interested only in values at low  $F$ 's and consider only first

power terms in F. Hence  $\bar{P}$  may be approximated by

$$\rho(\theta) = A \left[ 1 + \frac{\mu_F}{kT} \cos \theta \right]$$

whence from 6,

$$A = 1/2\pi$$

or

$$\rho(\theta) = 1/2\pi \left[ 1 + \frac{\mu_F}{kT} \cos \theta \right] \quad \underline{8}$$

The mean dipole moment  $\bar{P}$  is given by

$$\begin{aligned} \bar{P} &= \int_0^{2\pi} \rho(\theta) \mu \cos \theta d\theta \\ &= 1/2\pi \int_0^{2\pi} \left[ 1 + \frac{\mu_F}{kT} \cos \theta \right] \mu \cos \theta d\theta \\ &= 1/2 \frac{\mu^2_F}{kT} \quad \underline{9} \end{aligned}$$

Thus if there are n dipoles per cc. the contribution to the volume polarization becomes

$$\Delta P = \bar{P} \cdot n$$

The dielectric constant can be calculated by application of the Clausius-Mosotti equation

$$\frac{\epsilon - 1}{\epsilon + 2} = \frac{4\pi \Delta P}{F}$$

It should be noted that for the two dimensional case normally considered  $\bar{P}$  becomes

$$\bar{P}' = 1/3 \frac{\mu^2_F}{kT}$$

The above calculations correspond to the case of statistical equilibrium. We wish now to consider the case where the distribution given by equation  $\underline{8}$  is disturbed, and try to compute the rate at which the distribution function will change. This has been treated in some detail by Debye in connection with anomalous dispersion for rotations

of two degrees of freedom. To set up the equations involved it is necessary to consider the rotations produced by the action of the electrical field and the rotary diffusion arising from Brownian motion.

The moment  $m$  acting on a dipole oriented at an angle  $\theta$  to the electric field may be written

$$m = -\mu F \sin \theta \quad \underline{10}$$

the minus sign indicating that the couple acts opposite to the direction of increasing  $\theta$ .

Disregarding Brownian motion for the present and neglecting inertial effects, this couple will cause the dipole to rotate at an angular velocity such that the couple required to overcome the viscous drag will be counterbalanced. If  $\omega$  is the angular velocity

$$\omega = \frac{d\theta}{dt} = \frac{M}{\zeta} \quad \underline{11}$$

where  $\zeta$  is the coefficient of rotary friction (couple required to produce unit angular velocity). The coefficient of rotary friction can be shown to depend on the geometry of the rotating unit and the frictional resistance of the medium. Usually the latter is considered to be the macro viscosity.

Suppose at any instant of time the distribution of orientations is  $\phi(\theta)$ . Then in the absence of Brownian motion, the electric field will cause  $\phi(\theta)$  to change. We can compute this effect as follows. Consider an interval of time  $\delta t$ , and the interval of orientations  $\theta$  and  $(\theta + \delta\theta)$ .

The number of dipoles passing into the interval in unit time is

$$+ \phi(\theta) \cdot \omega(\theta)$$

The number passing out is

$$-\phi(\theta + \delta\theta) \omega(\theta + \delta\theta)$$

Thus the net change in dipoles in the interval per unit time is:

$$\frac{\partial(\omega\phi)}{\partial\theta} \cdot d\theta$$

Thus the net change of  $\phi(\theta)$  due to the electric field alone is given

by

$$\frac{\partial\phi_e}{\partial t} = - \frac{\partial(\omega\phi)}{\partial\theta}$$

12

(b) Let us next consider the effect of Brownian motion in the absence of an electric field. We assume an analogue of Fick's diffusion law (19) applied to rotary motion. The net number of dipoles  $dn$  whose orientation shifts in the time  $dt$  across the angle  $\theta$  from lower to higher values due to Brownian motion is

$$\frac{dn}{dt} = -K \left( \frac{\partial\phi}{\partial\theta} \right)_{\theta}$$

where  $K$  = rotary diffusion constant.

Considering an interval  $d\theta$  the number leaving per unit time across  $(\theta + d\theta)$  is

$$-K \left( \frac{\partial\phi}{\partial\theta} \right)_{\theta + d\theta}$$

Thus the net change in the interval  $d\theta$  in unit time is

$$K \frac{\partial^2\phi}{\partial\theta^2} \cdot d\theta$$

Thus the net change in the distribution function is

$$\frac{\partial\phi_{\theta}}{\partial t} = K \frac{\partial^2\phi}{\partial\theta^2}$$

13

which gives the rate of change of orientation due to Brownian motion alone.

(c) When both mechanisms operate let us assume additivity or simple superposition of the effects. The net change in  $\phi$  can be written

$$\frac{\partial \phi}{\partial t} = \frac{\partial \phi_e}{\partial t} + \frac{\partial \phi_s}{\partial t}$$

or 
$$\frac{\partial \phi}{\partial t} = -\frac{\partial(\omega\phi)}{\partial \theta} + K \frac{\partial^2 \phi}{\partial \theta^2} \quad \underline{14}$$

Substituting  $\omega$  from 11 we obtain

$$\frac{\partial \phi}{\partial t} = \frac{\partial}{\partial \theta} \left( \frac{\phi \mu_F}{J} \sin \theta \right) + K \frac{\partial^2 \phi}{\partial \theta^2} \quad \underline{15}$$

Clearly at statistical equilibrium,  $\frac{\partial \phi}{\partial t} = 0$ . Thus  $\rho(\theta)$

defined by 7 must satisfy the equation:

$$\frac{d}{d\theta} \left( \rho \frac{\mu_F}{J} \sin \theta \right) = -K \frac{d^2 \rho}{d\theta^2} \quad \underline{16}$$

Writing  $\rho(\theta) = A e^{-\frac{\mu_F}{kT} \cos \theta}$

$$\frac{d\rho}{d\theta} = A e^{-\frac{\mu_F}{kT} \cos \theta} \cdot \frac{\mu_F}{kT} \sin \theta = -\frac{\mu_F}{kT} \sin \theta \cdot \rho$$

$$\frac{d^2 \rho}{d\theta^2} = -\frac{\mu_F}{kT} \cos \theta \cdot \rho + \left( \frac{\mu_F}{kT} \right)^2 \sin^2 \theta \cdot \rho$$

We obtain by substituting 16

$$\rho \frac{\mu_F}{J} \cdot \cos \theta - \left( \frac{\mu_F}{J} \right) \left( \frac{\mu_F}{kT} \right) \sin^2 \theta \cdot \rho = -K \left[ -\frac{\mu_F}{kT} \cos \theta \rho + \left( \frac{\mu_F}{kT} \right)^2 \sin^2 \theta \rho \right]$$

$$\cos \theta - \mu_F \sin^2 \theta = \frac{KJ}{kT} \left[ \cos \theta - \frac{\mu_F}{kT} \sin^2 \theta \right]$$

Thus the identity is fulfilled if

$$\frac{KJ}{kT} = 1$$

or 
$$K = \frac{kT}{J} \quad \underline{17}$$

We thus see that the rotational diffusion constant is evaluated explicitly. We may then rewrite 15 in the form

$$\frac{\partial \phi}{\partial t} = \frac{\partial}{\partial \theta} \left[ \phi \frac{\mu F}{\gamma} \sin \theta \right] + \frac{kT}{\gamma} \left( \frac{\partial^2 \phi}{\partial \theta^2} \right) \quad \underline{18}$$

This equation serves as the basis for computing  $\phi$  in a varying electric field and thence anomalous dispersion effects. It will be shown in a later section that  $\gamma$  can in principle be computed from the anomalous dispersion. It should also be noted that  $\gamma$  could be calculated directly from the geometry of the particle.

(d) We may now consider the effect of impressing a shear motion. Let the system be subjected to a field of simple shear.

$$v_x = G y$$

where  $v_x$  is the velocity along the X axis. This defines the shear rate G.

In the absence of an electrical field and of Brownian motion, the shear field will cause the particle to rotate at an angular velocity  $\omega$ . This angular velocity is proportional to G, and, for a particle of generalized shape, to some function of  $\theta$ , the orientation of the particle with the field of motion. Let us write

$$\omega = G \cdot f(\theta)$$

where  $f(\theta)$  is a function whose explicit form we ignore for the moment.

The rotation thus imposed will tend to establish an orientation of the particles in the same manner as considered above for the case of an electric field.

Proceeding as in section (a) above, the change in

at any instant due to the impressed rotation from the field may be written

$$\frac{\partial \phi_s}{\partial t} = - \frac{\partial (\omega_s \phi)}{\partial \theta} = - G \frac{\partial f(\theta) \cdot \phi}{\partial \theta}$$

If this effect can be regarded as superimposed upon the separate influences of the electric field and Brownian motion, we obtain as an extension of 18

$$0 = \frac{\partial \phi}{\partial t} - \frac{\partial}{\partial \theta} \left[ \phi \left( \frac{\mu F \sin \theta}{\gamma} - Gf(\theta) \right) + \frac{kT}{\gamma} \left( \frac{\partial^2 \phi}{\partial \theta^2} \right) \right] \quad \underline{19}$$

It is clear from this equation that, if G is changed,  $\phi$  will change, provided  $f(\theta) \neq$  constant, i.e. provided the particle is asymmetric. Consequently  $\bar{P}$  and the dielectric constant will change. We seek to evaluate the effect of G for certain specific cases, corresponding to a condition of statistical equilibrium, i.e. we seek a solution to the equation

$$\frac{d}{d\theta} \left[ \phi \left[ \frac{\mu F}{\gamma} \sin \theta - Gf(\theta) \right] \right] + \frac{kT}{\gamma} \frac{\partial^2 \phi}{\partial \theta^2} = 0$$

It will be noted that this equation integrates to:

$$\phi \left[ \frac{\mu F}{\gamma} \sin \theta - Gf(\theta) \right] + \frac{kT}{\gamma} \frac{\partial \phi}{\partial \theta} = C_1 \quad \underline{20}$$

where  $C_1$  is a constant of integration. The bracketed term is zero at a particular value of  $\theta$  for which the rotation imposed by the electrical field is exactly counterbalanced by that imposed by the rotating field.

From the above analysis it can be seen that, in principle, a dependence of the dipole orientation on rate of shear could be expected under appropriate conditions. A rigorous solution of equation 20 was not obtained. Nevertheless, it was believed that the theoretical analysis was pursued to the point where experimental work was

desirable.

We have thus far considered measurements performed at low frequencies where the contribution of the permanent dipoles is present. It was believed that useful information could also be obtained from measurements in the region of anomalous dispersion.

### Dielectric Dispersion at High Frequencies

In the above discussion, the fact that the orientation polarization would vanish at sufficiently high frequencies was mentioned several times. In connection with equation 18 it was also stated that the rotary diffusion constant could be evaluated from measurements of dielectric dispersion.

Let us now limit our attention to the behavior of polar molecules in electric fields near this critical frequency region.

The discussion is greatly simplified if (following Debye) we consider the dielectric constant in vector notation as being complex

$$\epsilon = \epsilon' - j\epsilon'' \quad \underline{21}$$

where  $j = \sqrt{-1}$ ,  $\epsilon'$  is the dielectric constant,  $\epsilon''$  is dielectric loss factor. Corresponding to this complex dielectric constant we consider a complex polarization

$$P = P' - j P'' \quad \underline{22}$$

The values of the dielectric constant and polarization can be found as done by Debye (20), by solving an equation similar to 18 in our discussion. The values of the vector components of the dielectric constant are found to be

$$\epsilon' = \epsilon_{\infty} + \frac{(\epsilon_0 - \epsilon_{\infty})}{1 + \omega^2 \tau^{*2}} \quad \underline{23}$$

$$\epsilon'' = \frac{(\epsilon_0 - \epsilon_{\infty}) \omega \tau^*}{1 + \omega^2 \tau^{*2}} \quad \underline{24}$$

where  $\epsilon_0, \epsilon_{\infty}$  are dielectric constants at very low and very high frequencies relative to the dispersion region.

$$\omega = 2\pi f \quad \underline{25}$$

where  $f$  is the frequency

$$\tau^* = \frac{\epsilon_0 + 2}{\epsilon_{\infty} + 2} \tau \quad \underline{26}$$

where  $\tau$  is the relaxation time

and

$$\tau^* = \frac{1}{2\pi f \max}$$

where  $f \max$  is frequency of maximum absorption.

The relaxation time is to be regarded as the time for the polarization to fall to  $1/e$  th of its initial value upon instantaneous removal of the field.

It should be noted that equations 23, 24 can be obtained simply on the basis of the Clausius-Mosotti equation and the following two assumptions (21):

- a.  $\epsilon - \epsilon_{\infty}$  is a linear function of the dipole polarization:
- b. a dipole polarization which has been set up in the dielectric declines exponentially after removal of the field,

$$\frac{dP}{dt} = -P/\tau$$

The factor  $\frac{\epsilon_0 + 2}{\epsilon_{\infty} + 2} \tau$  occurs in Debye's equations. There is considerable evidence that the Clausius-Mosotti relation is invalid for the

internal field in polar liquids, and Onsager (10) and others (22) (23) have suggested that this factor be replaced by unity. In the present work the relaxation time has been evaluated as  $\frac{1}{2\pi f_{\max}}$ , where  $f_{\max}$  is the experimentally determined frequency for maximum absorption.

The fact that there are two vector components of the dielectric constant and polarization in the dispersion region is readily understood. Its significance is that the two components of the dielectric constant are 90° out of phase. In terms of electrical measurements it is seen that this corresponds to a resistive and capacitative component. The complex component  $\epsilon''$  is determined from the alternating current conductivity. Although it can be regarded as an apparent conductance, a real dissipation of energy is involved, and the phenomenon of dielectric heating results.

The dispersion region is completely defined by the equations 23, 24. It can be seen that at the frequency  $\omega = \frac{1}{\tau}$ .

$$\epsilon' = \frac{\epsilon_0 + \epsilon_\infty}{2} \quad \underline{27}$$

$$\epsilon'' = \frac{\epsilon_0 - \epsilon_\infty}{2} \quad \underline{28}$$

From measurements of either of these components of the dielectric constant the relaxation time can be found. In the Debye picture we have

$$\tau = \frac{K}{2kT} \quad \underline{29}$$

where  $K$  is rotary diffusion constant. Considering the dipole as a sphere of radius "a" rotating in a medium of viscosity  $\eta$  and applying Stoke's Law we have

$$\tau = \frac{4\pi\eta a^3}{kT} \quad \underline{30}$$

Thus, according to Debye, from a knowledge of the viscosity of the medium and the frequency and temperature of maximum absorption the size of the rotating unit can be estimated. Attempts have been made to adapt the Debye-Stokes relation to cylindrical particles (26). The correction, however, is a minor one in comparison with the general limitations of this relationship.

### Some Criticisms of the Debye Theory

The introduction of Stoke's Law and the macro viscosity is one of the most serious defects of the Debye Theory. Although the values of the effective volume of the rotating dipole are sometimes in agreement with 30 above, very serious discrepancies are found to occur (24).

An analysis of the assumptions made in introducing Stoke's Law at this point shows that Debye was not justified in doing this (25).

(a) Stoke's Law is derived hydrodynamically assuming stream-line motion in the surrounding fluid, and using as one boundary condition that the layer of liquid in contact with the surface moves with the same velocity as the sphere. For the latter condition to be met by a molecule surrounded by others of about the same size would mean that the effective radius of the sphere would have to be multiplied by three. If, on the other hand, we are to allow for a certain amount of slippage, the entire picture of stream-line flow becomes questionable.

(b) The present ideas of the structure of liquids are quite incompatible with the picture of a dipole molecule as a sphere immersed in a homogeneous viscous fluid. Instead we would expect a quasi-crystalline arrangement in the neighborhood of a polar molecule. Debye has tried to take this into account (27).

(c) The method of introducing the viscosity in the Debye theory throws the burden of formulating a molecular theory of dielectric relaxation upon those who seek to explain liquid viscosity on the basis of a molecular theory. It would be more reasonable to expect a theory of dielectric relaxation to help in formulating a molecular theory of viscosity, since the latter probably represents a more complex phenomenon. Furthermore, when considering solids the concept of "internal viscosity" must be invented, and it is doubtful whether anything useful has been gained by introducing the viscosity in this way.

#### Dielectric Relaxation as a Chemical Kinetic Process

A new approach to the problem of dielectric relaxation has been adopted by several authors in recent years. Frank (28) was one of the first to treat dielectric relaxation from the point of view of chemical kinetics. Eyring (29)(30), Kauzmann (25) and others have applied the theory of absolute reaction rates to the problem.

The assumption that the dielectric relaxation time serves to define a molecular rate constant seems to be quite reasonable. The fact that the dielectric relaxation time is markedly dependent on temperature is very significant from this point of view.

Whenever the rate of a process depends markedly on the temperature, it is quite certain that at some stage the molecule, or other unit involved, is forced to wait until it has acquired by thermal fluctuation a considerable amount of energy in excess of the thermal energy of the medium. It is therefore natural to apply kinetic methods to dielectric relaxation rates, and thus try to gain a better understanding of the fundamental mechanism.

Proceeding this way we can define a free energy for dielectric relaxation  $\Delta F^\ddagger$  by the equation

$$\frac{1}{\tau} = \frac{kT}{h} e^{-\frac{\Delta F^\ddagger}{RT}} \quad 31$$

where  $k$  and  $h$  are the Boltzmann and Planck constants. This equation can be rewritten

$$\frac{1}{\tau} = \frac{kT}{h} e^{-\frac{\Delta S^\ddagger}{R}} e^{-\frac{\Delta H^\ddagger}{RT}} \quad 32$$

Thus from a measurement of the dielectric relaxation time we can obtain  $\Delta F^\ddagger$ , while if the temperature variation of  $\tau$  is known we can obtain  $\Delta H^\ddagger$ . By subtraction values of  $\Delta S^\ddagger$  can be obtained. Similar equations can be written for the process of viscous flow. It is found that better correlation between the processes of dielectric relaxation and viscous flow can be obtained in this way than by application of the Debye theory (31). When the free energies are nearly equal it is now generally assumed that there is a close correlation between the two processes (32).

### The Distribution of Relaxation Times

In the previous discussion it was implicitly assumed that there was a single value of the relaxation time. There is

good reason to believe that in many cases, especially for complex molecules, a distribution of relaxation times exists. In the Debye theory the shape of the dispersion curves for dielectric constant and loss are completely described by equations 23, 24. It is found experimentally that the dielectric loss curve is often much broader and lower than expected on the basis of the theory. The slope of the dielectric constant curve is also found to be less than predicted by Debye. Extreme examples of such behavior are found for solid polymers and rubbers. Equations 23, 24 predict a drop of the dielectric constant from its low frequency to its high frequency value over a frequency variation of a factor of 10. For rubber this factor is found to be 300 (23), while the extreme case reported is a factor of 5,000,000 for polyvinyl chloride.

Although such extreme deviations are readily noticed, it is much more difficult to assess a slight broadening of the dispersion curves. Cole and Cole (33) suggested a convenient empirical plot for estimating such deviations quantitatively.

Equations 27, 28 may be rewritten

$$\epsilon^* - \epsilon_\infty = \frac{\epsilon_0 - \epsilon_\infty}{1 + j\omega\tau_0} \quad \underline{33}$$

$$\epsilon' - \epsilon_\infty = \frac{\epsilon_0 - \epsilon_\infty}{1 + (\omega\tau_0)^2} \quad \underline{34}$$

$$\epsilon'' = \frac{(\epsilon_0 - \epsilon_\infty)\omega\tau_0}{1 + \omega^2\tau_0^2} \quad \underline{35}$$

We can define vectors  $\bar{u}$  and  $\bar{v}$  on an Argand diagram where  $\epsilon'$  is

plotted on the real axis, and  $\epsilon''$  on the imaginary axis in the complex plane with values

$$\begin{aligned}\bar{u} &= \epsilon' - \epsilon_{\infty} \\ \bar{v} &= j \omega \tau_0 (\epsilon' - \epsilon_{\infty})\end{aligned}$$

These vectors in the complex plane are perpendicular and their vector sum is the constant quantity  $\epsilon_0 - \epsilon_{\infty}$ . Thus we can see that a plot of  $\epsilon'$  vs  $\epsilon''$  at varying frequency should yield a semi-circle with its centre on the X axis and whose diameter is  $\epsilon_0 - \epsilon_{\infty}$ . Real dielectrics, however, are often found to yield arcs of circles whose centres lie below the X axis as shown in diagram 3, Figure 1. The extent of this depression is measured by an angle  $\alpha'$  between the radius and the X axis. The value of  $\alpha$  is stated to be related to the distribution of relaxation times. Cole and Cole have suggested as an empirical modification to Debye's equations the following relations for  $\epsilon'$  and  $\epsilon''$  :

$$\epsilon' = \frac{1}{2} (\epsilon_0 - \epsilon_{\infty}) \left[ 1 - \frac{\sinh \frac{(1-\alpha) X}{\cos \frac{1}{2} \alpha \pi}}{\cosh \frac{(1-\alpha) X}{\cos \frac{1}{2} \alpha \pi}} \right] \quad 36$$

where  $X = \ln \omega \tau_0$

$\tau_0 =$  is most probable relaxation time.

$$= \frac{\frac{1}{2} (\epsilon_0 - \epsilon_{\infty}) \cos \frac{1}{2} \alpha \pi}{\cosh \frac{(1-\alpha) X}{\cos \frac{1}{2} \alpha \pi}} \quad 37$$

Recently Smyth (34) has used the above as a more accurate method of evaluating the relaxation time.

The actual form of the distribution functions has been approximated empirically by several workers. Wagner and Yager (35) have suggested a Gauss error function of the form

$$f(t) = e^{-b^2 t^2} \quad \underline{38}$$

where  $f(t) dt$  represents the probability that  $t$  lies in the interval  $dt$ , and where  $t = \ln \frac{\tau_0}{\tau}$  and  $\tau_0$  is the most probable relaxation time. Kirkwood and Fuoss (36,37) proposed a logarithmic distribution function. Cole and Cole have shown that the Kirkwood-Fuoss distribution could be rewritten using the parameter obtained in the circular arc plots. The distribution function is given by

$$F(s) ds = \frac{A \sin \alpha \pi}{2 \cosh(1-\alpha) s - \cos \alpha \pi} ds \quad \underline{39}$$

where  $s = \ln \frac{\tau}{\tau_0}$  where  $A$  is defined by condition  $\int_{-\infty}^{\infty} F(s) ds = 1$ .

Kauzmann has compared these and other distribution functions, and has shown that the general distributions predicted are in good agreement with one another.

### Viscosity and Streaming Birefringence of Asymmetric Particles

Previous work on large anisometric molecules in solution has largely been confined to studies of viscosity and streaming birefringence. The hydrodynamic aspects of the problem have been carefully investigated. Einstein (38), Boeder (39), Kuhn (40) and Jeffery (41) have dealt with the orientation of cylindrical particles in a velocity gradient. From their work it was seen that, when Brownian motion was negligible, the viscosity increase of the solution over that of the solvent depended upon the shape of the particles. In the presence of Brownian motion a second important viscosity effect was predicted. Under these conditions the apparent viscosity is a

function of the rate of shear at which it is measured. Such non-Newtonian viscosity is quite general for systems of large anisometric particles. Thixotropic behavior, or decrease of viscosity with increasing rate of shear, is usually found in such systems. This can be regarded as a particular type of non-Newtonian viscosity.

The hydrodynamical concepts of orientation under shear have been applied in the formulation of a theory of streaming birefringence (1). Referring to our previous discussion on the influence of shear on the dielectric constant equation 14 showed that

$$\frac{\partial \phi}{\partial t} = K \frac{\partial^2 \phi}{\partial \theta^2} - \frac{\partial (\omega \phi)}{\partial \theta}$$

Assuming statistical equilibrium after the flow has proceeded for some time we may consider that  $\phi$  does not vary with time or  $\frac{\partial \phi}{\partial t} = 0$ .

Integrating

$$K \frac{\partial \phi}{\partial \theta} - \omega \phi = C \quad \underline{40}$$

For thin rods whose diameters are negligible in comparison to their lengths Jeffery showed that

$$\omega = -G \sin^2 \theta \quad \underline{41}$$

Substituting in 40 we obtain

$$\frac{\partial \phi}{\partial \theta} - \frac{G}{K} \phi \sin^2 \theta = C \quad \underline{42}$$

Boeder (39) has given the solution of this equation, which is fundamental to the theory of streaming birefringence. Graphically the solution consists of families of bell shaped distribution curves on a plot of  $\phi$  vs.  $\theta$ , for differing values of  $G/K$ . The height of these curves determines the intensity of birefringence, and the

position of the maximum determines the extinction angle. Briefly stated, the double refraction is a measure of the difference in two refractive indices measured perpendicular to one another in the anisotropic liquid. The extinction angle measures the angle between the optic axis of the anisotropic liquid and the stream-lines of flow.

The analogy between streaming birefringence and the phenomenon of photo-elastic behavior should be recalled in this connection. It is well known that many amorphous isotropic materials when subjected to strain show anisotropic behavior, as was first observed by Brewster (42) in glass. These mechanical-optical effects have recently been extensively investigated and have been developed into a powerful tool for determining experimentally the distribution of stresses in structural models.

The photo-elastic behavior of an ideally elastic amorphous material can be readily understood. Under the action of a tensile stress in a given direction the molecules will be pulled apart in this direction. The electronic clouds will likewise be displaced and will interact in a different manner from the unstressed condition. Thus a material which is optically isotropic in the absence of stress will become anisotropic in the stressed condition. A light ray normal to the direction of stress will suffer a phase retardation whose magnitude will depend upon the orientation of the plane polarization relative to the direction of stress. Two such rays, one polarized in the direction of stress and the other across this direction, will experience a relative shift in passage through the sample. The

magnitude of the relative phase retardation can be related to either the stress or the strain. Experimentally it has been shown that the facts point to a strain optical effect rather than a stress optical phenomenon (43).

If we consider the concentrated polymer solutions as possessing a degree of structure due to the presence of complex interaction of chains then the photo-elastic phenomenon may be closer to the true picture of birefringence than is the phenomenon of orientation in the absence of interaction as discussed by Edsall.

#### Aluminum Soap - Benzene Systems

The system aluminum soap - benzene was investigated in connection with the work of Part I on dielectric behavior under shear. This type of system possesses rather unusual physical properties, and a brief description of these may be of value.

The addition of a few per cent of an aluminum soap to a suitable organic medium (e.g. benzene) produces a system with properties similar to those of high polymer solutions. A very great increase in viscosity is obtained, usually representing an increase of ten to one hundred times over that of the pure solvent. In the higher concentration ranges the systems show marked elasticity. Simultaneous measurement of viscosity and streaming birefringence of these systems have recently been reported by Gray and Alexander (6). They have found that in some instances birefringence could even be observed in the absence of flow, pointing to a "liquid crystal" type of orientation.

Although their general properties are similar to those of

polymers the aluminum soaps differ from these in several respects. The particle size in the aluminum soap systems appears to depend on the concentration (44) and the presence of peptizers (e.g. phenols, alcohols). Otherwise, their rubber-like bulk properties, the influence of plasticizers, and the fact that crystals do not seem to have been isolated class them as a type of polymeric material. A safe assumption is to class these systems as polymers, with the reservation that the linkage between the monomeric units is weaker than that for the usual natural and synthetic polymers (45).

#### Previous Work

##### PART I

The measurement of the dielectric constant of systems subjected to varying rates of shear is essentially a new experimental technique, and very little previous work is reported in the literature. Singh and Singh (46) measured the dielectric constant of pure liquids under flow conditions. They did not observe any significant changes in dielectric constant in their work which was confined to small symmetrical molecules. Recently Voet (47) measured the dielectric constants of suspensions of conducting particles in non-conducting media in a velocity gradient. He found that when such systems were caused to flow large changes in dielectric constant occurred. These results were interpreted in a semi-empirical manner to show that the changes in dielectric constant were due to changes in the "agglomeration" of the particles in solution.

## PART II

Dielectric dispersion measurements on polymeric materials have been reported by Fuoss, Smyth and coworkers (48) and others. Most of the work reported was performed on solid polymer samples, although these were sometimes plasticized. The work of Fuoss and coworkers is particularly comprehensive (49-60), and probably represents the major contribution in this field. The electrical properties of solid polymers are of great technical and commercial importance, and it is not surprising that the major part of the experimental work was performed on solids.

In addition it has been found possible to relate mechanical and electrical properties of polymer samples. Davies, Miller and Busse (61) succeeded in correlating the mechanical properties of polyvinyl chloride plasticized with tricresyl phosphate with the entropy for dielectric relaxation. The influences of thermal history (51) (52), type and concentration of plasticizers (60), molecular weight (56) and chemical composition of solid polymers on dielectric dispersion measurements have been investigated by Fuoss. He has reported measurements on samples of polyvinyl acetate and polyvinyl chloroacetate (59) which have a direct bearing on the present work.

The essentially amorphous, though partly crystalline structure, of most polymers presented a new medium for investigation. The work of Plessner and Richards (62) on dipole orientation in solutions of esters in solid polyisobutylene and polythene offer an example of the techniques that have been employed in this respect.

Dielectric dispersion studies of proteins in solution have been reported by several investigators (63)(64). In particular Oncley (65)(66) has reviewed the value of correlating data from dielectric dispersion and streaming birefringence measurements.

Comprehensive reviews on the interpretation of dielectric dispersion data have appeared recently. Kauzmann (25) and Powell and Eyring (31) have treated the subject on the basis of the theory of absolute reaction rates. Morgan and Yager (67) have summarized much of the available data on high polymers. Moullin (68) has treated the subject on a classical basis.

PART I

Measurements of the Dielectric Constant of Solutions  
of Macromolecules under Shear

- PART I -

EXPERIMENTAL

The nature of the experimental problem of measuring dielectric constants under shear required:

(1) an accurate and instantaneous method of measuring capacitance;

(2) a rotating condenser in which solutions could be subjected to varying rates of shear.

Electrical Apparatus

The most reliable and commonly accepted means of capacitance measurement at audio frequencies is the Bridge method (69). A Schering bridge was used throughout the course of this work. The first bridge was constructed by the author, but, though it possessed high precision, the requirements of versatility to a wide range of frequencies and accurate knowledge of residual impedances were not met. Consequently, a commercial General Radio Type 716 C Schering Bridge was used for the major part of the work.

The principle of the Schering bridge is readily understood. In Figure 2 the bridge is shown schematically as used in the "Substitution Method". The unknown condenser, in general not a pure capacitance, is represented by a pure capacitance,  $C_{xp}$ , and a pure resistance,  $R_{xp}$ , in parallel. The capacitor,  $C_s$ , was a precision air condenser incorporated in the bridge, calibrated to read capacitance values from

### SCHERING BRIDGE

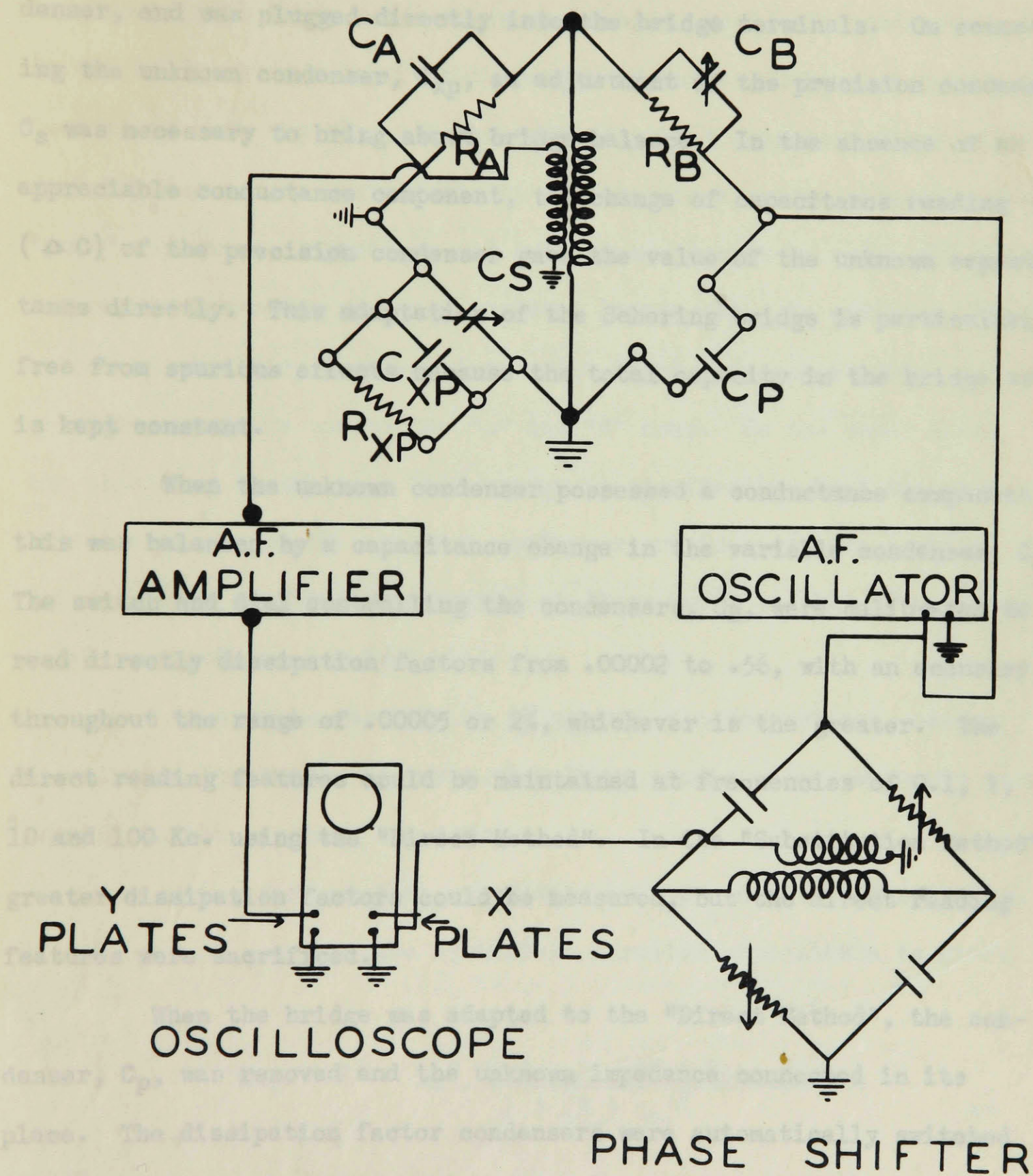


Figure 2: Schering bridge and auxiliary apparatus.

100 to 1100 uuf. with an absolute accuracy of 0.1 uuf. The capacitor,  $C_p$ , was a General Radio Co. Type 505, high quality, 1000 uuf. mica condenser, and was plugged directly into the bridge terminals. On connecting the unknown condenser,  $C_{xp}$ , an adjustment of the precision condenser,  $C_s$  was necessary to bring about bridge balance. In the absence of an appreciable conductance component, the change of capacitance reading ( $\Delta C$ ) of the precision condenser gave the value of the unknown capacitance directly. This adaptation of the Schering bridge is particularly free from spurious effects because the total capacity in the bridge arms is kept constant.

When the unknown condenser possessed a conductance component, this was balanced by a capacitance change in the variable condenser,  $C_B$ . The switch and dial controlling the condensers,  $C_B$ , were calibrated to read directly dissipation factors from .00002 to .56, with an accuracy throughout the range of .00005 or 2%, whichever is the greater. The direct reading features could be maintained at frequencies of 0.1, 1, 10 and 100 Kc. using the "Direct Method". In the "Substitution Method" greater dissipation factors could be measured, but the direct reading features were sacrificed.

When the bridge was adapted to the "Direct Method", the condenser,  $C_p$ , was removed and the unknown impedance connected in its place. The dissipation factor condensers were automatically switched to the "A" arm by setting a selector switch at the "Direct" position. When bridge balance was established, reading the precision condenser,  $C_p$ , then gave the value of the unknown capacitance, and the dissipation factor could also be read directly.

These direct reading features, however, did not prove to be particularly advantageous in the experimental work. When measuring impedances with large conductance components, residual impedances in the bridge arms necessitated the use of rather cumbersome correction factors in both the "Direct" and "Substitution" methods. These residual impedances are unavoidable in any practical bridge circuit. Since "pure" resistors, capacitors and inductances cannot be made, all bridge components introduce unwanted residual impedances. In addition, the method of shielding employed introduced fixed, but appreciable, capacitive components across the "A" and "B" arms. On the other hand, the shielding on the type 711C bridge is so effective that the zero capacitance across the unknown condenser arm is less than 1 uuf. This provides an inherent accuracy at least equal to that of any other model available commercially.

An example may help to illustrate the corrections necessary to maintain the bridge accuracy when large conductance components were present in the measured impedance.

Using the parallel substitution method and with a dissipation factor of 1 or greater, the equivalent parallel capacitance is given by

$$C_{\text{exp}} = \Delta C \frac{1 + (D + D_0) \left( D' + D_0 - \Delta D \frac{C}{\Delta C} \right)}{1 + (D + D_0)^2} \quad 43$$

where

$C'$  is initial reading of capacitance dial

$C$  is final reading of capacitance dial

$$\Delta C = C' - C$$

$D'$  is initial dissipation factor reading

$D$  is final dissipation factor reading

$D_0$  .035 for this model bridge.

The dissipation factor  $D_x$  under similar conditions is given by

$$D_x = \frac{C'}{\Delta C} \frac{\Delta D}{1 + (D + D_0 - \Delta D \frac{C}{\Delta C})} \quad \underline{44}$$

The meaning of the various relations discussed above may be recalled by reference to a simple circuit diagram. Considering the capacitance being measured as being represented by a pure capacitance in parallel with a pure resistance, a vector diagram illustrating existing relationships. These are shown in diagram 4, Figure 1.

$$\frac{C_{xp}}{C_g} = \epsilon' \quad \text{where } C_g \text{ is geometric capacity}$$

$$D_x = \frac{\epsilon''}{\epsilon'} = \frac{X}{R} = \frac{1}{RC\omega} = \tan \delta = \cot \theta$$

where  $\delta = 90^\circ - \theta$  is phase angle

$$\sin \delta = \cos \theta \text{ is power factor}$$

$X$  is reactance

$$\omega = 2\pi f, \text{ where } f \text{ is frequency.}$$

The two components of the dielectric constant are derived quite simply once the dissipation factor and corrected capacitance are known,

$$\epsilon' = \frac{C_{xp}}{C_g} \quad \text{and} \quad \epsilon'' = \epsilon' D.$$

The auxiliary equipment used in conjunction with the bridge is also shown in Figure 2. The bridge was energized by a Hewlett-Packard audio frequency oscillator which was continuously variable

from 35 c./second to 35 Kc./second. The oscillator signal was fed to the bridge and thence through an audio frequency amplifier to a 5" Sylvania cathode ray oscilloscope which served as null detector. The a.f. amplifier was constructed from the amplifying section of the a.f. oscillator described by N. R. Hollies (70), and the constant voltage power supply employed by the latter was used.

The method of null detection possessed some unusual features. The amplified bridge signal was fed to the vertical plates of the oscilloscope. The horizontal plates were connected to the oscillator through a variable phase shifter described by Lamson (71). In this way a lissajous pattern was formed on the oscilloscope screen. By proper adjustment of the phase shifting network a change in the conductance component could be made to produce a tilting of the ellipse, while a capacitance change could be made to produce a tilting of the ellipse. Complete bridge balance was indicated by the degeneration of the ellipse to a horizontal straight line.

The sensitivity of the detecting circuit was very high, and its response instantaneous. A sensitivity of .03 uuf. in measuring 1000 uuf. could be obtained. The inherent accuracy, however, was lower than this, being limited by the accuracy of calibration of the bridge's precision condenser and by the limitations of the correction factors for residual impedances.

### Rotating Condensers

The design of suitable liquid condensers presented a formidable problem. The choice of the shape of the condenser was readily

made; a coaxial cylindrical arrangement in which one of the cylinders is rotated possessed the advantage of constant shear gradient and ease of construction. The actual choice of the geometry of the condenser, however, involved the careful balancing of important theoretical variables against the difficulties and limits of precision of machining. The requirements to be fulfilled by a suitable condenser may be listed as follows:

- (1) a capacitance between 100 and 200 uuf. to ensure maximum precision of reading on the bridge;
- (2) absence of variation of capacitance greater than .2% during rotation;
- (3) production of a suitable range of shear gradients;
- (4) absence of turbulent flow at the highest rates of shear employed;
- (5) ease of filling with viscous solutions or gels;
- (6) absence of end effects due to disturbance of liquid surface during flow, or to slight variations in liquid level resulting from evaporation or method of filling.

The only geometrical quantities that could be adjusted to fulfil the above requirements were the radius,  $r$ , the spacing between the cylinders,  $d$ , and the length,  $l$ . It is interesting to examine these relationships more quantitatively. The capacitance of a coaxial cylindrical arrangement is given by

$$C = \frac{0.2416 l}{\log_{10} r_1/r_2}$$

where  $r_1$  and  $r_2$  are the inner and outer radii, respectively. When  $r_1$  is approximately equal to  $r_2$ , then approximately

$$C \propto \frac{r}{d} \quad \text{where } d = r_2 - r_1.$$

One can reach this same conclusion if one considers the coaxial cylindrical arrangement as a particular form of parallel plate condenser. It is evident that the capacity is directly proportional to the length and the radius, and inversely proportional to the spacing.

On the other hand, the rate of shear,  $G$ , at the distance  $r$  is given

$$G = \frac{dV}{dr} = \frac{\omega r_1^2}{r_1^2 - r_2^2} \left( 1 + \frac{r_2^2}{r^2} \right) \quad 45$$

which if  $d \ll r_1$  is given by

$$G \approx \frac{r_1 \omega}{d} \approx \frac{r_2 \omega}{d} \quad 46$$

where  $\omega$  is angular velocity.

Now since

$$\omega = 2 \frac{\pi \text{RPM}}{60} \quad G = \frac{r_2}{60} \frac{2 \pi \text{RPM}}{d} \quad 47$$

The conditions for turbulent flow in a coaxial cylindrical system of this type were thoroughly investigated by G. I. Taylor (72) (73). Both theory and experiment showed that

$$\frac{\omega_c^2}{(\eta/\rho)^2} = \frac{4}{\pi} \frac{r_1 + r_2}{2P d^3 r_1^2} \quad 48$$

where

$V$  is the velocity of liquid

$\omega$  angular velocity                       $\omega_c$  critical angular velocity for turbulence

$\eta$  its viscosity

$\rho$  its density

$r_1, r_2$  radii of inner and outer cylinders respectively

$G$  velocity gradient in  $\text{secs}^{-1}$

and  $P$  is a numerical factor given by

$$P = .0571 \left( 1 - .652 \frac{d}{r_1} + \frac{.00056}{1 - .652 d/r_1} \right)$$

If  $r_1 \approx r_2$

$$\frac{\omega_c^2}{(\eta/\rho)^2} = \frac{\pi^4}{2P d^3 r_1}$$

or

$$\omega_c \propto \frac{\eta}{\rho d^{3/2} r_1^{1/2}}$$

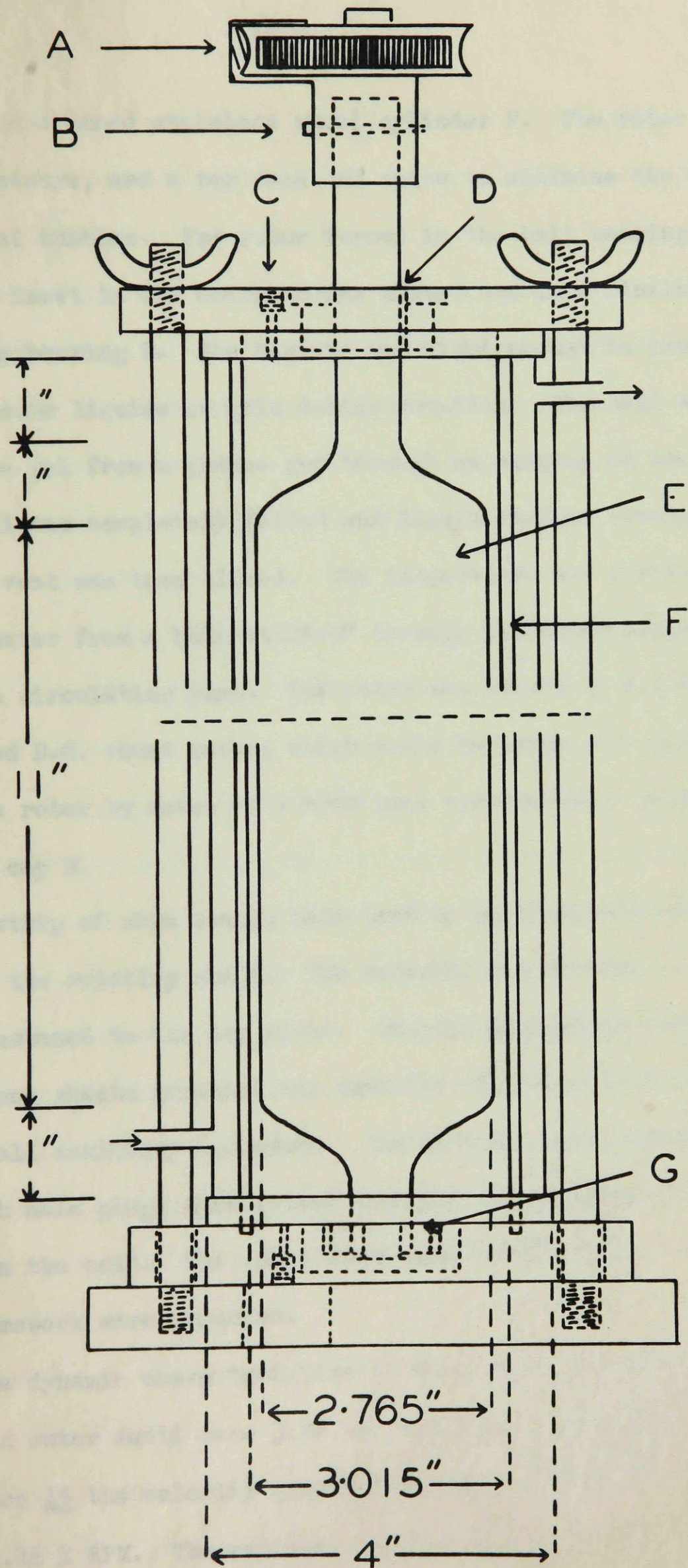
Hence the critical angular velocity varies approximately as the inverse 3/2 power of the gap and the inverse root of the radius. Similarly the critical velocity gradient

$$G_c = \frac{r \omega_c}{d}$$

must vary as the inverse 5/2 power of the gap.

The first cell (cell A) that was specifically designed to meet many of these requirements is shown in Figure 3. In this cell the disadvantages of large dimensions and low shear rate were balanced by large gap dimensions which were believed necessary to ensure negligible eccentricity (and consequently small capacitance variation) on rotation.

The cell consisted of a solid brass chrome plated rotor E



Rotating condenser A.

rotating inside a honed stainless steel cylinder F. The rotor had smooth end contours, and a top dead end space to minimize the effect of any residual bubbles. The rotor turned in the ball bearing ring G in a bakelite inset in the bottom brass plate, and in a similarly insulated oilite bearing D. The bearing was tight enough to prevent the escape of viscous liquids or gels during rotation. The cell was filled by forcing the gel from a grease gun through an opening in the bottom until the cell was completely filled and liquid emerged through the vent C; this vent was then closed. The temperature was controlled by circulating water from a bath at  $25.0^{\circ}$  through the outer copper jacket by means of a circulating pump. The rotor was turned by a 1/10 H.P. variable speed D.C. shunt motor, which could be swung into position to engage the rotor by means of a worm gear arrangement A mounted on the bakelite cap B.

A strip of shim stock, held taut by springs, made electrical contact with the rotating shaft. The assembly was mounted on a bakelite block fastened to the top plate. Coaxial microphone cable, with the outer steel sheath grounded was used for all leads both to the cell and to all auxiliary equipment. The ends of these cables were equipped with male plugs that fitted directly into terminals on the bridge and on the cell. The outer stationary cylinder and its surrounding framework were grounded.

The dynamic characteristics of this cell were calculated. The inner and outer radii were 3.52 cm. and 3.84 cm. respectively. Using equation 45 the velocity gradient in seconds<sup>-1</sup> was found to be  $1.10\omega$ , or 1.16 X RPM. The critical rate of rotation for turbulence

was evaluated as  $(\text{RPM})_c = 1.20 \times 10^4 \frac{\eta}{\rho}$  using equation 48. Thus with a rate of rotation of 1000 RPM for cell A the velocity gradient was  $1160 \text{ sec}^{-1}$  and  $\frac{\eta}{\rho}$  had to exceed 0.8.

The cell was calibrated in the manner recommended by Smyth (74). The capacitance of the empty cell was first measured and found to be 227.2 uuf. The cell was then filled with dried A.R. benzene and the capacitance again measured at  $25.0^\circ$  and found to be 465.9 uuf. Denoting the geometrical capacitance by  $C_g$  and the stray capacitance by  $C_o$  we have

$$C_g + C_o = 227.2$$

$$\epsilon C_g + C_o = 465.9$$

Subtracting we have

$$(\epsilon - 1) C_g = 238.7$$

Assuming the value of 2.276 for the dielectric constant of benzene at this temperature, we obtain  $C_g = 187.5$  uuf.  $C_o = 39.7$  uuf. This agreed very well with the calculated value of 200 uuf. which the cell was designed to possess.

After the early work on aluminium soaps and the first investigations on high polymers it appeared desirable to obtain measurements (by analogy with streaming birefringence measurements) at higher rates of shear than were hitherto possible. The cell described above was not suitable, not only because of the low velocity gradients obtainable, but due to the large volume (over 600 ml.) of carefully dried solutions necessary for its filling.

A further cell (Cell B) was machined on the lathe by the author. The overall dimensions were 7" for the outer cylinder and 6"

for the effective length of the inner cylinder. The diameter was approximately  $1\frac{1}{2}$ " and the spacing  $1/16$ ". The rotor turned in ball bearings in both top and bottom bakelite, precision fitting caps. The temperature was controlled by circulating thermostated water through an outer water jacket. The shear rates obtainable in this cell were of the same order of magnitude as those in cell A, but the critical value for turbulence was higher and the volume smaller. The effective geometrical capacity  $C_g$  was found to be 86.1 uuf. and the velocity gradient calculated was  $G=1.01$  RPM ( $\text{sec}^{-1}$ ).

The final cell (Cell C) was closely modeled after those used in streaming birefringence studies for high shear gradients (75)(76)(77) and incorporated several unusual features. Cell C is shown in Figure 4. The inner rotor ( $F_1$ ) was machined from a solid piece of bakelite to approximately correct dimensions. A brass sleeve ( $E_1$ ) was fitted over this to act as the live electrode and the whole was then carefully machined to the proper dimensions. Small brass sleeves were used to eliminate wear on the bakelite in the ball bearings ( $C_1$ )( $K_1$ ). The spacing between inner and outer cylinders (F) and (G) was only .01". The design was expected to safeguard against any surface disturbance at high rates of rotation, since the  $\frac{1}{4}$ " bakelite at the top would experience the same streamline flow as the active electrode, and in addition there was a  $\frac{1}{4}$ " dead space filled with liquid above this region.

In order to reduce strains on the bakelite shaft the cell was mounted on a drill press stand and the rotor was held in the Jacob's chuck normally used for the drilling bit. Electrical contact (D) was made by a #32 B.S.S. gauge wire strung through a centrally

drilled hole in the shaft to an outer contact ring (B), where contact was established through a carbon brush (A). The cell was filled by forcing liquid in through the inlet (J). The temperature was controlled by thermostating the water jacket (H) with water circulated from a bath at 25.0°C.

The calculated velocity gradient for cell C was 18.7 RPM, and the cell possessed a capacitance of 137.0 uuf.

### Materials

All polymer samples and solvents were carefully dried. Metallic sodium was used for the drying of benzene and toluene. Other solvents were allowed to stand over "Drierite", and, in some cases, were finally dried over P<sub>2</sub>O<sub>5</sub> (when this was chemically feasible) before being distilled.

Solid samples were dried in vacuo at 60° for several hours. Polyvinyl acetate, however, softened when treated in this way, and these samples were dried in vacuo at room temperature. The following polymers were investigated:

Polyvinyl acetate: Gelva V 1 1/2, V 15, V 25 and V 200. The numbers refer to the viscosities of a monomer unit weight in grams in one liter of benzene. The molecular weights by the osmotic pressure method were given as: V 1 1/2 15,000, V 15 60,000, V 25 100,000. These samples and specifications were obtained from Canadian Resins and Chemicals Co.

Polyvinyl formal: also obtained from the above Company.

Cellulose acetate butyrate: obtained from the Tennessee Eastman Company.

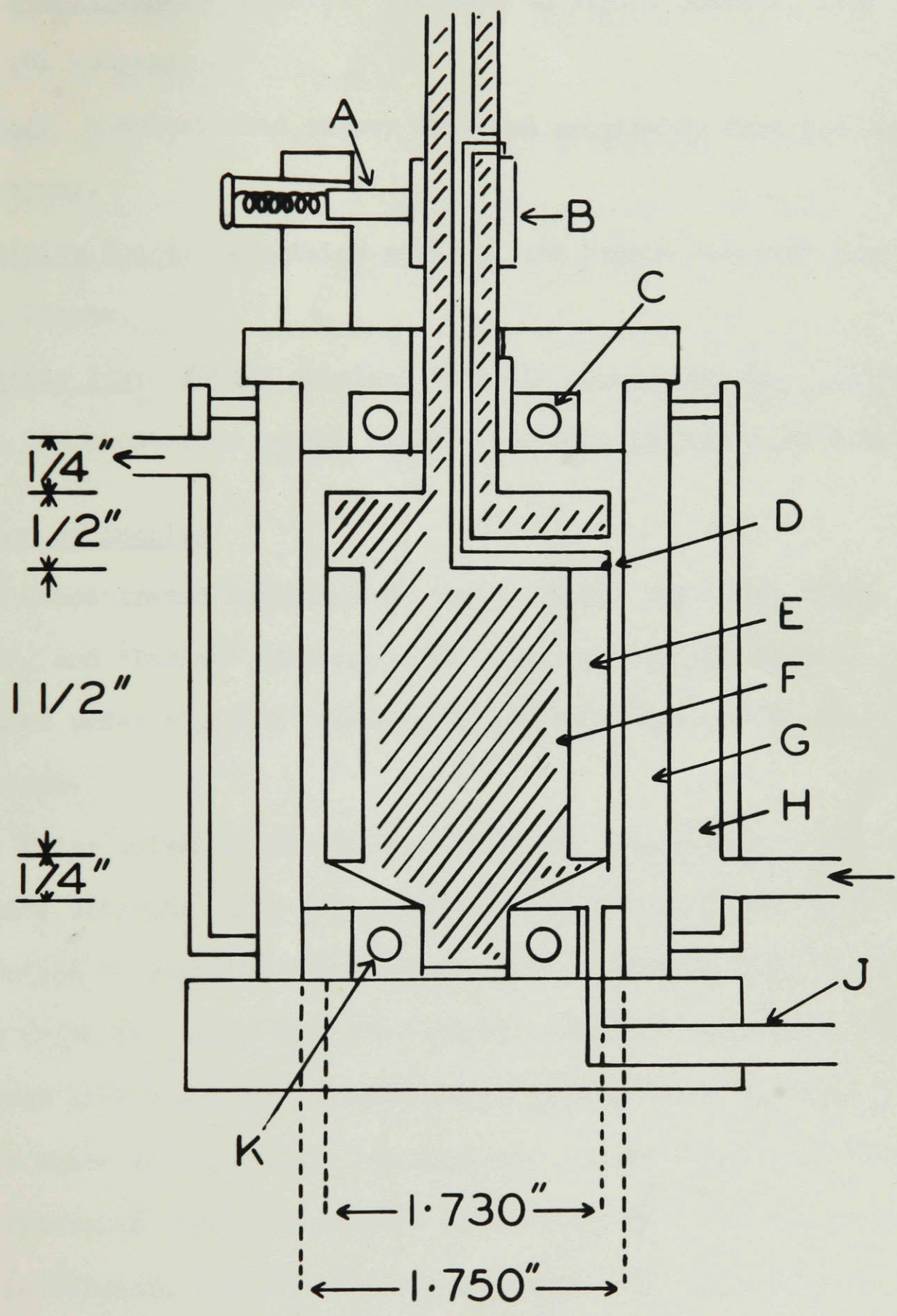


Figure 4: Rotating condenser C.

Ethyl cellulose: "Ethocel" standard 10 c.p.s. obtained from the Dow Chemical Company.

Parlon: a chlorinated rubber obtained originally from the Hercules Powder Company.

Aluminium Soaps: Aluminium stearate and Napalm obtained from D.R.C.L., Ottawa.

Printing Ink: #85323 obtained from the Canada Printing Ink Company as a representative carbon black suspension in petroleum base.

#### Preparation of Samples

Concentrated solutions of the polyvinyl acetates, "Ethyl Cellulose", and "Parlon" were prepared by dissolving the samples in A.R. benzene under vigorous stirring by a mercury seal stirrer for several hours.

Polar solvents were necessary in the preparation of cellulose acetate butyrate and polyvinyl formal solutions, since non-polar liquids failed to dissolve these substances. A wide variety of solvents was tried for these and other polymer samples which were available. Great difficulty was encountered in drying these suitably for dielectric measurements at low frequencies. It was found that under the most intensive drying conditions appreciable D.C. conductivity remained in solvents such as esters and ketones and the slightest exposure to the atmosphere during filling or during the progress of a run was sufficient to cause a very substantial increase in conductivity. Very often this was sufficient to make the resistive impedance

so small in relation to the capacitance that capacity measurements were impossible at low frequencies.

It was found, however, that chloroform could be used for the preparations of polyvinyl formal and cellulose acetate butyrate solutions. The cellulose ester could also be dissolved in a 2:1 volume mixture of butyl acetate and toluene. This latter solvent mixture had desirable electrical properties, although butyl acetate alone could not be used due to the high conductivity mentioned above.

The method of preparation of aluminium soap gels had a marked effect on their physical properties. A standard procedure was therefore adopted. The aluminium soaps were dried in a vacuum oven at 60° for 16 hours, and the benzene was dried over sodium metal. Napalm gels were prepared by adding the soap to the benzene at room temperature and stirring vigorously for 30 minutes with a special double paddle, fork-like stirrer. This type stirrer proved very effective in keeping the solid soap evenly distributed throughout the benzene prior to gelation. After gelation had begun ordinary propeller stirrers proved very ineffective, whereas this type stirrer produced thorough mixing.

Aluminium stearate gels are usually prepared by the addition of a small amount of a "peptizer" such as phenol which causes a rapid gelation of the soap in benzene at room temperature. The addition of such a polar substance, however, was undesirable, because of the increased difficulty of interpreting such dielectric data. It was found, however, that heating the benzene - aluminium stearate system produced a sharp gelation at about 50°C. Therefore, the preparation

of aluminium stearate gels was accomplished by suspending the powder in the benzene at 25°, accompanied by vigorous stirring through a mercury seal stirrer. The system was then heated until the gelation temperature was reached; heating was then stopped, but stirring continued for a further 30 minutes.

### Procedure

The following variables could be changed at will in performing the experiments: frequency, temperature, rate of shear, concentration and type of solvent and solute. The experimental variables measured were: capacitance, dissipation factor, rate of shear and time. The experimental work consisted of dynamic measurements carried out with few exceptions at constant temperature (25.0°) and constant frequency (10 Kc), (while in Part II static measurements at varying frequency and temperature are reported). When the cell was filled the concentration and type of solute could not be changed during a run. Thus the main experimental procedure consisted of varying the rate of shear at definite time intervals and measuring the changes in capacitance and dissipation factor. Another type of measurement could also be made. This was the measurement of "recovery" times, i.e. the rates of return of the capacitance and dissipation factor to their static values after the rate of shear is reduced to zero. Finally "cycling" runs could be performed. In this type of run the rate of shear was increased at the end of fixed time intervals until a maximum value was reached, and then the rate of shear was progressively decreased. This procedure was intended to test for the presence of hysteresis or "memory" effects.

## RESULTS

### Aluminum Soaps

The first systems investigated were "gels" formed in the system aluminum soap - benzene. The usage of the term "gel" rather than "solution" should be explained. For our purpose it is sufficient to say that these systems were semi-rigid, possessed marked elastic properties and exhibited thixotropic or non-Newtonian viscosity behavior. The question whether these unusual properties are due to the formation of aggregates in solution or to the dissociation of a high polymeric type of structure has not been satisfactorily settled (44)(45)(78). From the practical standpoint (e.g. their use as flame-thrower and incendiary bomb fuels) and from the theoretical point of view, a correlation between electrical and mechanical properties was of interest.

Preliminary experiments showed a marked correlation between change in dielectric constant and rate of shear in the cell. As the apparatus was refined, and a cell designed specifically for these systems brought into use, a more critical analysis of the results was necessary. In cell A a masking or distortion of the data due to the presence of air between the plates was not likely. The knowledge of the residual impedances in the commercial bridge, and the application of complete correction factors for conductance, however, completely changed the outlook on these data.

While changes in observed capacity of 70 to 100 uuf. were

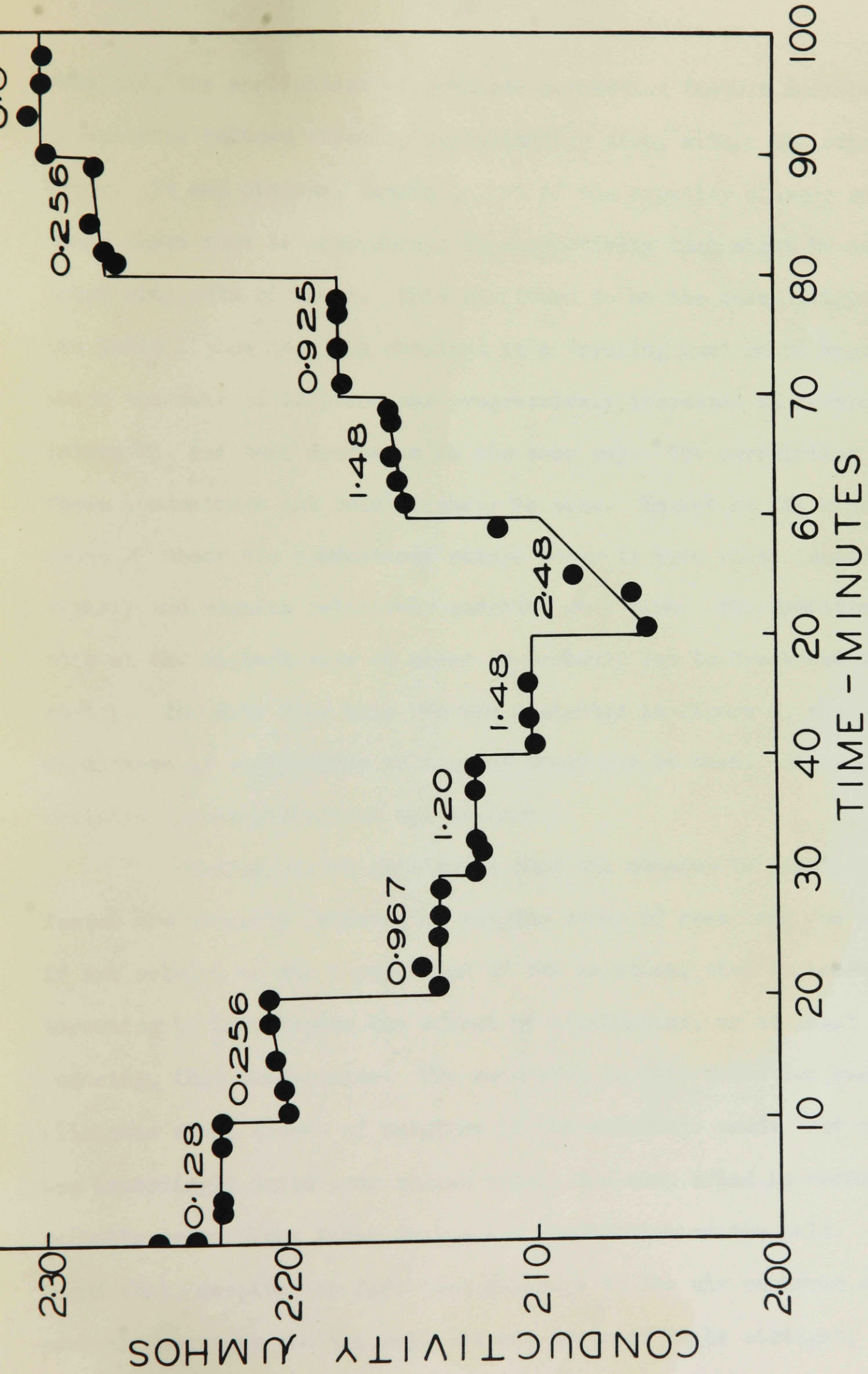


Figure 5: Conductivity of 5% Napalm at inscribed rates of shear.

obtained, the application of complete correction factors for the high conductance reduced these to approximately zero, within the experimental error. It was obvious, however, that if the capacity changes were spurious there must be some change in conductivity that might be correlated with rate of shear. This was found to be the case. Figure 5 and Table I show the data obtained in a "cycling run" on 5% Napalm in which the rate of rotation was progressively increased at 10-minute intervals, and then decreased in the same way. The correlation between conductance and rate of shear is seen. Except at the highest rates of shear the conductance change seems to take place instantaneously and remains relatively constant with time. The deviation from this at the highest rate of shear is probably due to breakdown of viscosity. The data from this run are replotted in Figure 6, where the dependence of conductance on rate of shear can be seen. Signs of a definite hysteresis effect are evident.

Working on the hypothesis that the changes in dissipation factor and capacity observed at varying rates of shear are due chiefly, if not solely, to the conductance of the solution, then it became interesting to investigate the effect of eliminating, or at least greatly reducing, this conductance. The main step in this direction was to eliminate small traces of moisture in the materials used. The benzene was accordingly dried over sodium metal, the soap dried in vacuo and suitable precautions taken during the preparation of the gels. It was found that, despite the fact that exposure to the air occurred at several occasions and the cell was not designed to be airtight, a

TABLE I

Variation of Conductance and Capacitance with Rate of Shear  
for 5% Napalm at 1 Kc

G = rate of shear;  $\Delta C$ ,  $\Delta D$  observed capacitance and dissipation factor;  
 $C_{xp}$ ,  $1/R_{xp}$  calculated equivalent parallel  
capacitance and conductance

Time min.	G sec <sup>-1</sup>	$\Delta C$	$\Delta D$	$C_{xp}$ uuf.	$1/R_{xp}$	Time min.	G sec <sup>-1</sup>	$\Delta C$	$\Delta D$	$C_{xp}$ uuf.	$1/R_{xp}$
0	0	735.0	.4410	567.	2.259	43.0	1.48	703.8	.3968		2.102
0.5	0.128	731.1	.4349		2.240	44.0	1.48	703.6	.3968		2.102
2.5	0.128	725.0	.4321		2.229	46.0	1.48	704.0	.3968	557.	2.103
3.3	0.128	729.3	.4325		2.231	51.0	2.48	695.4	.3840		2.053
5.0	0.128	729.7	.4330		2.233	52.0	2.48	696.6	.3855		2.059
8.0	0.128	729.4	.4325		2.231	53.5	2.48	698.7	.3882		2.068
10.0	0.128	729.2	.4322	563.	2.230	55.0	2.48	701.4	.3930		2.084
11.5	0.272	723.6	.4242		2.203	55.5	2.48	701.4	.3950		2.094
12.5	0.272	724.0	.4250		2.205	59.0	2.48	703.0	.4010	555.	2.117
14.0	0.272	724.0	.4250		2.205	61.5	1.48	708.6	.4100		2.152
15.0	0.272	724.3	.4255		2.207	63.0	1.48	709.0	.4112		2.156
15.5	0.272	724.2	.4253		2.206	65.0	1.48	708.6	.4115		2.157
17.0	0.272	724.7	.4260		2.209	68.0	1.48	708.8	.4118		2.158
18.0	0.272	724.8	.4262		2.210	69.0	1.48	709.0	.4121	555.	2.160
19.0	0.272	724.6	.4262	561.	2.210	71.0	1.07	712.8	.4178		2.178
21.0	0.967	711.6	.4076		2.140	74.0	1.07	712.9	.4180		2.179
22.5	0.967	712.6	.4091		2.147	77.0	1.07	712.6	.4178		2.178
25.0	0.967	711.4	.4077		2.140	78.0	1.07	713.2	.4184	555.	2.181
26.0	0.967	710.4	.4062		2.133	81.0	0.256	730.2	.4430		2.270
27.0	0.967	711.1	.4074		2.139	82.0	0.256	731.4	.4445		2.275
29.0	0.967	711.0	.4072	560.	2.138	84.0	0.256	732.4	.4460		2.279
30.5	1.20	708.4	.4034		2.126	89.0	0.256	731.8	.4450	557.	2.276
31.0	1.20	708.6	.4028		2.129	90.5	0	736.0	.4520		2.296
32.0	1.20	707.8	.4028		2.123	91.5	0	737.6	.4530		2.301
33.0	1.20	708.0	.4030		2.124	93.0	0	737.8	.4540		2.305
35.0	1.20	707.8	.4027		2.123	95.0	0	737.6	.4534		2.303
37.0	1.20	707.8	.4030		2.124	96.0	0	737.4	.4529		2.300
39.0	1.20	707.3	.4027	558.	2.123	97.0	0	737.4	.4529		2.300
41.0	1.48	703.6	.3962		2.099	98.0	0	737.0	.4529	558.	2.298

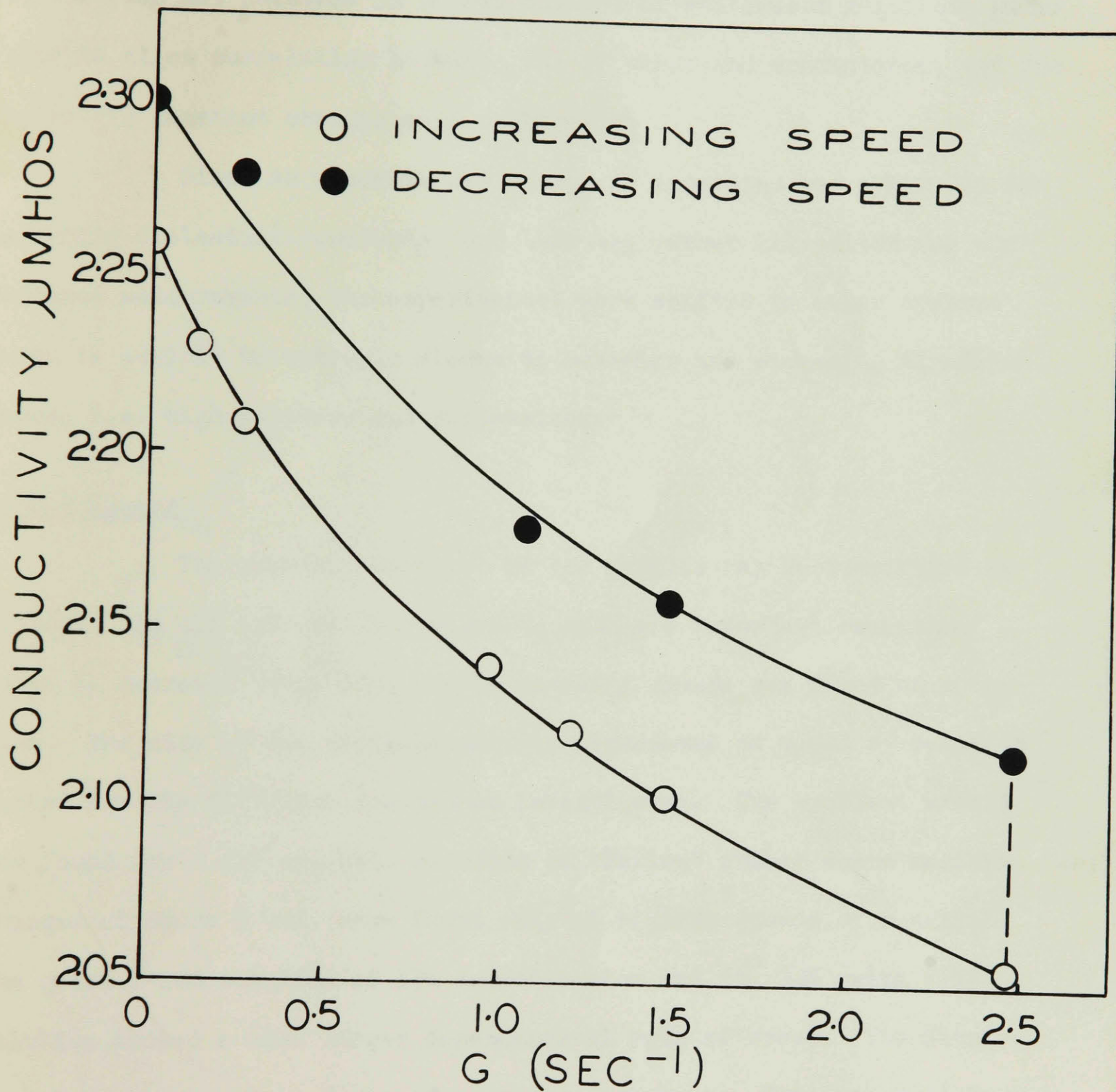


Figure 6: Effect of rate of shear on conductivity of 5% Napalm.

ten-fold drop in conductance was obtained. With such a relatively low value it was not possible to obtain changes of sufficient magnitude under shear to allow correlation between rate of shear and conductance, and the dielectric constant changes were negligible.

Since an accurate and elaborate apparatus was available for measuring dielectric constants, and this was rather ill-suited for conductance measurements, the experimental work shifted to other systems known to exhibit thixotropic viscosity behavior and streaming birefringence, i.e. high polymers and suspensions.

#### High Polymers

The general character of the results may be summarized as follows. In all systems investigated, with one important exception, a capacity decrease or no appreciable capacity change was found on rotation. The size of the decrease and its dependence on speed of rotation varied for the different substances investigated. The smallest effect was found for a 22% wt./vol. solution of "Parlon" rubber where maximum changes of about 2 uuf. were found only at highest speeds of rotation. The gelva V-200 solution of 13% concentration and the 30% gelva V-15 solution showed a much larger dependence on rate of shear. The data have been expressed in terms of percentage changes. This was done by expressing the capacity change as

$$\frac{\Delta \epsilon}{\epsilon_s - \epsilon_o} \times 100$$

where  $\Delta \epsilon$  is dielectric constant change under shear,  $\epsilon_s$  dielectric constant of solution,  $\epsilon_o$  dielectric constant of pure solvent. It can

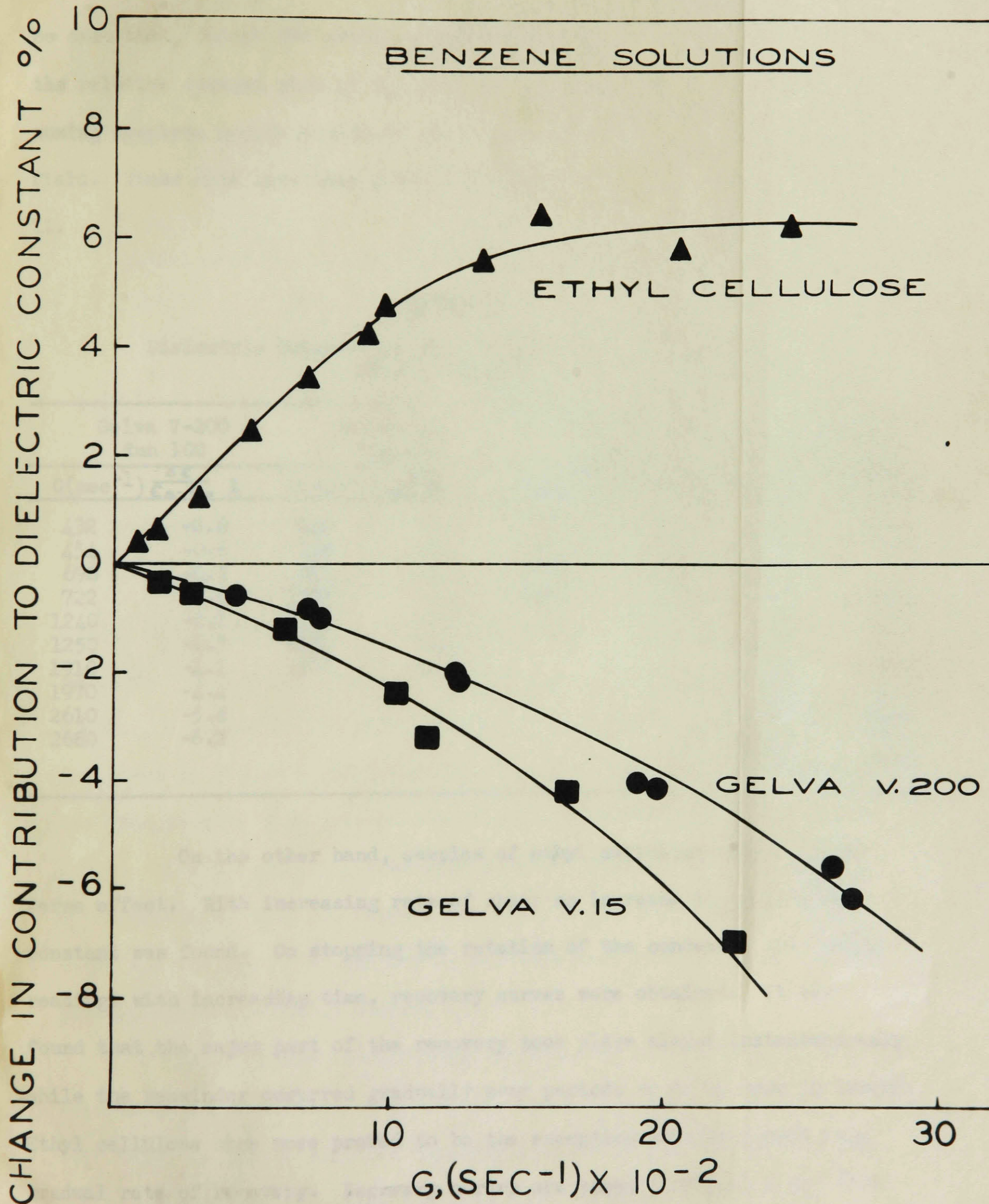


Figure 7: Change of dielectric constant with rate of shear.

be seen that, though the actual changes in dielectric constant were small, the relative changes were of the order of 5-10% of the total possible, assuming complete counteraction of the dipole orientations in the electric field. These data have been plotted in Figure 7 and are listed in Table II.

TABLE II

Dielectric Behavior of Polymer Samples at Various Rates of Shear

Gelva V-200 Run 100		Gelva V-15 Run 106		Parlon Run 112		Ethyl Cellulose Run 128	
$G(\text{sec}^{-1})$	$\frac{\Delta \epsilon}{\epsilon_s - \epsilon_0} \%$	$G(\text{sec}^{-1})$	$\frac{\Delta \epsilon}{\epsilon_s - \epsilon_0} \%$	$G(\text{sec}^{-1})$	$\frac{\Delta \epsilon}{\epsilon_s - \epsilon_0} \%$	$G(\text{sec}^{-1})$	$\frac{\Delta \epsilon}{\epsilon_s - \epsilon_0} \%$
432	-0.6	162	-0.3	88	-0.2	84	+0.3
454	-0.6	279	-0.5	565	-0.2	154	+0.6
696	-0.8	615	-1.2	1520	-2.5	295	+1.2
722	-1.0	1025	-2.4	2480	-4.0	478	+2.5
1240	-2.1	1125	-3.2			695	+3.4
1250	-2.3	1650	-4.1			910	+4.3
1910	-4.1	2260	-7.1			960	+4.8
1970	-4.4					1330	+5.6
2610	-5.8					1540	+6.5
2680	-6.2					2040	+5.8
						2440	+6.2

On the other hand, samples of ethyl cellulose showed an inverse effect. With increasing rate of shear an increase in dielectric constant was found. On stopping the rotation of the condenser and taking readings with increasing time, recovery curves were obtained. It was found that the major part of the recovery took place almost instantaneously while the remainder occurred gradually over periods up to an hour in length. Ethyl cellulose once more proved to be the exception showing a much more gradual rate of recovery. Recovery curves are shown in Figure 8 and Table III for these samples.

TABLE III

Recovery Curves of Polymer Samples

Gelva V-200 Run 101			Gelva V-15 Run 106			Ethyl Cellulose Run 128		
Time (min)	$\frac{\Delta \epsilon}{\epsilon_s - \epsilon_0}$	%	Time (min)	$\frac{\Delta \epsilon}{\epsilon_s - \epsilon_0}$	%	Time (min)	$\frac{\Delta \epsilon}{\epsilon_s - \epsilon_0}$	%
0	-5.3		0	-7.1		0	+6.1	
.25	-2.1		3.0	-3.0		1.0	+5.0	
1.0	-1.0		9.0	-2.5		3.0	+4.5	
8.0	-0.5		12.0	-2.2		6.0	+4.1	
11.0	-0.3		30.0	-1.1		12.0	+3.4	
			44.0	-0.7		20.0	+2.7	
			62.0	-0.5		41.0	+2.1	
			67.0	-0.5		50.0	+1.7	
				-0.4		62.0	+1.2	

With polymer samples in polar solvents it was harder to assess the contribution to dipole orientation of the dissolved polymer. The general character of the results remained the same, however, and data for polyvinyl formal and cellulose acetate butyrate are given in Figure 9 and Table IV. It can be seen that the percentage changes were much greater than for the polyvinyl acetate samples, but the relative capacity increases observed were of the same order of magnitude as with the former. It has not yet been possible to account for the shapes of the curves obtained when rate of shear (G) is plotted against capacity change.

In all cases except ethyl cellulose it was possible to get reasonable duplication of experimental results on subsequent runs. With ethyl cellulose positive capacity increments were always observed, but after the first few runs the data could only be duplicated at

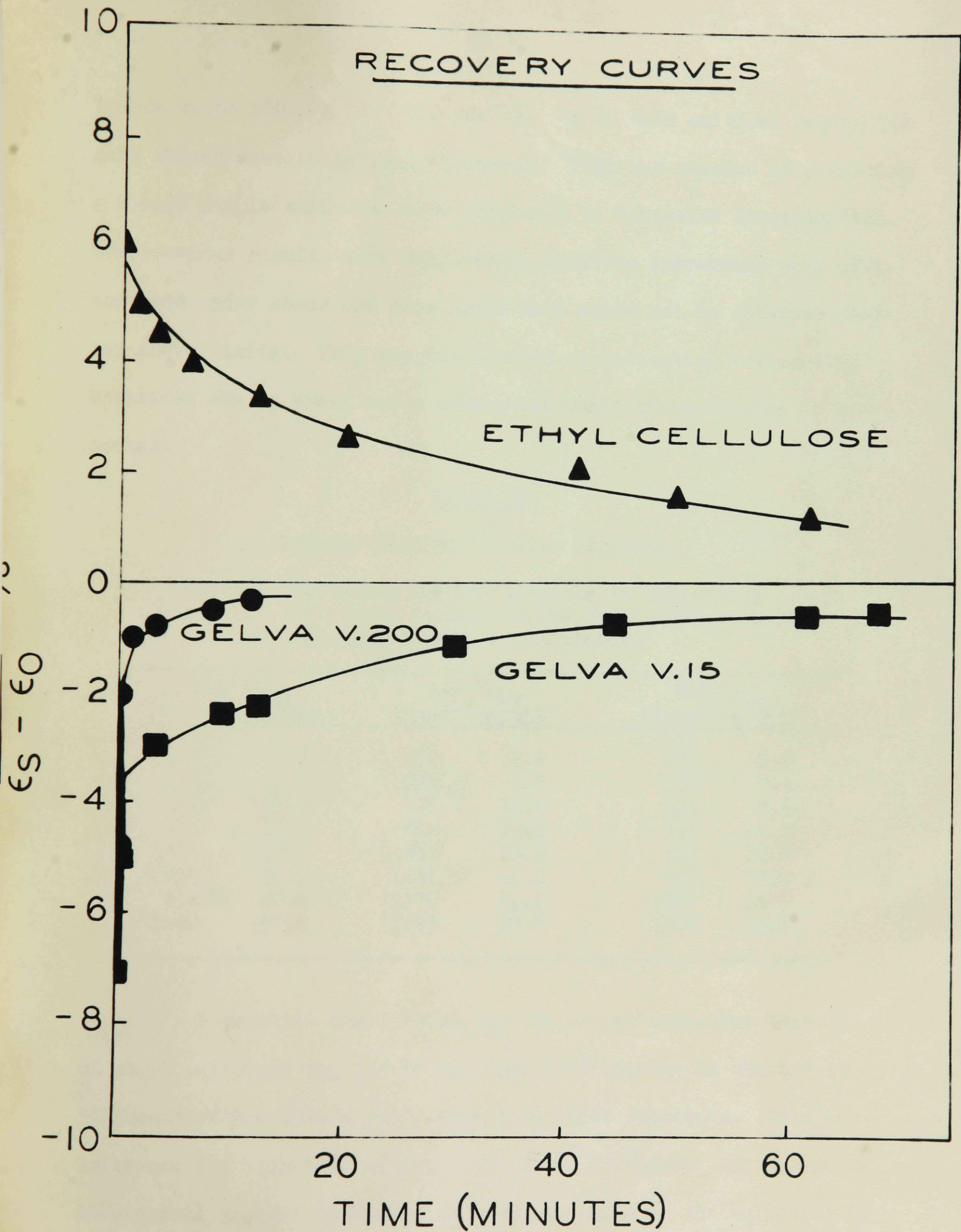


Figure 8: Recovery of dielectric constant with time.

speeds up to 600 RPM ( $G = 700 \text{ sec}^{-1}$ ). Up to this critical region the data showed reasonably good agreement. This was checked by preparing a second sample which was also subjected to intensive investigation. The previous results were duplicated, positive increments were again observed under shear and once again data could not be obtained over the above limits. This was interpreted as indicating a viscosity breakdown due to shear and a consequent onset of turbulence is suspected.

TABLE IV

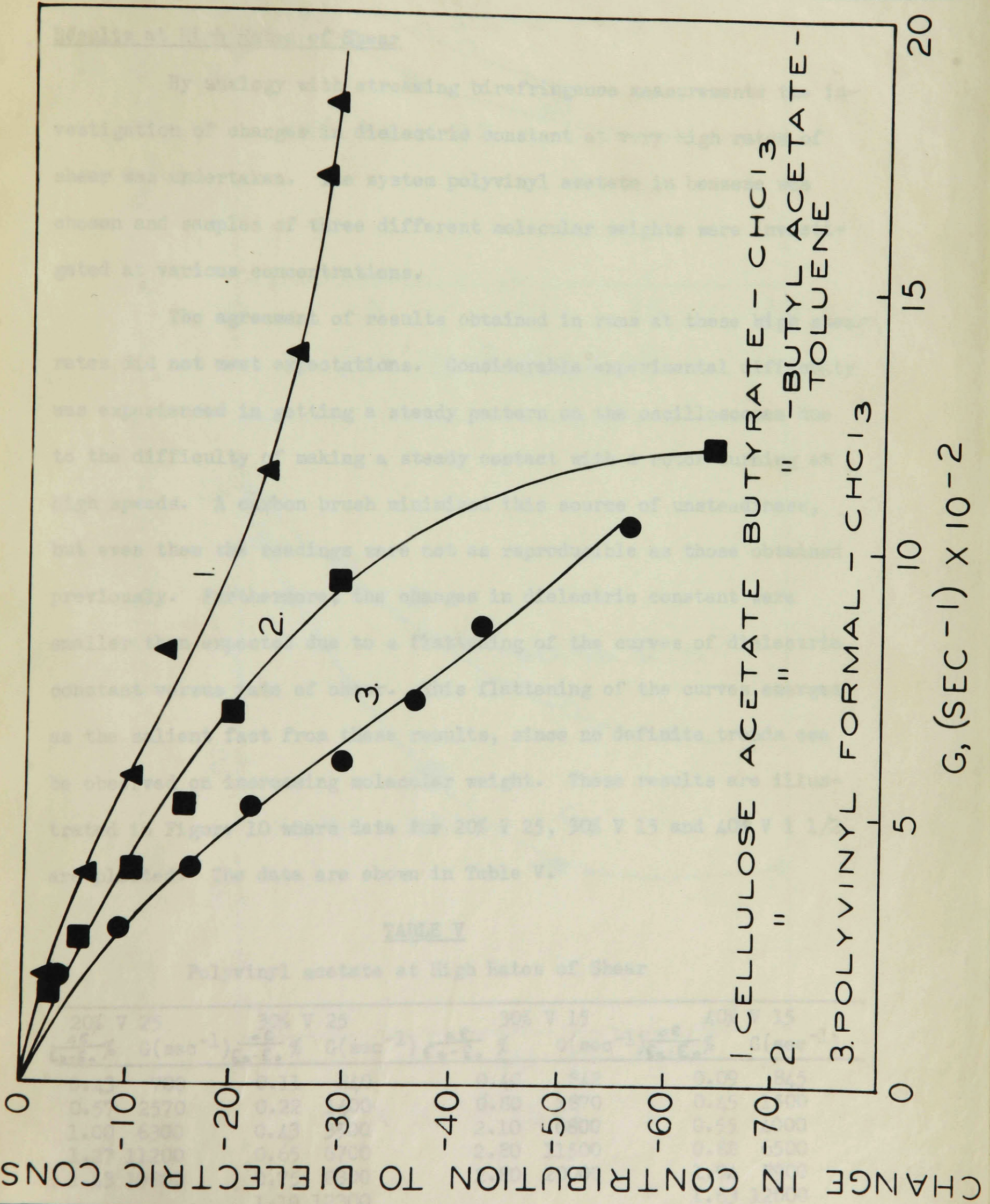
Polymer Samples in Polar Solvents

Run 141 Cellulose acetate butyrate in chloroform  
 146 Cellulose acetate in 1:2 butyl-acetate-toluene  
 165 Polyvinyl formal in chloroform

Run 141		Run 146		Run 165	
$G(\text{sec}^{-1})$	$\frac{\Delta\epsilon}{\epsilon_s - \epsilon_0} \%$	$G(\text{sec}^{-1})$	$\frac{\Delta\epsilon}{\epsilon_s - \epsilon_0} \%$	$G(\text{sec}^{-1})$	$\frac{\Delta\epsilon}{\epsilon_s - \epsilon_0} \%$
200	-3.6	200	2.2	172	2.6
286	-9.0	389	5.6	286	5.1
400	-15.3	572	10.0	400	9.8
515	-20.6	800	13.3	515	14.9
600	-29.3	858	13.3	685	18.9
715	-36.0	1141	22.2	943	28.9
858	-42.4	1370	24.4	1030	49.0
1060	-57.0	1695	27.8	1200	63.6

A possible explanation for the rather anomalous behavior of ethyl cellulose may lie in the fact that benzene is classed as a "diluent" rather than a good solvent for this substance. This may influence the stability of the solution to breakdown, and should on theoretical grounds influence the configuration of the molecules in solution (79).

Figure 9: Changes in dielectric constant of polymers in polar solvents.



Results at High Rates of Shear

By analogy with streaming birefringence measurements the investigation of changes in dielectric constant at very high rates of shear was undertaken. The system polyvinyl acetate in benzene was chosen and samples of three different molecular weights were investigated at various concentrations.

The agreement of results obtained in runs at these high shear rates did not meet expectations. Considerable experimental difficulty was experienced in getting a steady pattern on the oscilloscopes due to the difficulty of making a steady contact with a rotor turning at high speeds. A carbon brush minimized this source of unsteadiness, but even then the readings were not as reproducible as those obtained previously. Furthermore, the changes in dielectric constant were smaller than expected due to a flattening of the curves of dielectric constant versus rate of shear. This flattening of the curves emerges as the salient fact from these results, since no definite trends can be observed on increasing molecular weight. These results are illustrated in Figure 10 where data for 20% V 25, 30% V 15 and 40% V 1 1/2 are plotted. The data are shown in Table V.

TABLE V

Polyvinyl acetate at High Rates of Shear

20% V 25		30% V 25		30% V 15		40% V 15	
$\frac{\Delta\epsilon}{\epsilon_s - \epsilon_0} \%$	G(sec <sup>-1</sup> )	$\frac{\Delta\epsilon}{\epsilon_s - \epsilon_0} \%$	G(sec <sup>-1</sup> )	$\frac{\Delta\epsilon}{\epsilon_s - \epsilon_0} \%$	G(sec <sup>-1</sup> )	$\frac{\Delta\epsilon}{\epsilon_s - \epsilon_0} \%$	G(sec <sup>-1</sup> )
0.43	700	0.11	840	0.40	842	0.09	845
0.57	2570	0.22	1400	0.80	1870	0.45	1500
1.00	6300	0.43	3500	2.10	6800	0.55	4000
1.27	11200	0.65	6700	2.80	11500	0.82	6500
1.43	19800	0.75	8300	2.80	20000	1.04	8900
		1.19	12300			1.63	12000

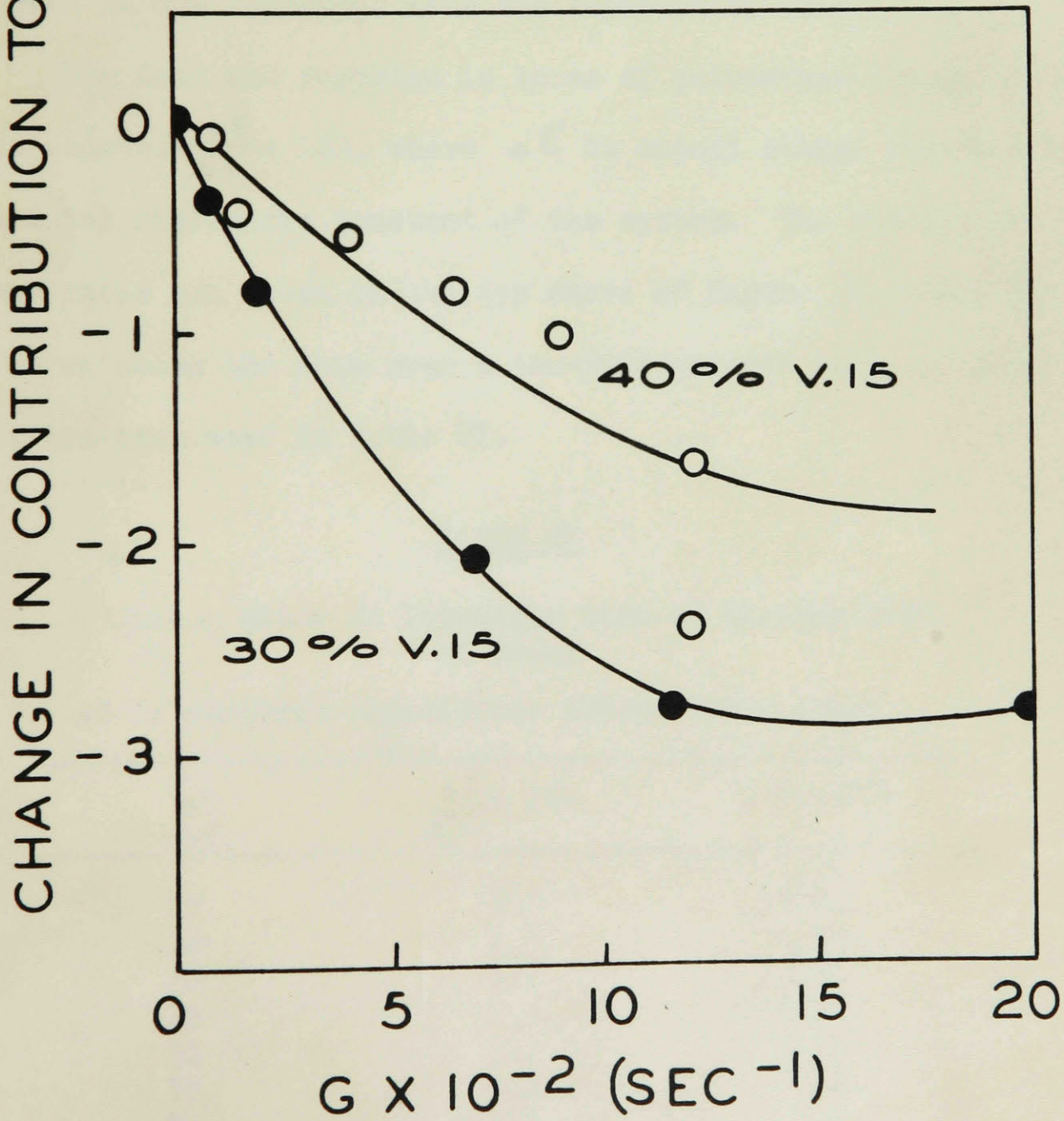
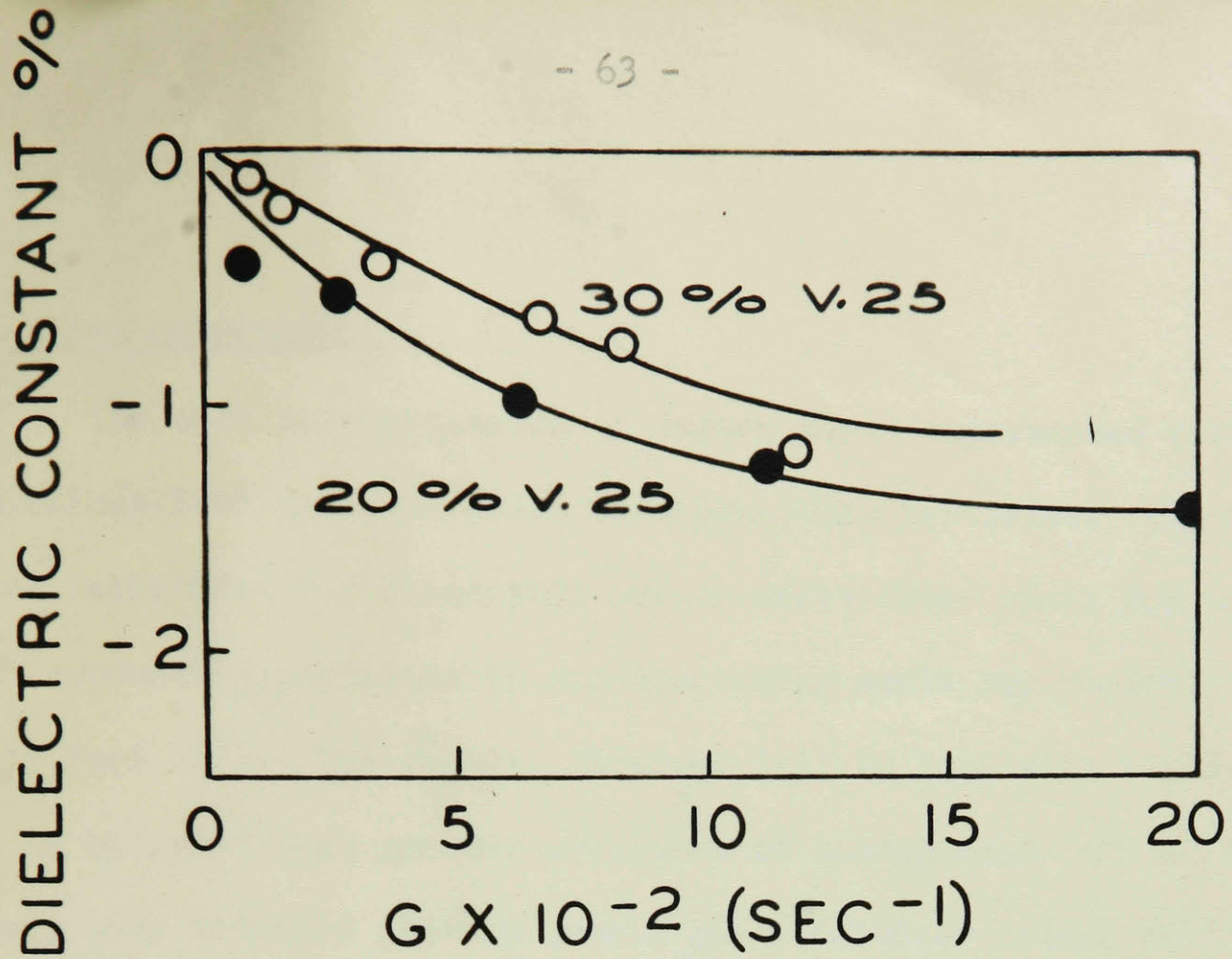


Figure 10: Changes in dielectric constant at high rates of shear.

Carbon Black Suspensions

The work on suspensions of carbon black represented a change in dimensions from macromolecules to microscopic particles. The theoretical background for dielectric measurements under shear for systems of conducting particles in non-conducting media has recently been given by Voet (47). The results obtained fall in line with his data, and it is believed that greater precision of measurement (and a resultingly more detailed picture over a range of shear rates) could be obtained on our apparatus than was reported by Voet.

The data are reported in terms of percentage change of dielectric constant  $\frac{\Delta \epsilon}{\epsilon_T} \times 100$ , where  $\Delta \epsilon$  is actual change observed and  $\epsilon_T$  is total dielectric constant of the system. The results for very low shear rates are shown in the top curve of Figure 11, while the bottom curve shows the data over a ten-fold greater range of shear. The data are tabulated in Table VI.

TABLE VI

Carbon Black in Petroleum Base at Varying Rates of Shear

$\Delta C$  is observed capacitance change under shear

$\Delta C$ uuf.	$\frac{\Delta \epsilon}{\epsilon_T} \times 100$	G (sec <sup>-1</sup> )
23	2.0	0.91
26	2.3	1.00
30	2.7	1.49
32	2.9	3.15
34	3.1	3.34
36	3.2	5.80
39	3.5	8.09
45	4.0	34.8
50	4.5	43.5
52	4.6	69.5
54	4.8	87.0

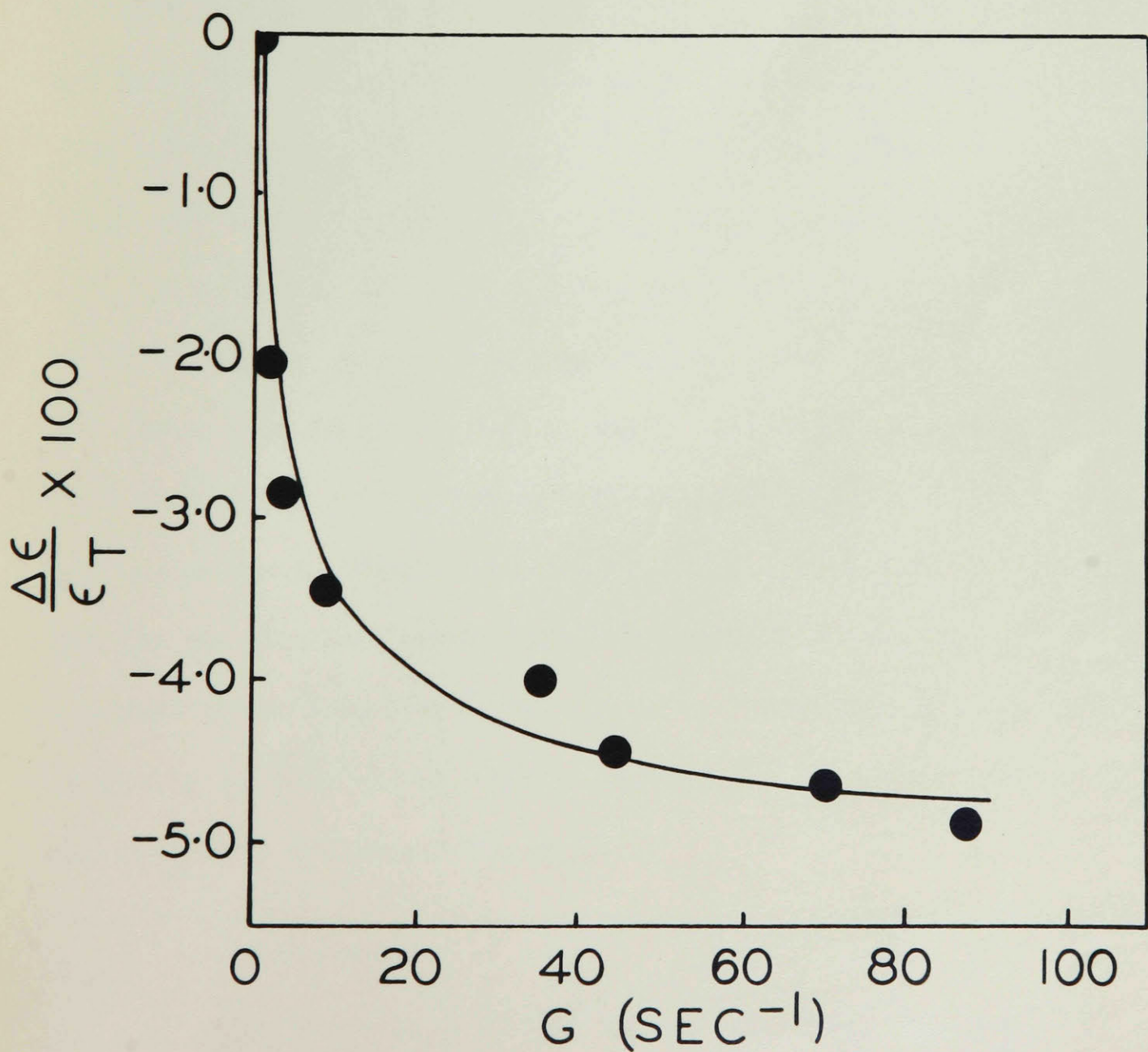
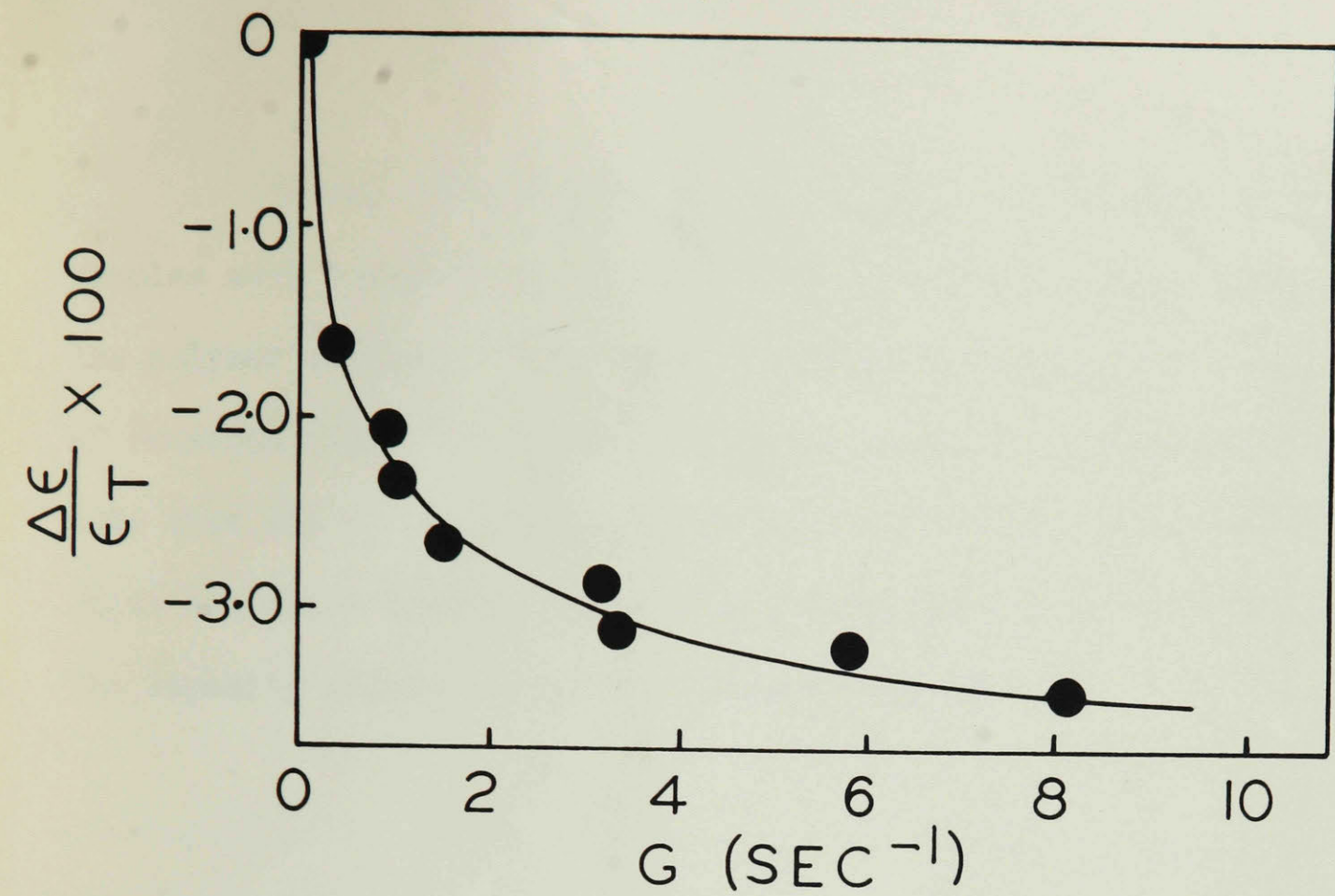


Figure 11: Change in dielectric constant of a carbon black suspension with rate of shear.

Actual changes 500% greater than those observed with polymer samples were obtained at one hundredth the rate of shear necessary for the polymer samples. Good reproducibility was obtained at low rates of rotation (less than 1/10 RPM) of the cell. It is interesting to note that the plots of percentage capacity change versus the rate of shear are approximately exponential; straight lines were obtained when the capacity change was plotted against  $\log G$ .

## DISCUSSION OF RESULTS

Dynamic measurements of dielectric constant are subject to a greater degree of uncertainty than static measurements. Since the measured changes in dielectric constant were relatively small, it is advisable to analyze the sources of error.

### (a) Eccentricity of the rotating condenser:

Eccentricity in the rotating condensers limited the precision of measurements. Mechanical defects of this type produced cyclic changes in pattern which were readily distinguished on the oscilloscope screen. The elliptical pattern was observed to close to a straight line at balance, and to open to a flattened ellipse at maximum unbalance. It was usually possible to obtain maximum and minimum readings, and the extent of the error introduced was readily determined. It is believed that only a precessional movement of the rotor was responsible for these variations in capacitance. A slight deviation of the rotor from a circular to a slightly ellipsoidal shape was not believed to influence the readings. The cells A and C were precisely machined, and the maximum deviation found was about 0.2 uuf. in air and about 0.5 uuf. when filled with the solution. Since this error could be partially eliminated by taking maximum and minimum readings, it did not seriously influence the data.

### (b) Escape of liquid from the region between the plates of the condenser:

The prevention of the escape of liquid from the gap between the cylinders of the condenser presented a serious experimental difficulty. A characteristic of the behavior of non-Newtonian liquids is

the presence of a component of force perpendicular to the direction of shear. This phenomenon is evident, for example, when such solutions are stirred, being manifested in a pronounced tendency to climb rotative shafts.

A considerable amount of preliminary experimental data were nullified by this effect, which resulted in introducing air bubbles into the system. The rotating condenser A, however, was designed specifically to prevent the occurrence of this error in measurements of the aluminum soaps. The provision of the top "dead space" and the tightly fitting bearings are believed to have eliminated this source of error. The cell, C, was also carefully designed to eliminate errors due to this cause.

(c) Heating effects:

When high rates of shear are applied to viscous systems considerable energy is dissipated as heat. Since the dielectric constant of polar substances is sensitive to temperature changes, this introduced a possible source of error.

The main precaution taken was the thermostating of the cell with a stream of rapidly circulating water. About 500 cc./minute were circulated through the cell.

The presence of heating effects was also checked experimentally in several ways. It was found that decreasing by half the flow of water circulated through the outer jacket did not change the capacitance readings at the highest rates of shear.

A further check was possible by the performance of the "cycling runs" previously described. In the great majority of experiments

very little change in capacitance with time was observed when the cell was allowed to rotate at a given rate of shear. If heating effects were of significant magnitude a steady decrease of capacitance with time would be expected. This was not found.

It should also be noted that the experimental data for ethyl cellulose, which showed an increase of dielectric constant with increasing rate of shear, refuted the presence of heating effects. No mechanism can be readily envisaged in which the dipole polarization would increase with increasing temperature.

(d) Turbulent flow:

The normal limits of turbulent flow were calculated as indicated previously. These limits were not exceeded, and on the basis of the behavior of normal liquids turbulent effects should not have been present.

Aluminum Soaps

Systems of aluminum stearate and Napalm were subjected to a rather intensive investigation. The data presented in Figure 5 represented quite typical behavior of these systems. Although only data for Napalm were recorded here, the results obtained with aluminum stearate were of the same nature.

It was seen that the conductance of the system decreased with increasing rate of shear, while no significant changes in capacitance were found. It was extremely difficult to assess the magnitude of any capacitance change with these systems. Since the aluminum soaps were relatively non-polar, only a small increase in dielectric constant of

the gel over that of the solvent was found. This shortcoming was magnified by the fact that only relatively low concentrations of soap could be added. Gels prepared with more than 6% soap by weight possessed properties approximating those of a solid, and were too viscous to handle.

It was important to ascertain whether this conductance of the aluminum soap gels arose from dielectric loss in a dispersion region, or whether simple ionic conductance was involved. Static measurements were carried out over a wide frequency range in order to clarify this question.

A region of dielectric dispersion was not found at audio frequencies. Instead the data showed that the measured conductance varied inversely with the frequency. This definitely pointed to d.c. conductance (48). As a further check measurements were made with a d.c. ohmmeter, and a conductance of approximately 1 megohm was found.

These measurements have not been reported in detail in the present work. Mr. G. B. Gunn, working in collaboration with the author, has thoroughly investigated the dielectric behavior of aluminum soaps at both audio and radio frequencies. These results will be reported separately by Mr. Gunn.

It should be noted that the above explanation assumes a similarity between the measured macro viscosity and the internal friction experienced by a moving particle on the micro scale. If the concept of non-Newtonian behavior due to orientation in a shear field were applicable here, the viscosity on the micro scale would be essentially that of the solvent (7). Since there is evidence that gels of the

aluminum soaps possess a certain degree of structure due to Van der Waal's attraction, the orientation theory of non-Newtonian viscosity is not strictly applicable.

It therefore seems probable that the conductance of aluminum stearate and Napalm gels is related to the viscosity, although a direct relationship cannot be assumed.

### High Polymers

The experimental data on high polymers showed that changes of dielectric constant occurred in a velocity gradient. These were approximately 5-10% of the calculated dipole contribution to the dielectric constant. With one exception, ethyl cellulose, in benzene, a decrease in dielectric constant was always found.

If we assume a mechanism of particle orientation in a velocity gradient, then it can be concluded that these changes are due to the counteraction of dipole orientation in an electric field by orientation in a shear field. We would thus infer that the axis of the dipole lies along the major axis of a rod-like particle.

On this basis we would conclude that in ethyl cellulose the axes of the dipoles are perpendicular to the major axis of the particle. With such a configuration one would expect an enhancement of the orientation in an electric field through orientation under shear. On this basis the observed phenomena could be explained.

Some features of the experimental results, however, throw doubts on the validity of the above approach. If the changes in dielectric constant were due solely to orientation in a velocity gradient

one could reasonably expect an immediate recovery of the dielectric constant to its initial value on ceasing rotation.

It can be seen from Figure 8 that the major part of the recovery took place instantaneously in the Gelva samples. A time dependence of the recovery was evident, however, even for these. For ethyl cellulose, the return of the dielectric constant to its original value was relatively gradual. In this case, particularly, it is difficult to explain the deviation from the expected instantaneous recovery.

If one assumes a great degree of interaction between the polymer molecules in concentrated solution, then the considerations of photo-elastic behavior may be applicable.

For an amorphous linear polymer the mechanical effect of a stress is shown in a series of retarded elastic effects besides the instantaneous elastic response. The total elastic strain is thus a function of time as well as stress (79).

The instantaneous response can be regarded as resulting from an elastic strain. By analogy with the photo-elastic phenomena this corresponds to a general stretching, with neighboring atoms being pulled apart slightly. This introduces a degree of anisotropy which would be evident as a double refraction corresponding to a change of refractive index in two directions perpendicular to one another. Similarly it can be regarded as giving rise to two dielectric constants perpendicular to one another, of slightly differing magnitudes.

The retarded photo-elastic response is regarded as resulting from a time dependent segmental diffusion of the polymer chains. An

uncurling and orientation of the polymer chains gives rise to further configurational strains and leads to additional anisotropy. The most significant aspect of such configurational strains is believed to be due to orientation of relatively short segments of molecular chains.

We thus see that from either the point of view of streaming birefringence or photo-elastic behavior we may regard the changes in dielectric constant under shear as due to partial orientation of polymeric chains. Although the phenomenon of streaming birefringence lends itself to simpler theoretical treatment, the photo-elastic effect seems to offer a basis for a more complete explanation of the experimental data.

Ostwald's concept of "strukturviskositat" (80)(81) appears to support the above views. As an example the shearing of a dispersion of elastically deformable particles will produce a change in particle shape which will make progressively easier flow, and hence lower viscosity. The particles need not be elastic. They may be polar and tend, when the system is at rest, to orientate themselves into some type of ordered structure which has to be destroyed before flow can take place (5). When the stress is removed the particles recover their original orientation. If this recovery is relatively slow we may observe thixotropic behavior.

#### Carbon Black Suspensions

With suspensions of Carbon Black the changes of dielectric constant under shear were very pronounced. The results confirmed Voet's work (47) on such systems. The experiments were carried out

over a wider range of shear than those reported by Voet, who merely reported the difference between the static dielectric constant and that at a high rate of shear. The experimental data obtained in the present work show an apparent logarithmic correlation between capacitance change and rate of shear.

The interpretation of the results is probably best approached in the manner suggested by Voet. In essence the latter's empirical "agglomeration factor" can be regarded as derived from Ostwald's conception of structural viscosity due to the formation of molecular aggregates.

PART II

Dielectric Dispersion Studies of Polyvinyl  
Acetate in Toluene

## PART II

### EXPERIMENTAL

#### Apparatus

Accurate measurements of capacitance and conductance at radio frequencies entail the use of carefully designed and well shielded apparatus. Unless such equipment is used the measurements are very liable to be distorted by changes in the measuring circuits. Very recently a new type of impedance measuring circuit has been developed and made available commercially. The General Radio Company's Type 821-A Twin-T Impedance Measuring Circuit is particularly well suited for measurements of dielectric dispersion, and several workers in this field have recently adopted it (48)(82).

The instrument can be used for impedance measurements at radio frequencies from .46 Mc. to 40 Mc. The accuracy of measurement at high frequencies is achieved by eliminating some of the residual impedances which normally limit the performance of bridge circuits. Errors inherent in variable resistors at high frequencies are avoided by measuring susceptance in terms of an especially designed variable air capacitor and a fixed resistor. When suitable corrections are applied capacitance measurements can be made with an accuracy of .1% or .5 uuf., whichever is the larger. Conductance measurements can be made with an accuracy of  $\pm 2\%$  of actual dial reading + .1% of full scale. The maximum capacitance that can be measured is 1000 uuf., while the conductance

range is proportional to frequency, being 100 umho at 1 Mc.

The Twin-T is used for measuring unknown impedances in terms of their parallel admittance components, namely susceptance B, and conductance G. The susceptance is obtained from capacitance increments read from a dial directly calibrated in capacitance by means of the relation  $B = \omega C$ . The conductance is obtained from a dial directly calibrated in conductance (in umho).

The circuit consists of two T networks so that they furnish parallel transmission paths, a-b-c- and a-d-c from a high frequency generator to a null detector as shown in Figure 12.

Zero energy transfer from the generator to the detector occurs when the transfer impedances of the two T networks are made equal and opposite and a null balance is obtained. The circuit conditions for which this occurs are expressed by

$$G_L - R\omega^2 C^1 C^{11} \left( 1 + \frac{C_G}{C^{III}} \right) = 0 \quad 49$$

$$C_B + C^1 C^{11} \left( \frac{1}{C^I} + \frac{1}{C^{II}} + \frac{1}{C^{III}} \right) - \frac{1}{\omega^2 L} = 0 \quad 50$$

From the initial capacitance values,  $C_{G_1}$  and  $C_{B_1}$ , and the final capacitance values,  $C_{G_2}$  and  $C_{B_2}$ , the unknown admittance components are found as follows

$$G_X = \frac{R\omega^2 C^1 C^{11}}{C^{III}} (C_{G_2} - C_{G_1}) \quad 51$$

$$B_X = \omega (C_{B_1} - C_{B_2}) \quad 52$$

Measurements of admittances are made by establishing an initial balance without the unknown and a second balance with the unknown in the circuit. The effective parallel capacitance  $C_{xp}$  of the unknown

is given by

$$C_{xp} = C_{B_1} - C_{B_2} \quad 53$$

The unknown conductance  $G_x$  is determined from the final setting of the conductance dial; the initial setting is always zero. The measurements are made direct reading at frequencies of 1, 3, 10 and 30 Mc. At other frequencies the dial reading must be multiplied by the square of the ratio of frequency used to that of the nominal switch position frequency.

A high frequency generator and method of null detection were needed in conjunction with the Twin-T circuit. A Clough-Brengle oscillator, variable from 0.1 to 40 Mc. was used as a source of high frequency signal. The signal strength from this unit was increased from .1 volt to 10 volts by a separate amplifier, and was then fed to the Twin-T network. A Hallicrafter S-140 radio receiver with internal beat oscillator was employed as a highly selective null detector. All units were fed from a constant voltage transformer for increased stability.

Thorough shielding of all units was essential. Coaxial cable, with the outer sheath grounded, was used to connect all units. The ends of the cable were fitted with special cable jacks for direct shielded connections to all parts of the apparatus. The Twin-T and auxiliary equipment were placed on a copper sheet, and all leads to ground were soldered to it. A heavy copper wire was led from the copper sheet to a steel building girder several feet away. This latter precaution was not essential as it was found that grounding was already complete.

The functions of the various units of the apparatus are easily understood. A high frequency carrier signal was generated by the oscillator. This signal could be modulated with a 400-cycle note generated by the same unit. After amplification the combined signal entered the Twin-T network. In the absence of balance conditions in this network a residual signal entered the radio receiver. When the receiver was tuned to the frequency of the carrier signal a 400-cycle hum could be heard in the loudspeaker, or through earphones which could be plugged into jacks in the receiver. The principle of operation was therefore analogous to the functioning of a radio receiver. On balancing the Twin-T network, the signal no longer entered the detector, and no sound could be heard.

Although the above procedure was used for rough balancing of the network, a more accurate balance could be obtained by a slight variation of this. In practice, an unmodulated signal was fed from the oscillator to the Twin-T network. When the network was unbalanced part of the carrier signal was fed into the receiver. An internal beat oscillator in the receiver was employed to produce beats with the carrier signal. This heterodyne signal was amplified and could be heard in the loudspeaker. The automatic volume control was turned off in order to secure a more precise balance. It was found that balance conditions could be established more readily when the signal strength was low. Best results could be achieved by progressively decreasing the attenuation on the oscillator volume control. The receiver r.f. sensitivity control was turned to its highest sensitivity and not varied; the audio volume control was adjusted to the highest sensiti-

vity obtainable without undue amplification of extraneous noise.

A drift in the values of the initial setting of the precision susceptance condenser occurred during the initial period after the oscillator was switched on. The magnitude of this drift decreased with time, and after about four hours the initial readings of the susceptance condenser would remain constant within 0.2 uuf. over a period of several hours. Consequently all units except the detector were allowed to "warm up" four hours before a run was performed. The initial readings ( $C_1$ ) of the precision condenser were checked, nevertheless, during the course of a run; significant variations were rare.

The author is indebted to Mr. G. B. Gunn, who performed much of the initial work of assembling the apparatus, and whose valuable advice was of great assistance in the present work.

### Dielectric Cell

A dielectric cell suitable for measurements over a wide temperature range was required. A comparatively simple model was made by the author and proved to be satisfactory. This condenser is shown in Figure 13. It consisted of two coaxial brass cylinders E, F held in position by accurately machined bakelite caps C, G. The bottom cap G fitted tightly into the outer cylinder, and was sealed with sodium silicate to be liquid tight. The inner cylinder was centered by sliding it along a bakelite projection in the bottom cap until a press fit was obtained at the top. The centering system employed had the advantage that no bakelite was present in the region between the plates. Thus dielectric losses in the bakelite could have little effect on

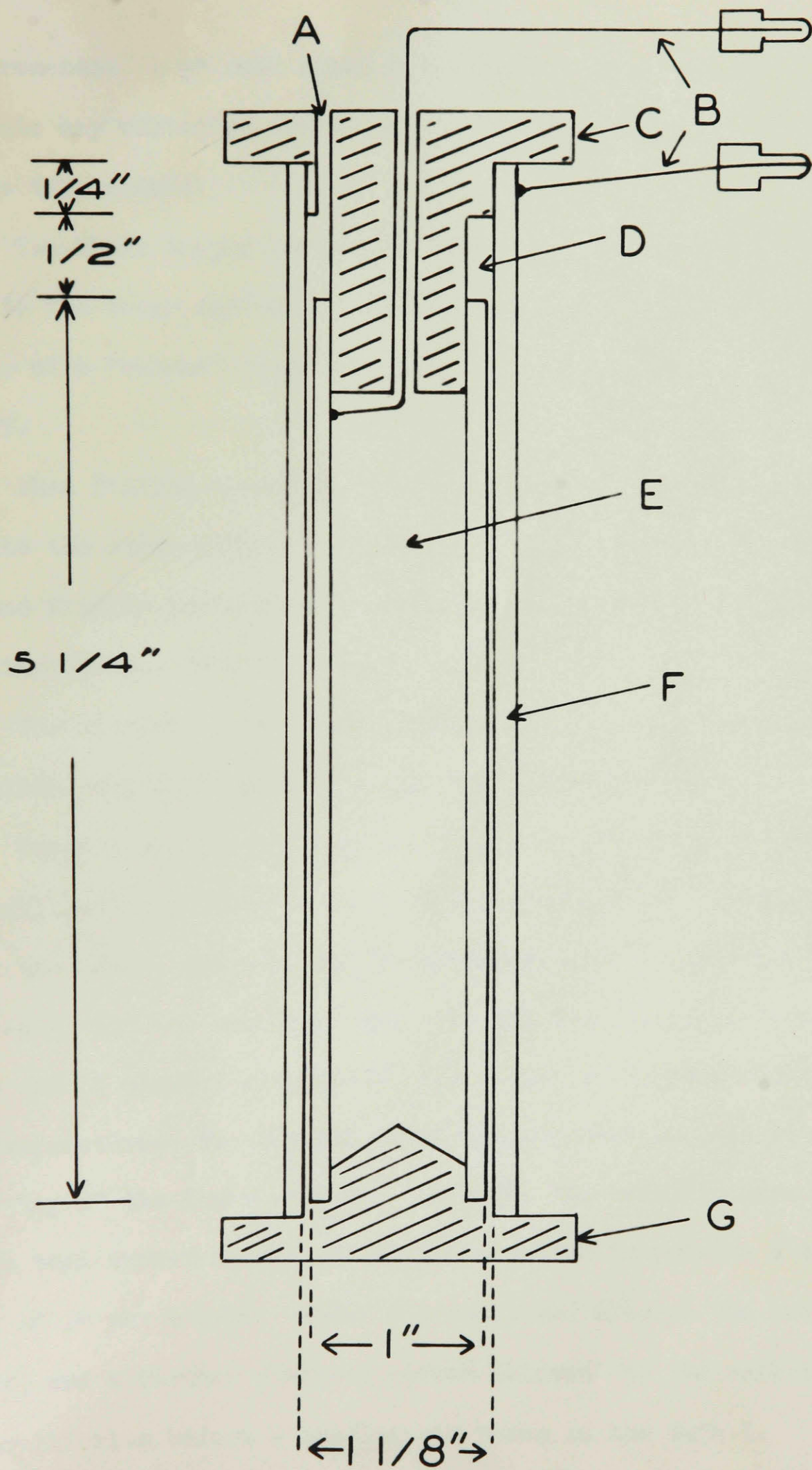


Figure 13: Condenser for R.F. measurements.

the measurements. A  $\frac{1}{2}$ " dead space D was left above the inner cylinder to eliminate any variation due to incomplete filling or volume shrinkage at low temperature.

Two short copper leads of #18 B.S.S. gauge wire were soldered directly to the inner and outer cylinders, and were fitted at their other ends with "banana" plugs B, which could be fitted into jacks in the Twin-T.

When filling the condenser a suitable quantity of liquid was poured into the outer cylinder. The inner cylinder was then slowly lowered and finally pressed into position. This resulted in excess liquid being ejected from the vent A.

The diameter of the inner cylinder was 1.0" and that of the outer cylinder was  $1-1/8$ ", and the gap was therefore  $1/16$ ".

Temperature control was maintained in a Dewar flask provided with a small heater controlled by a Variac transformer. Toluene was placed in the Dewar, and dry ice slowly added until a temperature of approximately  $-80^{\circ}$  was reached. The cell was then slowly lowered into the Dewar and 15 minutes allowed for it to come to thermal equilibrium at this temperature. The toluene level was adjusted so that it was above the top of the inner cylinder but below the bakelite cap. The heater was then turned on and the Variac adjusted to provide a temperature rise of  $2^{\circ}$  per minute. After 5 minutes had elapsed the heater was turned off, and a further 5-minute period allowed for the cell to reach thermal equilibrium before a reading was taken on the Twin-T.

Tests showed that there was no appreciable drift in readings after this period had elapsed. Since the spacing between the cylinders

in the cell was small, it is not surprising that the liquid in this region came to thermal equilibrium very quickly. Originally the Dewar was provided with an electrically driven stirrer. This was found to be unnecessary as the evolution of  $\text{CO}_2$  alone provided thorough agitation of the toluene.

Temperatures were read on a toluene thermometer immersed in the toluene. The thermometer calibration was checked and standardized at the freezing points of water and mercury, and was found to be correct to  $0.1^\circ$ .

The upper frequency limit of accurate operation of radio-frequency impedance measuring equipment is nearly always determined by residual parameters in the wiring and in the impedance elements, which are not taken into account in the ordinary theory of operation. While these have been made extremely small in the Twin-T network, they are still large enough to affect the performance at the higher frequencies, and limit the maximum usable frequency to approximately 30 Mc.

Only the residual parameters in the precision air condenser  $C_B$ , which is in parallel with the unknown impedance, need be considered. The residual effects of all other circuit elements on balance conditions have been made negligible. The residual parameters in the condenser  $C_B$  for which corrections may be required are:

(a) Inductance  $L'$ , between the condenser and the ungrounded terminal;

(b) Inductance  $L''$ , between the condenser and the point in the Twin-T circuit to which it is connected;

(c) Inductance  $L_c$ , in the metal structure of the condenser itself;

(d) Resistance  $R_c$  in the metal structure of the condenser.

Figure 14 is an equivalent circuit showing the residual parameters listed and their relative locations. They are all relatively constant, independent of the setting of the susceptance condenser, and had the following values at a frequency of 30 Mc.:

$$L' = 6.8 \times 10^{-9} \text{ h.}$$

$$L'' = 3.15 \times 10^{-9} \text{ h.}$$

$$L_c = 6.1 \times 10^{-9} \text{ h.}$$

$$R_c = .026 \text{ ohms.}$$

54

The inductances are independent of the frequency; the resistance varies directly as the square root of the frequency.

The inductance  $L'$  is directly in series with the unknown admittance. To correct for its effect it is therefore necessary to subtract its inductive reactance from the measured reactance.

The inductance  $L''$  has no appreciable effect on the susceptance balance, but causes the apparent conductance to differ from its true value. To a first approximation the true value of the unknown conductance  $G_x$  is found from the measured value of unknown conductance  $G''$  and the initial condenser capacitance  $C_1$ , by:

$$G_x = G'' (1 - \omega^2 L'' C_1)^2$$

55

The inductance,  $L_c$ , causes the high frequency effective capacitance of the precision susceptance condenser,  $C$ , to rise above the low frequency calibration. The apparent susceptance, measured

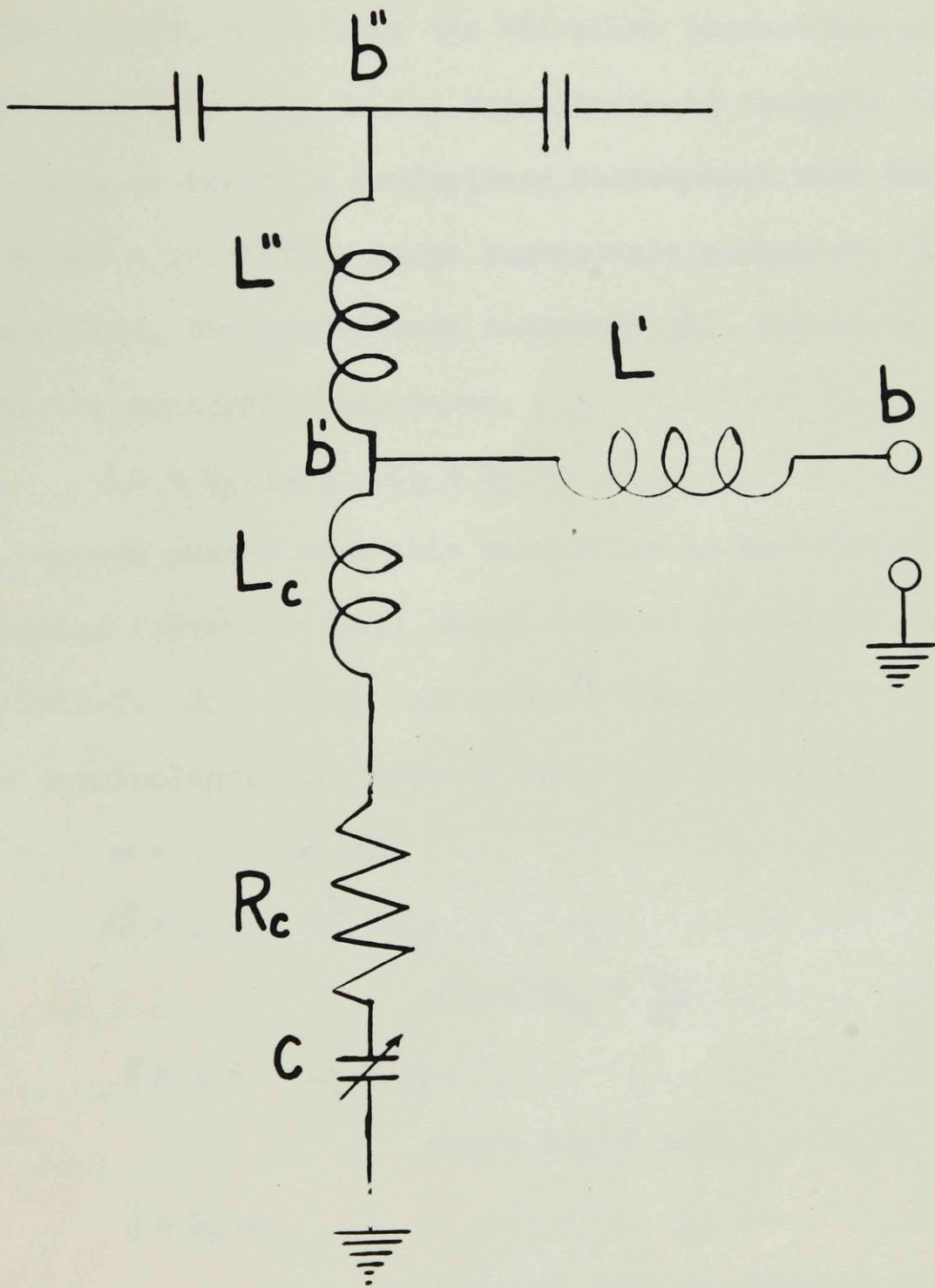


Figure 14: Equivalent circuit of precision condenser in Twin-T.

by this condenser, therefore differs from the true value. To a first approximation the true value of the unknown susceptance,  $B_x$ , is

$$B_x = \frac{\omega(C_1 - C_2)}{1 - \omega^2 L_c (C_1 + C_2)} \quad \underline{56}$$

The resistance,  $R_c$ , causes the effective conductance of the susceptance condenser  $C$  to vary as the capacitance is changed. It therefore introduces an error in conductance measurement when the unknown admittance has a relatively large susceptance component. To correct for its effect, the conductance component,  $\delta G$ , should be added algebraically to the measured conductance.

$$\delta G = R_c \omega B_x (C_1 + C_2) \quad \underline{57}$$

For capacitive unknown susceptance this correction is positive.

Correction factors for all these residual parameters were supplied with the Twin-T. Correction factors  $\alpha, \beta, \gamma$  were defined in order to simplify the terminology. In terms of the above discussion

$$\alpha = 1 - \omega^2 L_c C \quad \underline{58}$$

$$\beta = 1 - \omega^2 L' C_{e1} \quad \underline{59}$$

$$\text{where } C_{e1} = \frac{C_1}{\alpha} \quad \underline{60}$$

$$\gamma = 1 + \omega L' B'_x \quad \underline{61}$$

$$\text{where } B'_x = \omega(C_{e1} - C_{e2}) \quad \underline{62}$$

$$\delta = R_c \omega \quad \underline{63}$$

The unknown susceptance  $B_x$  and conductance  $G_x$  can be obtained from these as follows:

$$B_x = \frac{\omega \left( \frac{C_1}{\alpha_1} - \frac{C_2}{\alpha_2} \right)}{\gamma} = \frac{\omega(C_{e1} - C_{e2})}{\gamma} = \frac{B'_x}{\gamma} \quad \underline{64}$$

$$G_x = \frac{G'' \beta + \delta B'_x (C_{e1} + C_{e2})}{\gamma^2} \quad \underline{65}$$

Although the above corrections could be applied in a systematic form by employing data sheets and correction graphs supplied with the instrument, the arithmetical computations were found to be laborious and time consuming. Considerable simplification was possible, however, by a strict standardization of procedure and the formulation of accurate correction charts covering the range of frequencies and impedances actually encountered in the measurement of dielectric dispersion.

The first problem was to evaluate the correction for lead inductance. Although the leads were short (3"), they could introduce errors up to 100% unless corrections were applied. The apparent capacity  $C'$  measured with leads of inductance  $L_1$  is related to the true capacity  $C_{xp}$  by the law:

$$C' = \frac{C_{xp}}{1 - \omega^2 L_1 C_{xp}} \quad \underline{66}$$

This can be rewritten as:

$$\frac{1}{C'} = \frac{1}{C_{xp}} - \omega^2 L_1 \quad \underline{67}$$

Hence if  $\frac{1}{C'}$  is plotted vs.  $\omega^2$  the slope of the straight line yields  $L_1$  and the intercept is  $\frac{1}{C_{xp}}$ . This was done and good straight lines were obtained yielding a value of  $1.12 \times 10^{-7}h$  for  $L_1$  on the basis of two independent determinations for the empty cell and for the cell filled with benzene. This value was also checked by an algebraic method using the low frequency value of  $C'$  where the effect of lead inductance was negligible.

To this value of lead inductance the internal lead inductance of the precision condenser ( $6.9 \times 10^{-9}h$ ) was added, and new values of the correction factor  $\gamma$  were obtained. These data are

shown in Figure 15 for frequencies of 10, 20, 30 Mc. and were also plotted on a larger scale for 1, 3, 10 Mc. The significance of  $\gamma$  is  $\frac{C'}{\gamma} = C_{xp}$  where  $C'$  is apparent capacity uncorrected for effect of leads and  $C_{xp}$  is true capacity.

The original measurements obtained when the capacitance of the cell was measured in air and benzene are shown in Table VII. The actual capacitance change measured is shown in the column  $C_1 - C_2$ . The values  $C_{e1}$ ,  $C_{e2}$  represent the values of the capacitance corrected for all residual parameters except the lead inductance correction  $\gamma$ . The final column  $C_{xp}$  shows corrected capacitance values obtained with the application of the correction for lead inductance. Comparison of the data in this column with the values  $C_{e1} - C_{e2}$  shows the importance of the lead correction.

TABLE VII

Measured Capacitance of Condenser in Air and Benzene

f Mc	$\omega$ Mc	$C_1 - C_2$ uuf	$C_{e1} - C_{e2}$ uuf	$B'x$ umhos	$\gamma$	$C_{xp}$ uuf
<u>Air Capacitance</u>						
.55	3.455	83.2	83.2	288.9	1.000	83.2
1	6.282	83.9	83.9	526.0	1.000	83.9
3	18.55	83.7	83.1	1500	1.001	83.6
10	62.82	84.6	86.4	5430	1.039	83.5
20	125.6	90.9	97.7	12270	1.173	83.2
30	188.5	109.3	125.9	23740	1.357	80.8
<u>Benzene Capacitance</u>						
.55	3.455	152.0	152.0	525	1.000	152.0
1	6.282	152.6	152.6	960	1.000	152.6
3	18.55	152.6	152.6	2880	1.002	152.3
10	62.82	160.7	165.0	10370	1.078	153.0
20	125.6	215.8	229.1	28770	1.430	159.5

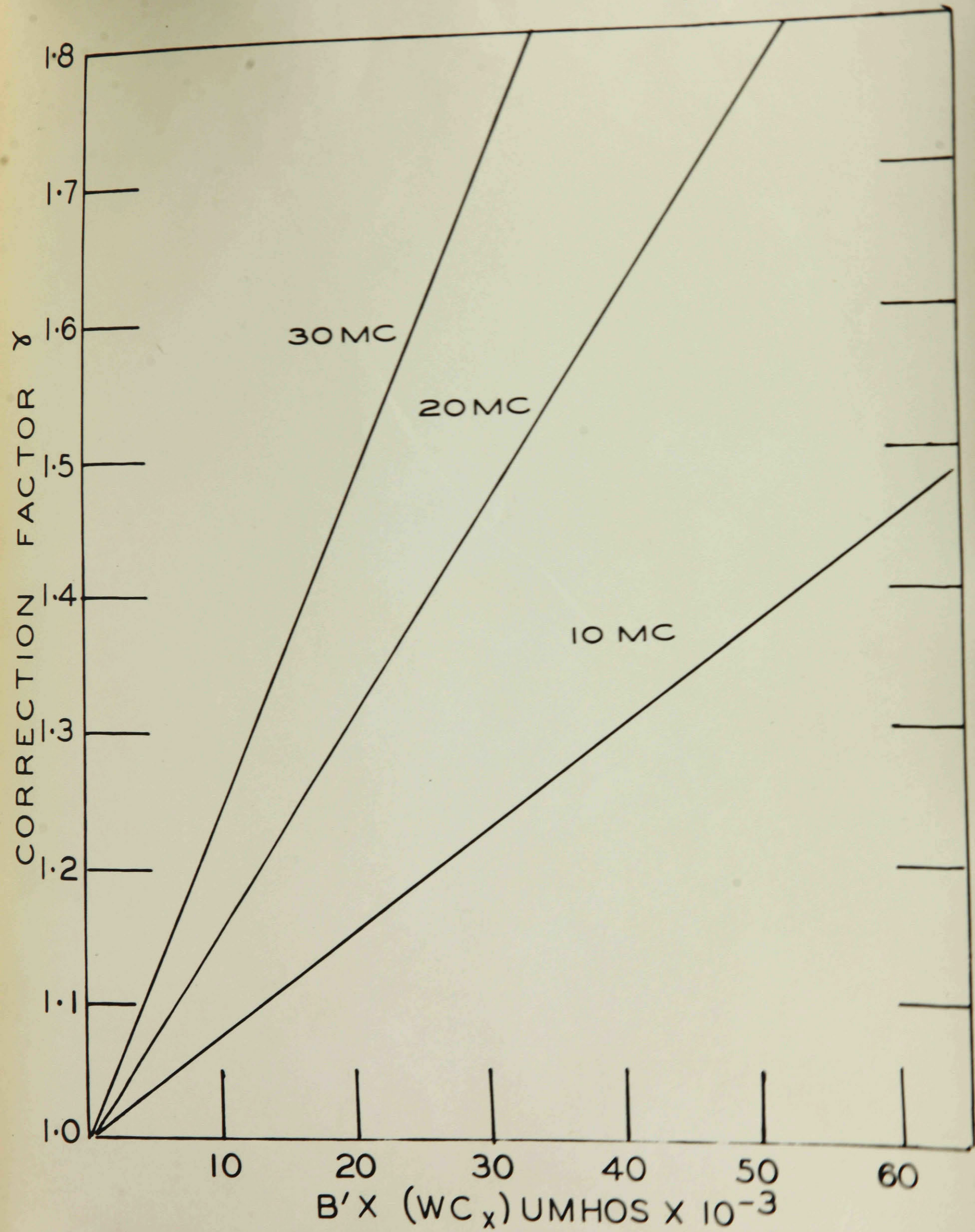


Figure 15: Correction graph for lead inductance.

The data for formulation of correction charts of the type shown in Fig.15 are shown in Table VIII.

TABLE VIII  
Correction Factor  $\gamma$  for Lead Inductance

f Mc	$\omega$ Mc	$C_{e1} - C_{e2}$ uuf	B'x umhos	$\gamma$
10	62.82	100	6282	1.0470
10	62.82	200	12564	1.0940
10	62.82	400	25128	1.1880
20	125.6	100	12564	1.1880
20	125.6	200	25128	1.3760
20	125.6	400	50256	1.7520
30	188.5	100	18850	1.4230
30	188.5	200	37700	1.8460
30	188.5	400	75400	2.6920

Further simplifications of the calculations were introduced by standardizing the capacitance setting  $C_1$  for each frequency and performing all runs at a given frequency with the same initial setting. Values of the correction factor  $\alpha$  for a fixed initial setting of  $C_1$  and final settings of  $C_2$  corresponding to measured capacitances of 150, 200, 250 and 300 uuf. were obtained from the General Radio charts. A plot of observed capacitance change versus B'x was possible from these data. This plot was found to be linear. The data for this chart at 10 Mc. are shown in Table IX.

TABLE IX

Values of B'x for Observed Capacitance Change at 10 Mc.

Where:  $C_1, C_2$  are initial and final settings of precision condenser

$$C_{e1} = C_1/\alpha, \quad \text{and } B'x = \omega(C_{e1} - C_{e2})$$

$C_1 - C_2$ uuf	$C_1$ uuf	$\alpha,$	$C_2$ uuf	$\alpha_2$	$C_{e1}$ uuf	$C_{e2}$ uuf	$C_{e1} - C_{e2}$ uuf	$B'x \times 10^{-3}$ umhos
150	615.0	0.9850	465	0.988	624.4	470.6	153.8	9.660
200	615.0	0.9850	415	0.990	624.4	419.2	205.2	12.88
250	615.0	0.9850	365	0.991	624.4	368.4	256.0	16.08
300	615.0	0.9850	315	0.992	624.4	317.5	306.9	19.28

The correction factor  $\alpha$  did not affect measurements at frequencies of 1 and 3 Mc. and hence was only used for the 10 Mc. data. Even at this frequency, where corrections had to be applied, the procedure was relatively simple. The measured capacitance  $C_1 - C_2$  could be converted directly into the corrected value  $B'x$  by means of the graph whose data are shown in Table IX above. This value of  $B'x$  was then used in evaluating the correction factor  $\gamma$  from Figure 15. The corrected capacitance  $C_{xp}$  was then found from the relation  $Bx = B'x/\gamma = \frac{\omega C_{xp}}{\gamma}$  or  $C_{xp} = \frac{B'x}{\omega \gamma}$

The correction factors  $\beta, \delta$  used in correcting the observed conductance  $G''$  were negligible at 1 and 3 Mc., and were well below the experimental error even at 10 Mc. The conductance was therefore only corrected for lead inductance, using the relationship  $G_x = G''/\gamma^2$ .

A sample calculation may help to illustrate this. Let us assume a measured capacitance change of 250.0 uuf. and a conductance

of 1000 umhos. at 10 Mc. The value of  $B'_{x'}$  from the graph (formulated from Table IX) is found to be 16.08 umhos. Using this value  $\delta$  is found to be 1.120 from the lead inductance correction graph (plotted from Table VIII). The corrected capacitance,  $C_{xp}$ , is thus found to be  $\frac{250.0}{1.120} = 223.2$  uuf. and the conductance is  $\frac{1000}{(1.120)^2} = 797$  umhos. Using the complete correction factors supplied with the Twin-T, values of 223.2 for  $C_{xp}$  and 796 for  $G_x$  are obtained.

The dielectric cell was calibrated with benzene at 25.0°C. The geometric capacitance ( $C_g$ ) was found to be 54.0 uuf., while the extraneous capacitance ( $C_o$ ) including leads was 29.7 uuf.

### Materials

Three samples of polyvinyl acetate, gelva V 1 1/2, V 15 and V 25 were used, corresponding to molecular weights of 15,000, 60,000 and 100,000 respectively. The samples were dried in vacuo, but were not further purified. Reagent grade toluene was used throughout. The toluene was dried over sodium metal, and then distilled prior to use.

The following samples were prepared:

15%, 30%, 40%, 60%	V 1 1/2
15%, 30%, 40%	V 15
15%, 30%	V 25

All concentrations are expressed as gms. Gelva/ml. toluene.

The choice of toluene rather than benzene as a solvent should be explained. Although benzene was an ideal solvent for dielectric work since its dipole moment is zero (74), the wide range of temperature over which toluene remained liquid was a distinct advantage.

Since the dipole moment of toluene is very small, it was not expected to provide any serious theoretical complications.

## RESULTS

Although dielectric dispersion data obtained at fixed temperature and varying frequency are easier to interpret theoretically, the majority of workers in this field have performed their experiments at fixed frequency and varying temperature. The experimental advantages of this procedure are obvious. Measurements performed over a wide temperature range can be used to bring dispersion regions normally out of the scope of an impedance measuring circuit into its most accurate range. Although it is normally difficult to perform measurements over a frequency variation of 1000 to 1, a temperature range of  $100^{\circ}$  will cover a dispersion region, and can be easily obtained in most instances. Furthermore, as it has already been shown, the effects of residual impedances seriously limited the performance of the Twin-T at its higher frequency limits. No such drawbacks existed in using temperature down to  $-80^{\circ}\text{C}$ . In fact most of the measurements would have been above the highest frequency limit of the Twin-T at room temperature, and could not have been performed.

Dielectric measurements were taken of samples of three molecular weights, at concentrations of 15, 30 and 40%, at 1, 3 and 10 Mc., over a temperature range of  $-80^{\circ}$  to  $80^{\circ}$ . The corrected values of the equivalent parallel capacitance  $C_{xp}$ , and conductance  $G_x$ , were interpreted in terms of the complex dielectric constant

$$\epsilon = \epsilon' - j\epsilon''$$

Hereafter  $\epsilon'$  will be referred to as dielectric constant, and  $\epsilon''$  as dielectric loss. The dielectric constant is defined as the ratio of the parallel geometric capacitance in the medium to that in vacuo.

The cell's parallel geometric capacitance,  $C_g$ , and its extraneous capacitance,  $C_o$ , were found from the calibration in benzene. Hence it can be seen that

$$\epsilon' = \frac{C_{xp} - C_o}{C_g}$$

It will be remembered that  $\epsilon''/\epsilon' \tan \delta = G/B$

But  $B = \omega C$  and  $\epsilon' = C/C_g$  so we have,

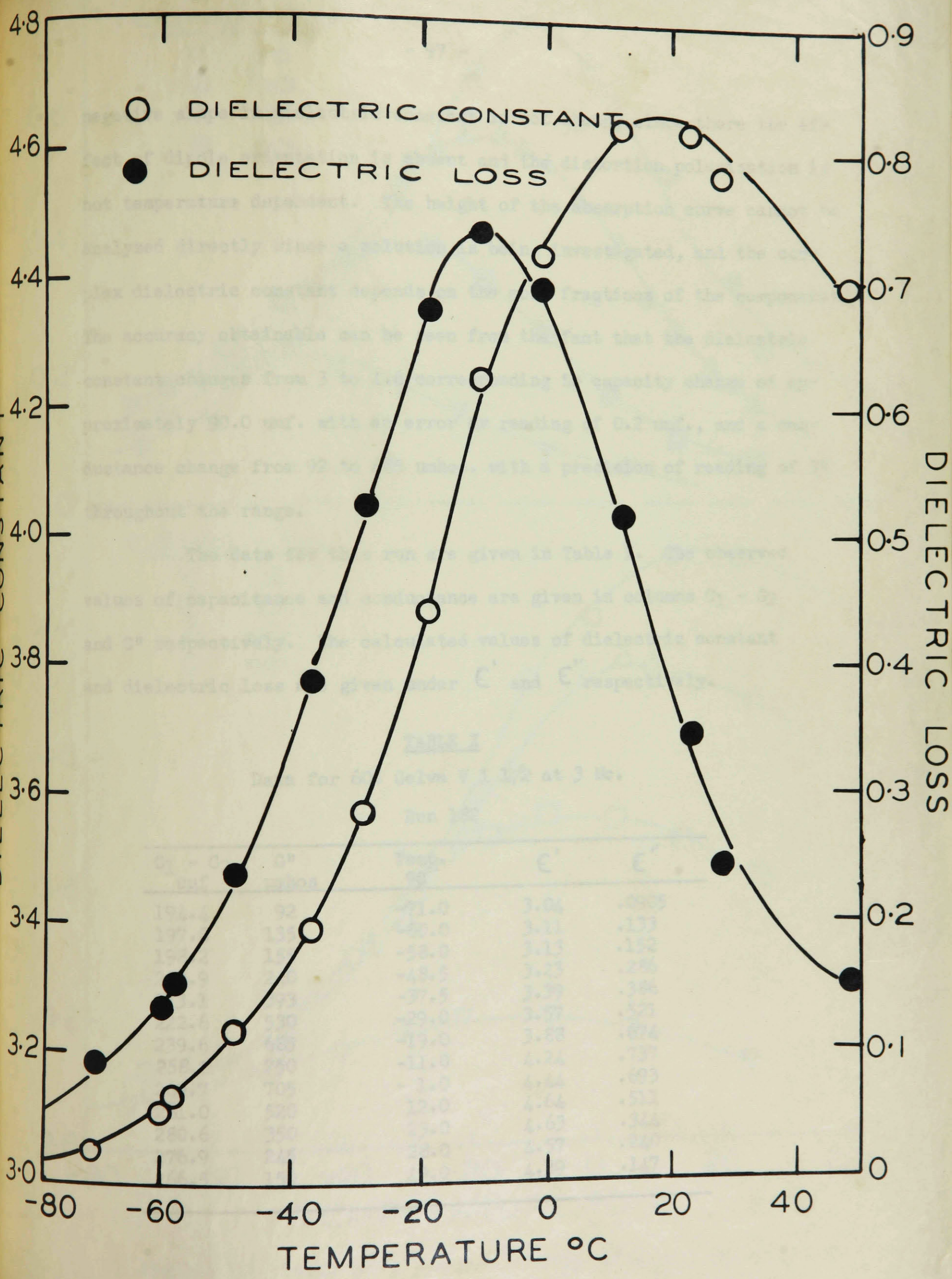
$$\epsilon'' = \epsilon' \frac{G}{B} = \frac{C/C_g G}{\omega C} = \frac{G}{\omega C_g}$$

At any frequency, therefore,  $\epsilon''$  is proportional to  $G$ . The proportionality constant,  $1/\omega C_g$ , was evaluated for 1, 3 and 10 Mc., and the conductance readings were then readily transformed into equivalent values of the dielectric loss.

The general nature of the results obtained is shown in Figure 16 for a typical run on 60% Gelva V 1 1/2 (Run 182). It is seen that the dielectric loss curve is symmetrical about a mean temperature, that the position of the maximum of the curve is well defined, and that a simultaneous change in dielectric constant occurs in the absorption region. Analyzing this in more detail one sees that a negative slope in the dielectric constant curve occurs at temperatures above the absorption region. This is due merely to the classical variation of dipole polarization with temperature at low frequencies and follows the relation

$$P = a + \frac{b}{T}$$

In addition there is a small density effect but this is almost negligible in comparison to the above even for the large density temperature coefficient for toluene. This can be seen to be true by observing that at the very low temperature region the effect of this



dispersion of 60% V-1 1/2 Gelva at 3 Mc.

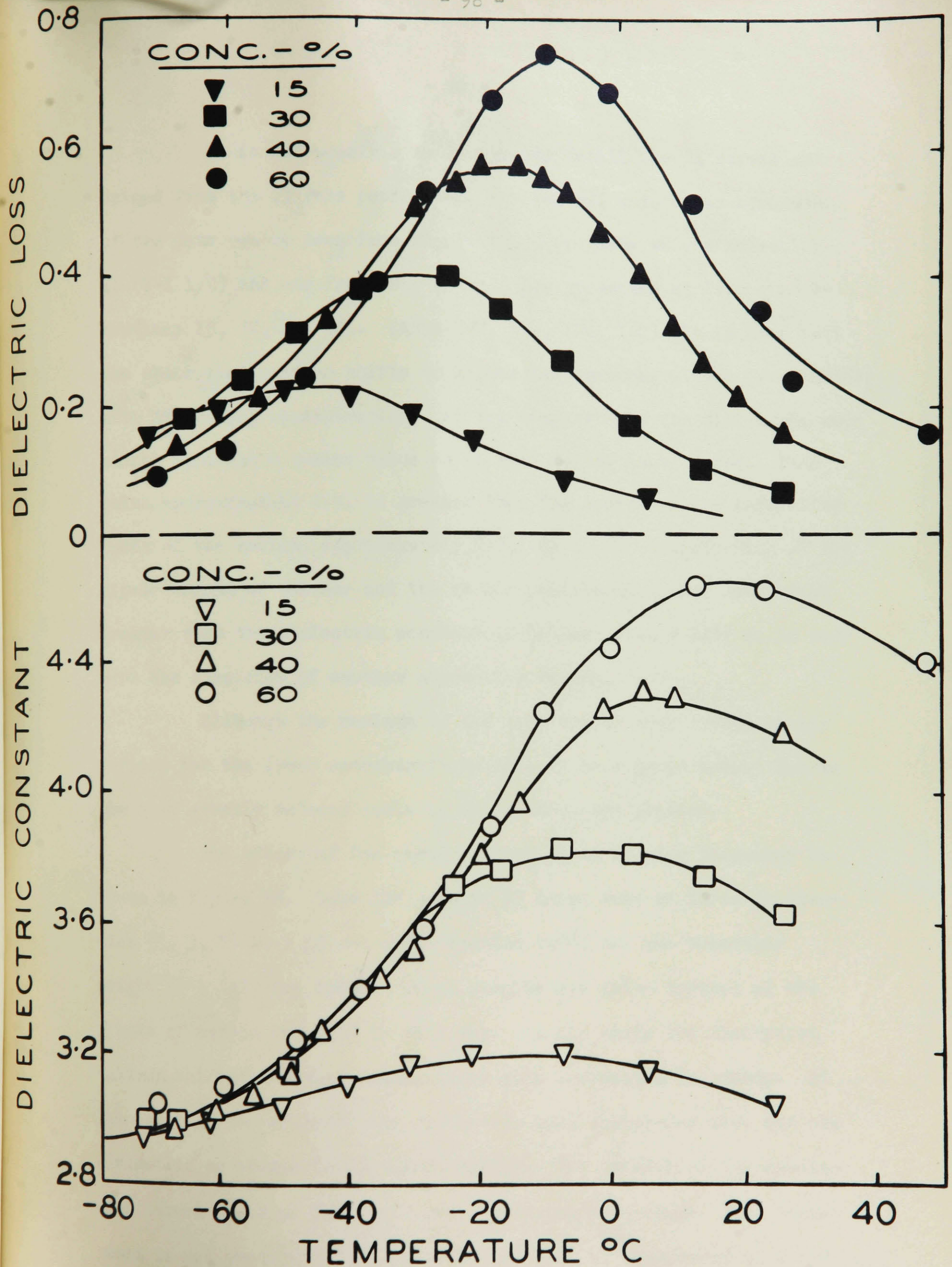


Figure 17: Dielectric dispersion of V-1/2 Gelva at 3 Mc. at the inscribed concentrations.

It is not possible to discuss in detail the 54 curves obtained from the 27 runs performed. The general nature and agreement of the data can be seen from Figure 17, where data at one molecular wt (V-1 1/2) and one frequency (3 Mc.) are presented at four concentrations 15, 30, 40, 60%. (Runs 185, 184, 179, 182) It is seen that the absorption maximum shifts to higher temperatures (lower frequencies) with increasing concentration. At low temperatures the dielectric constants approach a common value as is seen in the lower curve. This value, approximately 2.9, is greater than the square of the refractive index of the medium, approximately 2.3, due to the contribution of the dipole moment of toluene and the atomic polarization, but not so much greater than the dielectric constant of toluene (2.4 - 2.5) as to warrant the suspicion of another absorption region.

Although the maximum of the loss curves seem rather poorly defined for the lower concentrations this is to a great extent due to the very greatly reduced scale on which these are plotted.

The nature of the results obtained at varying frequency is shown in Figure 18. Here the results of three runs at three frequencies (1, 3, 10 Mc.) at one concentration (40%) and one molecular weight (V-1 1/2) are shown. These results are quite typical of the 8 sets of curves obtained in this way. In all cases the absorption maximum shifts to higher temperatures with increasing frequency. At low and high temperatures the dielectric loss approaches zero and the dielectric constants reach common values. The breadth of the absorption curves seems to increase with increasing frequency. This phenomenon is not predicted theoretically and will be considered at a future

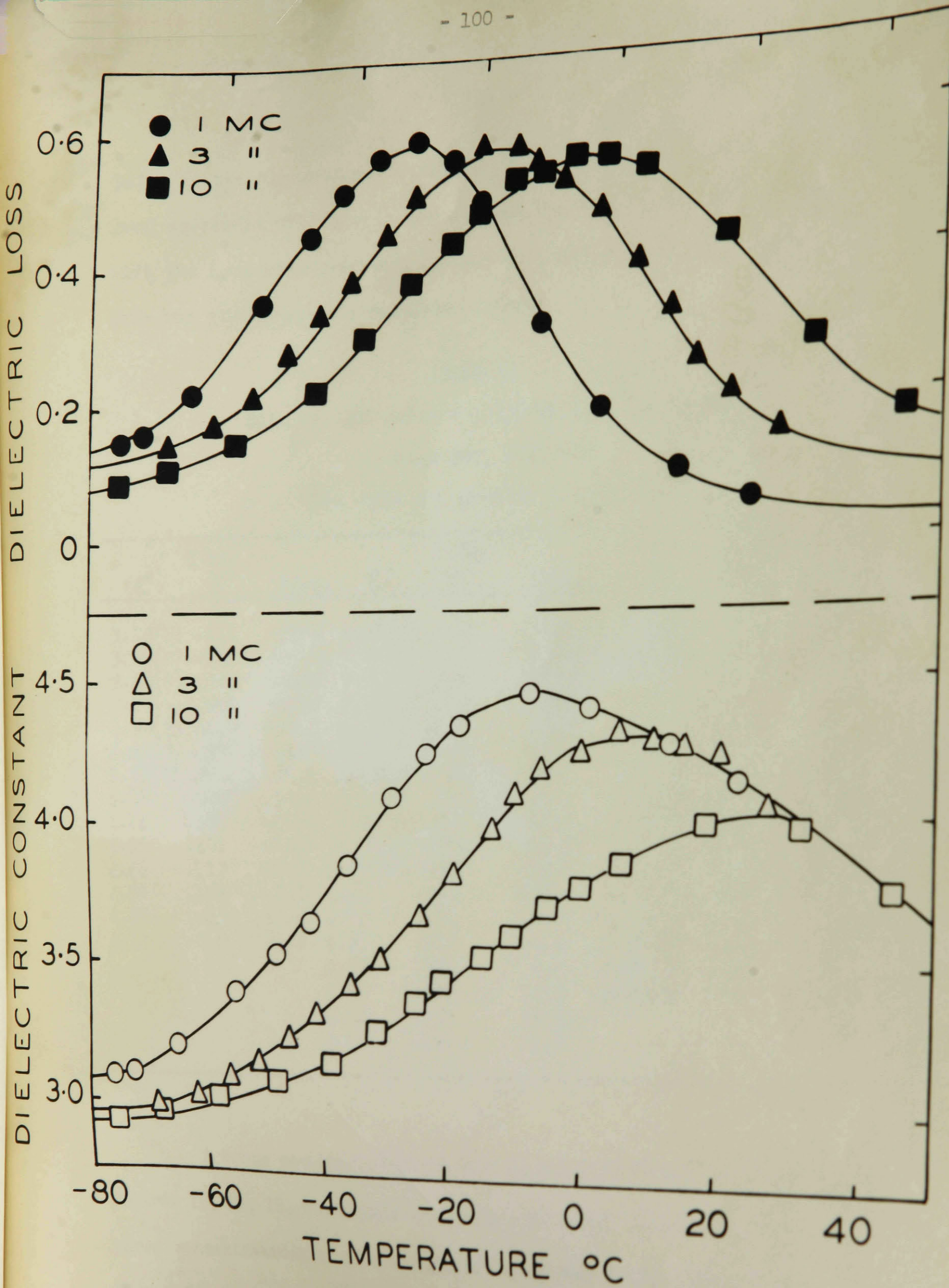


Figure 18: Dielectric dispersion of 40% V-1½ Gelva at 1, 3 and 10 Mc.

point in the discussion. Otherwise the curves seem to show remarkably good agreement with theory and reflect the high precision attainable with the apparatus over wide ranges of frequency and temperature. The data for these runs are tabulated below:

TABLE XI

Data for 40% Gelva V 1 1/2 at 1, 3 and 10 Mc.

Runs 207, 179, 208

(The data are plotted in Fig. 18)

1 Mc.			3 Mc.			10 Mc.		
$\epsilon'$	$\epsilon''$	Temp.	$\epsilon'$	$\epsilon''$	Temp.	$\epsilon'$	$\epsilon''$	Temp.
3.08(0)	.147	-75.0	2.97(8)	.143	-68.0	2.92(0)	.087	-75.0
3.10(0)	.158	-71.5	3.01(9)	.169	-61.0	2.97(0)	.107	-67.0
3.19(6)	.220	-64.0	3.07(8)	.208	-55.0	3.01(6)	.150	-57.0
3.37(6)	.354	-54.0	3.14(2)	.275	-50.0	3.09(0)	.222	-46.5
3.52(2)	.448	-47.0	3.23(0)	.328	-45.0	3.14(1)	.298	-38.2
3.63(8)	.508	-42.0	3.30(8)	3.84	-40.5	3.26(4)	.376	-31.0
3.83(6)	.561	-36.5	3.41(0)	.446	-35.5	3.36(4)	.439	-24.8
4.08	.582	-30.2	3.65(8)	.551	-25.0	3.43(8)	.474	-21.0
4.24	.552	-25.5	3.80(0)	.571	-20.5	3.53(0)	.519	-15.6
4.35	.491	-20.5	3.97(0)	.570	-14.8	3.61(4)	.534	-11.1
4.46	.310	-10.5	4.08(8)	.553	-12.0	3.71(0)	.550	- 6.0
4.39	.186	- 1.1	4.19	.521	- 8.0	3.78(0)	.551	- 1.4
4.27	.098	11.5	4.24	.472	- 2.0	3.86(2)	.532	4.5
4.13	.056	21.8	4.31	.398	4.0	3.98(6)	.427	17.5
			4.28	.324	8.5	3.97(0)	.281	31.3
			4.26	.258	13.5	3.89(0)	.165	45.0
			4.24	.206	18.5			
			4.16	.147	26.0			

A cross sectional view of the data is presented graphically in Figures 18, 19, 20, where data on samples of three molecular weights and three concentrations at frequencies of 1, 3, and 10 Mc. are plotted. Figure 19 shows the data for 30% V 15 at three frequencies, and the results are tabulated in Table XII. Figure 20 shows the data for 15% V 25

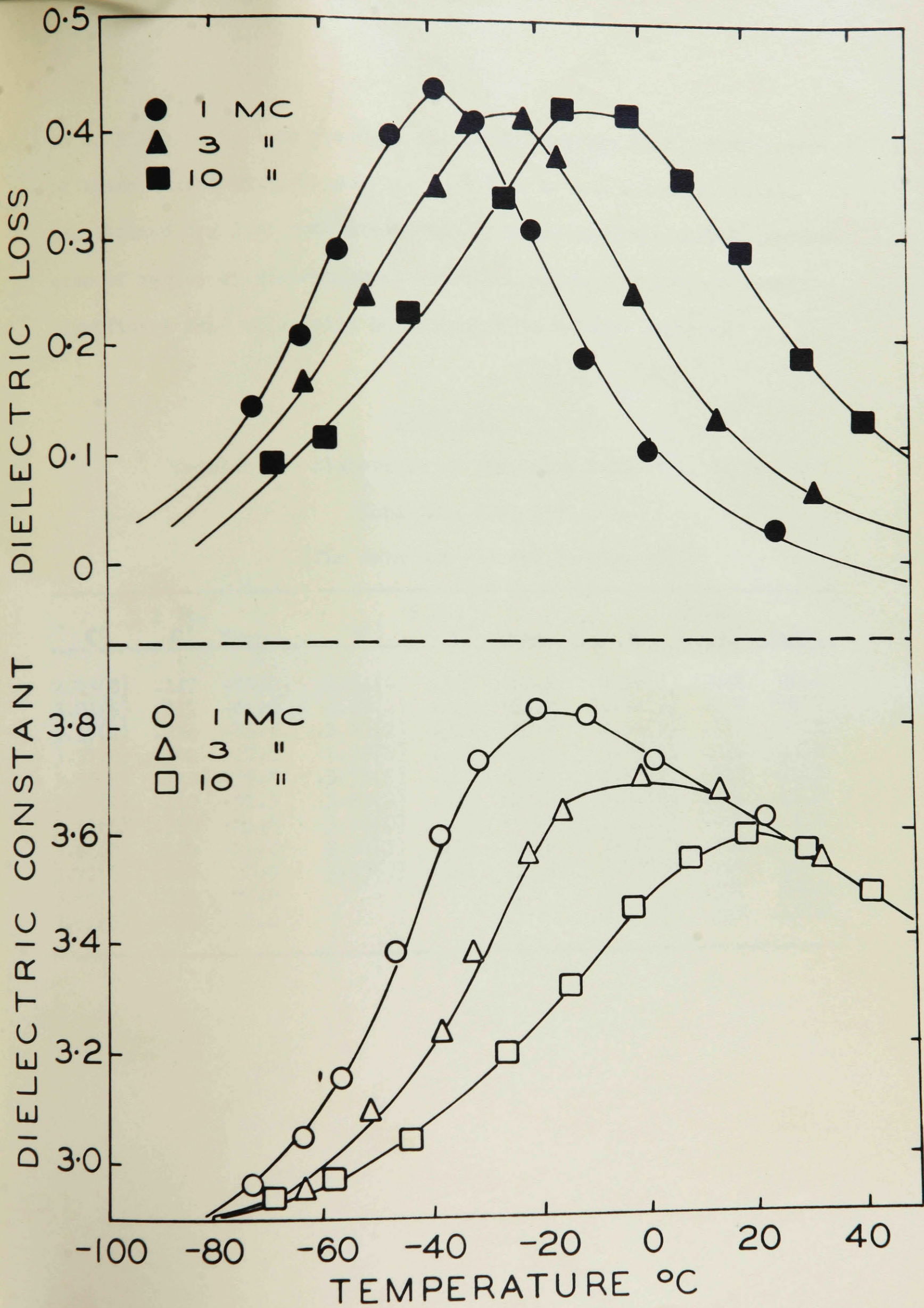


Figure 19: Dielectric dispersion of 30% V-15 Gelva at 1, 3 and 10 Mc.

at 1, 3 and 10 Mc. and the data are given in Table XIII. Comparison of these curves with Figure 17, where data at one molecular weight are plotted for four concentrations, does not show any marked dependence of region of absorption on molecular weight. This is a rather significant fact which will be discussed in a later section.

TABLE XII

Dielectric Dispersion of 30% Gelva V 15 at 1, 3, 10 Mc.

Runs 189, 186, 188

(The data are plotted in Fig. 19)

1 Mc.			3 Mc.			10 Mc.		
$\epsilon'$	$\epsilon''$	Temp.	$\epsilon'$	$\epsilon''$	Temp.	$\epsilon'$	$\epsilon''$	Temp.
2.95(8)	.147	-73.2	2.94(6)	.162	-63.5	3.58(3)	.242	20.0
3.03(5)	.212	-64.0	3.09(2)	.246	-52.0	2.94(3)	.089	-66.8
3.15(0)	.286	-56.8	3.23(2)	.346	-39.0	2.96(9)	.113	-58.5
3.37(0)	.392	-47.0	3.38(0)	.403	-32.5	3.03(5)	.230	-44.0
3.58(5)	.440	-38.8	3.55(5)	.408	-22.5	3.19(0)	.340	-25.5
3.72(9)	.410	-31.5	3.63(9)	.374	-16.0	3.31(9)	.424	-11.0
3.82(6)	.310	-21.0	3.70(0)	.249	- 1.5	3.45(7)	.420	- 2.5
3.81(0)	.189	-11.0	3.67(3)	.130	14.0	3.54(7)	.358	8.0
3.72(6)	.103	0.9	3.53(8)	.061	32.5	3.58(5)	.291	18.8
3.65(6)	.035	21.0				3.55(8)	.191	30.2
3.61(6)	.031	25.0				3.48(7)	.127	42.0

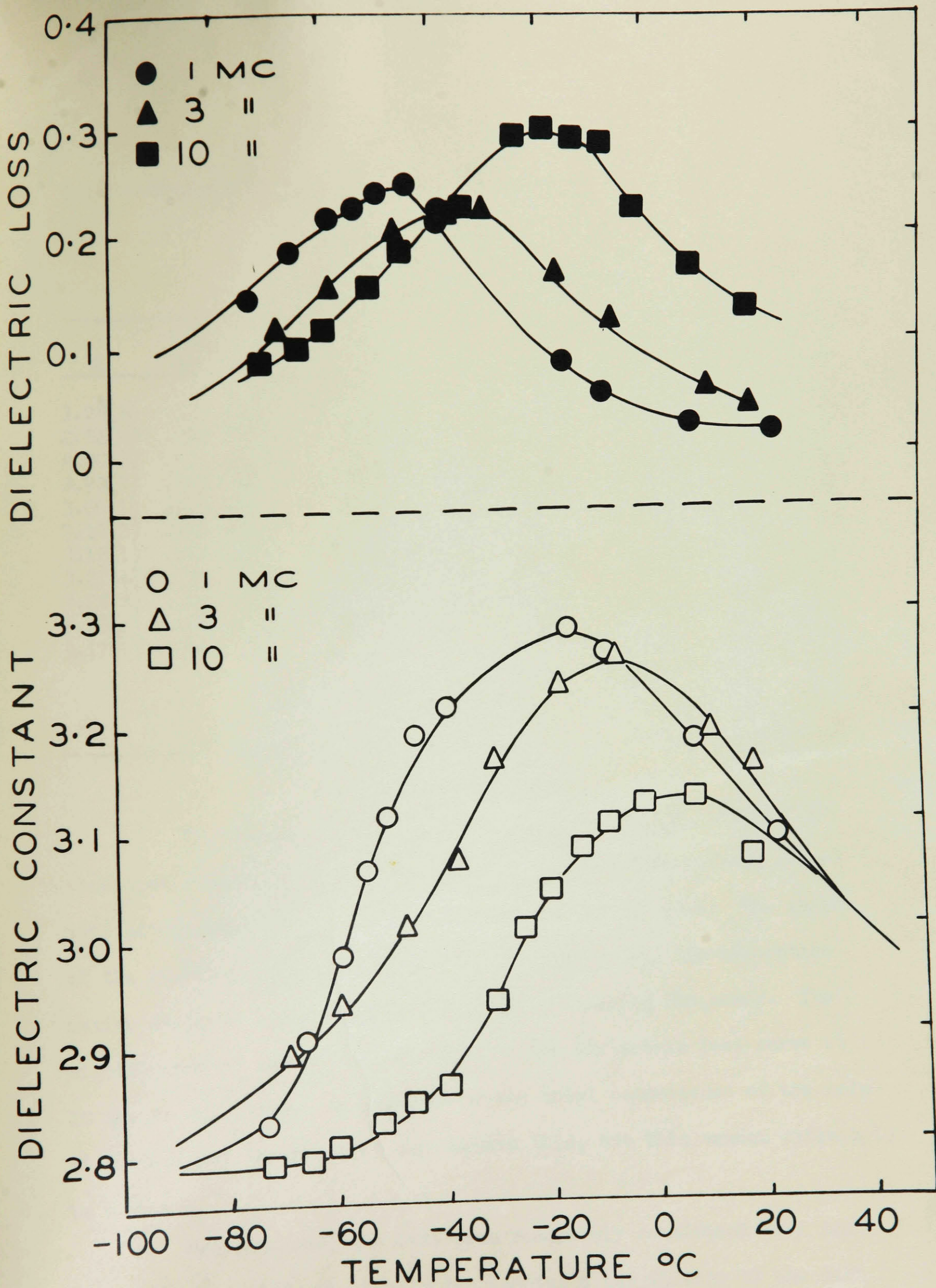


Figure 20: Dielectric dispersion of 15% V-25 Gelva at 1, 3 and 10 Mc.

TABLE XIII

Dielectric Dispersion of 15% V 25 at 1, 3, 10 Mc.

Runs 205, 190, 206

(The data are plotted in Fig. 20)

$\epsilon'$	1 Mc.		$\epsilon'$	3 Mc.		$\epsilon'$	10 Mc.	
	$\epsilon''$	Temp.		$\epsilon''$	Temp.		$\epsilon''$	Temp.
3.08(8)	.019	23.0	3.12(4)	.0388	25.0	2.79(0)	.0865	-72.0
2.84(6)	.147	-73.5	2.89(3)	.113	-69.0	2.79(2)	.102	-65.0
2.90(3)	.191	-66.0	2.94(0)	.155	-59.5	2.80(6)	.119	-60.0
2.98(2)	.218	-59.0	3.00(9)	.206	-47.0	2.82(6)	.159	-52.0
3.06(1)	.226	-54.2	3.06(8)	.223	-37.0	2.84(3)	.191	-46.0
3.12(2)	.242	-50.0	3.16(3)	.224	-30.5	2.86(0)	.223	-39.5
3.18(1)	.226	-45.0	3.23(5)	.168	-17.5	2.86(4)	.260	-35.0
3.21(6)	.215	-39.0	3.25(9)	.124	- 7.0	3.00(8)	.293	-25.0
3.28(2)	.086	-16.0	3.19(0)	.058	10.5	3.04(1)	.300	-20.0
3.26(4)	.058	- 9.0	3.15(3)	.046	19.0	3.07(8)	.287	-14.0
3.17(8)	.029	7.5				3.10(2)	.287	- 9.0
						3.12(2)	.227	- 2.2
						3.12(6)	.176	7.5
						3.07(0)	.134	18.0

The results at the lowest concentration, 15%, (Figure 20) show some inconsistencies, but in view of the low capacitance increment being measured, the agreement seems reasonably good. The shapes of the curves are in accordance with the theory, and the absorption maxima shift to higher temperatures with increasing frequency. The significance of the increased height of the dielectric loss curve at 10 Mc. is not clear. An increase of the total conductance of the solution at higher temperatures may explain this, but this cannot definitely be assumed.

Nevertheless, the data seem remarkably consistent when one considers that each run usually represented a new filling of the cell

with the solution. The three runs on the same sample at different frequencies were not in chronological order, and were sometimes carried out a month apart. The runs are numbered chronologically, and an indication of the order of performance of the experimental work can be obtained in this way.

The data for the remaining runs performed on polyvinyl acetate are tabulated below.

TABLE XIV

Dielectric Dispersion of 30% Gelva V 1 1/2 at  
1, 3, 10 Mc.

Runs 198, 184, 199

1 Mc.			3 Mc.			10 Mc.		
$\epsilon'$	$\epsilon''$	Temp.	$\epsilon'$	$\epsilon''$	Temp.	$\epsilon'$	$\epsilon''$	Temp.
3.17(2)	.224	-69.0	2.97(7)	.181	-67.5	3.76(4)	.232	26.0
3.27(5)	.295	-60.2	3.01(2)	.236	-58.5	2.99(7)	.129	-68.6
3.48(1)	.406	-50.7	3.16(0)	.311	-49.5	3.01(8)	.156	-59.5
3.78(0)	.473	-40.0	3.39(2)	.383	-39.0	3.09(2)	.232	-47.9
3.91(3)	.443	-32.0	3.66	.396	-26.0	3.18(1)	.311	-38.0
4.05(7)	.329	-21.5	3.76	.353	-18.0	3.27(9)	.397	-27.2
4.09(0)	.176	- 7.1	3.83	.265	- 8.0	3.40(2)	.440	-17.2
3.87(6)	.054	15.2	3.80	.172	2.5	3.55(1)	.455	- 7.2
3.78(1)	.036	25.0	3.72	.106	13.5	3.66(2)	.415	1.9
			3.62	.063	26.0	3.72(2)	.332	13.5
						3.70(7)	.209	28.2
						3.63(0)	.140	40.0

TABLE XV

Dielectric Dispersion of 15% V 1 1/2 Gelva at 1, 3, 10 Mc.

Runs 200, 185, 201

1 Mc.			3 Mc.			10 Mc.		
$\epsilon'$	$\epsilon''$	Temp.	$\epsilon'$	$\epsilon''$	Temp.	$\epsilon'$	$\epsilon''$	Temp.
3.10	.015	23.0	2.88	.153	-73.0	2.81	.123	-69.2
2.97	.206	-74.5	2.95	.197	-62.0	2.79	.147	-59.8
3.01	.230	-64.0	3.04	.226	-51.0	2.90	.202	-48.3
3.06	.236	-55.0	3.10	.216	-41.5	2.96	.221	-42.0
3.29	.218	-46.0	3.16	.187	-31.5	3.00	.238	-33.5
3.33	.171	-38.5	3.19	.143	-22.0	3.08	.244	-25.8
3.36	.118	-29.8	3.21	.090	- 8.0	3.14	.237	-19.0
3.33	.053	-13.0	3.16	.055	5.0	3.16	.229	-11.2
3.25	.029	0	3.04	.028	24.5	3.18	.177	- 1.8
3.14	.015	17.2				3.18	.143	5.8
						3.12	.100	18.2
						3.08	.073	27.2

TABLE XVI

Dielectric Dispersion of 40% V 15 Gelva at 1, 3, 10 Mc.

Runs 196, 194, 197

1 Mc.			3 Mc.			10 Mc.		
$\epsilon'$	$\epsilon''$	Temp.	$\epsilon'$	$\epsilon''$	Temp.	$\epsilon'$	$\epsilon''$	Temp.
3.78(1)	.0425	26.1	3.72(6)	.0983	24.5	2.97(2)	.120	-59.0
3.14(5)	.236	-61.8	2.96(3)	.0935	-74.5	3.00(5)	.186	-48.0
3.28(2)	.331	-52.6	2.96(7)	.105	-68.5	3.06(3)	.244	-40.0
3.49(0)	.449	-44.0	3.06(7)	.194	-55.0	3.14(5)	.327	-31.0
3.72(2)	.484	-35.5	3.17(6)	.287	-47.6	3.22(3)	.384	-23.9
3.91(6)	.463	-27.2	3.30(1)	.382	-38.2	3.33(2)	.438	-15.5
4.05(4)	.328	-16.3	3.51(9)	.469	-27.5	3.43(0)	.458	- 8.0
4.01(4)	.153	- 3.0	3.70(2)	.463	-18.0	3.54(2)	.448	- 0.9
3.89(7)	.076	+11.0	3.83(9)	.378	-17.5	3.63(8)	.405	8.3
3.79(0)	.040	23.1	3.88(0)	.251	+ 4.8	3.68(1)	.325	18.0
			3.80(1)	.128	19.5	3.67(6)	.234	28.5

TABLE XVII

Dielectric Dispersion of 15% V 15 Gelva at 1, 3, 10 Mc.

Runs 204, 187, 203

1 Mc.			3 Mc.			10 Mc.		
$\epsilon'$	$\epsilon''$	Temp.	$\epsilon'$	$\epsilon''$	Temp.	$\epsilon'$	$\epsilon''$	Temp.
3.02(8)	.139	-72.5	3.21(6)	.055	20.0	2.91(6)	.0875	-74.0
3.07(2)	.186	-67.0	2.90(2)	.118	-73.5	2.92(0)	.109	-65.5
3.13(8)	.239	-61.2	2.94(9)	.142	-61.0	2.94(8)	.166	-54.0
3.25(0)	.295	-52.5	3.01(7)	.207	-48.8	3.00(6)	.247	-43.1
3.36(4)	.316	-47.0	3.12(6)	.260	-37.8	3.07(8)	.320	-33.1
3.44(2)	.310	-41.0	3.22(0)	.273	-29.1	3.17(8)	.363	-20.0
3.47(8)	.280	-35.0	3.30(4)	.236	-18.0	3.32(2)	.357	- 5.5
3.53(0)	.218	-27.0	3.32(1)	.155	- 9.5	3.38(2)	.308	7.8
3.55(0)	.162	-20.0	3.28(3)	.087	8.0	3.39(5)	.200	19.5
3.47(9)	.106	- 6.0	3.21(2)	.051	24.5	3.34(2)	.144	27.8
3.39(6)	.037	11.8						

TABLE XVIII

Dielectric Dispersion of 30% V 25 Gelva at 1, 3, 10 Mc.

Runs 192, 191, 193

1 Mc.			3 Mc.			10 Mc.		
$\epsilon'$	$\epsilon''$	Temp.	$\epsilon'$	$\epsilon''$	Temp.	$\epsilon'$	$\epsilon''$	Temp.
3.59(1)	.0326	24.5	3.60(3)	.085	22.2	2.94(9)	.0763	-72.0
3.02(8)	.130	-72.5	2.93(5)	.101	-70.5	2.96(5)	.177	-54.8
3.15(3)	.206	-60.3	3.006	.138	-64.3	3.03(9)	.232	-42.3
3.26(7)	.345	-51.9	3.06(5)	.211	-54.0	3.13(0)	.326	-30.4
3.42(5)	.396	-45.3	3.23(8)	.321	-42.5	3.26(0)	.405	-18.5
3.58(3)	.437	-38.5	3.44(8)	.400	-29.9	3.38(0)	.434	- 7.8
3.74(8)	.410	-29.5	3.59(2)	.389	-20.0	3.44(9)	.391	- 0.2
3.85(2)	.342	-20.2	3.69(3)	.321	- 7.5	3.54(2)	.322	11.0
3.87(7)	.218	-10.9	3.72(9)	.232	0.9	3.56(1)	.217	25.5
3.81(5)	.109	- 1.8	3.70(2)	.141	11.8			
3.71(6)	.053	12.5	3.59(7)	.082	22.8			

A knowledge of the refractive index and density of the samples of dielectric is needed in the interpretation of the data in terms of the Debye theory. The refractive indices of all samples were measured on a Bausch and Lomb refractometer, whose prisms were thermostated at 25.0°C. The measurements were performed with light from an incandescent lamp; no effort was made to use light of a fixed wave length. Table XIX shows the readings obtained in this way. Each value presented represents the mean of three readings of the instrument.

TABLE XIX

Refractive Indices of Samples used in Obtaining Dielectric Dispersion Data

Gelva Type	Concentration			
	15%	30%	40%	60%
V 1 1/2	1.4908	1.4883	1.4869	1.4849
V 15	1.4903	1.4886	1.4874	
V 25	1.4904	1.4885		
Pure Toluene	1.4931			

The densities of the samples were measured on a Westphal balance. The accuracy obtainable on such an instrument is seriously lowered when measurements are performed on viscous solutions. The lowest sensitivity, however, was 0.5%, and this was deemed sufficient. The measurements were performed at 20.0°C. and are shown in Table XX.

TABLE XX

Results of Density Measurements of Gelva Samples on  
Westphal Balance

Temperature - 20.0°C.

Gelva Type	Concentration			
	15%	30%	40%	60%
V 1 1/2	0.904	0.939	0.957	0.981
V 15	0.909	0.935	0.953	
V 25	0.905	0.936		
Pure Toluene	0.866			

DISCUSSION OF RESULTS

Application of the Theory of Absolute Reaction Rates

From the temperatures at which maxima on the dielectric loss curves are found, relaxation times can be evaluated. We have seen that, if dielectric relaxation is treated as a molecular rate process, the free energy  $F^\ddagger$  can be defined as in equation 31.

$$\frac{1}{\tau} = \frac{kT}{h} e^{-\frac{\Delta F^\ddagger}{RT}}$$

which can be written as

$$\frac{1}{\tau} = \frac{kT}{h} e^{+\Delta S^\ddagger/R} e^{-\frac{\Delta H^\ddagger}{RT}}$$

Hence,

$$H^\ddagger = R \left( d \ln \tau / d \frac{1}{T} \right) - R T$$

If  $\sigma$  is the slope of the curve  $\log \tau$  is plotted versus  $1/T$

$$H^\ddagger = 2.303 R \sigma - R T.$$

Plots of  $\log \tau$  vs.  $1/T$  are shown in Figures 21 for 15, 30 and 40% concentrations of V 15 gelva, and are seen to yield straight lines, thus indicating a constant  $\Delta H^\ddagger$  and  $\Delta S^\ddagger$ .

The data obtained in this way from all the runs performed are summarized in Table XXI. This table shows values of  $\Delta F^\ddagger$  obtained from the temperatures of maximum absorption. Values of  $\Delta H^\ddagger$  were obtained from the temperature variation of  $\tau$ , and  $\Delta S^\ddagger$  values were obtained by subtraction.

These data have been interpreted as showing that the dipoles are rotating almost freely in the system.

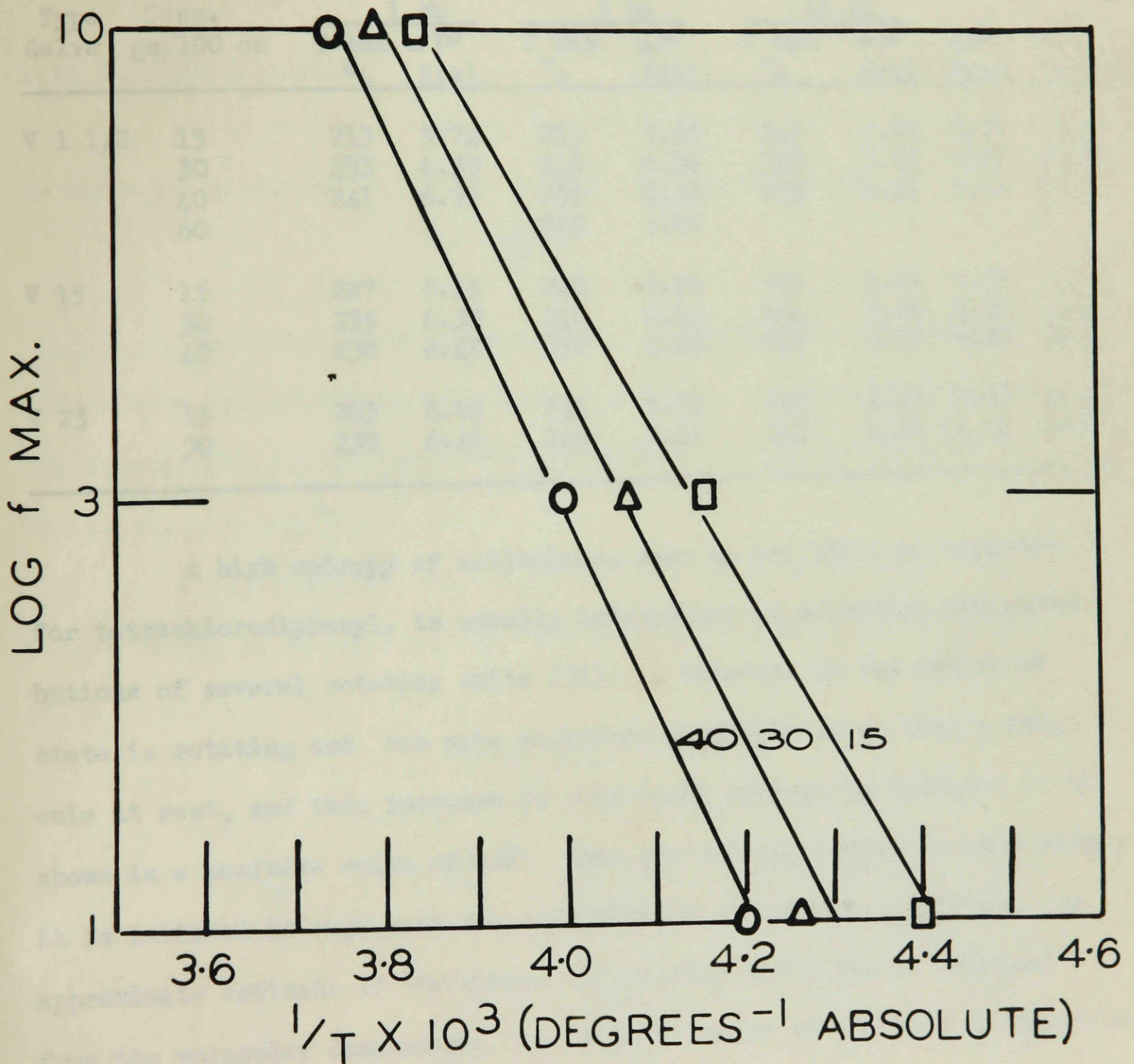


Figure 21: Logarithmic plot of frequency of absorption against reciprocal of absolute temperature for 15, 30 and 40% V-15 gelva.

TABLE XXI

Evaluation of  $F^\#$ ,  $H^\#$ ,  $S^\#$  from Dielectric Dispersion Data

Type Gelva	Conc. gm/100 cc	1 Mc		3 Mc		10 Mc		$\Delta H^\#$ Kcal	$\Delta S^\#$ cal/°A
		T max °A	$\Delta F^\#$ Kcal	T max °A	$\Delta F^\#$ Kcal	T max °A	$\Delta F^\#$ Kcal		
V 1 1/2	15	213	5.74	233	5.55	246	5.59	6.97	5.9
	30	233	6.30	243	6.09	262	5.95	9.51	14.2
	40	241	6.35	256	6.46	269	6.15	9.91	14.3
	60			263	6.62				
V 15	15	227	6.15	240	5.99	259	5.89	7.59	6.0
	30	235	6.38	246	6.12	264	6.05	8.90	11.2
	40	238	6.48	250	6.26	267	6.09	9.92	10.4
V 25	15	223	6.05	234	5.72	253	8.40	8.38	11.0
	30	239	6.46	245	6.11	263	6.00	11.31	20.5

A high entropy of activation, such as the 150 e.u. reported for tetrachlorodiphenyl, is usually interpreted as requiring the contributions of several rotating units (31). A molecule in the activated state is rotating and has more positions available to it than a molecule at rest, and this increase in rotational entropy is believed to be shown in a positive value of  $\Delta S^\#$ . When the entropy change is very large, it is believed to represent the contribution of several molecules. An approximate estimate of the number of rotating units can be obtained from the molecular dimensions, the heat of fusion or the heat of vaporization (30).

On the other hand, values of zero or slightly negative values of the entropy have been found for hexasubstituted benzenes (83) and for highly plasticized polyvinyl chloride. This is interpreted by Eyring and others as indicating that the molecules are rotating freely in the normal state.

The values of  $\Delta F^\ddagger$ ,  $\Delta H^\ddagger$ , and  $\Delta S^\ddagger$  obtained in the present work are approximately those obtained for alcohols of about 6 to 8 chain atoms (84).

### Size of Rotating Units

An approximate size of the rotating unit can be obtained by the application of the Debye formula from equation 30,

$$\tau = \frac{4\pi\eta a^3}{kT}$$

The viscosity of toluene over a temperature range was obtained from the International Critical Tables. The viscosities at the appropriate temperatures were determined by extrapolation of a linear plot of  $\log \eta$  vs.  $1/T$ .

A molar volume  $V_m = 4/3\pi N a^3$  was also calculated. The values of  $V_m$ ,  $a$ , as well as  $\eta$  and temperature are shown in Table XXII.

TABLE XXII

Radius of Rotating Unit and Molar Volume for 3 Mc Data

Type Gelva	Conc. gms/100 cc	T max °A	$\eta \times 10^3$ poise	$a \times 10^8$ cm	$V_m$ cc
V 1 1/2	15	223	18.5	19.1	17500
	30	243	12.7	22.2	28000
	40	256	10.6	24.1	35300
	60	263	9.2	25.6	42600
V 15	15	240	15.0	21.9	26600
	30	246	11.8	22.8	30200
	40	250	11.1	23.1	29800
V 25	15	234	15.0	20.8	22800
	30	245	12.2	22.0	26100

The bulk density of gelva is approximately 1.2. By multiplication of the molar volumes in Table XXII by this density approximate values of the molecular weight can be obtained. These values can be seen to be about 30,000, which is the order of magnitude obtained by the osmotic pressure method.

It is significant that no trend to larger values of the molecular weight of the rotating particle is obtained as one proceeds from V 1 1/2 to V 25. The approximate molecular weights obtained by the osmotic pressure method are 15,000, 60,000 and 100,000 for V 1 1/2, V 15 and V 25 respectively. It would thus appear that the rotating unit is smaller than the molecule. On the other hand the large molar volumes and radii obtained indicate that these units must represent large portions of the molecule.

The limitations of the Debye-Stokes equation must be realized in interpreting these data, even though the agreement seems good in this case. For comparison the data for 30% Gelva at 10 Mc. are shown in Table XXIII.

The fact that  $\tau$  and  $\eta$  do not show the same temperature dependence is probably the main reason for the poor agreement of the calculated values. An equivalent statement is that the activation energies for viscous flow and for dipole rotation are not equal in the present case. Such behavior is quite common and has been reported by many investigators (21)(25). The Debye-Stokes equation is thus seen to yield only approximate values, although these do appear to be of the correct order of magnitude.

TABLE XXIII

Radius of Rotating Unit and Molar Volume for 10 Mc. Data

Type Gelva	gms/100 cc	T max oA	$\eta \times 10^3$ poise	a x 10 <sup>8</sup> cm	V <sub>m</sub> cc
V 1 1/2	15	246	12.0	17.8	15000
	30	262	9.2	16.7	12300
	40	269	8.2	16.2	11200
V 15	15	259	9.6	16.9	12800
	30	264	8.9	16.6	12000
	40	267	8.5	16.3	11500
V 25	15	253	10.8	17.4	13900
	30	263	9.0	16.1	12100

It can be seen that the viscosity of the solvent and not of the solution is the significant factor, in agreement with the Debye theory. The viscosities of solutions of V 1 1/2, V 15 and V 25 are approximately in the ratio of 1:10:16. For a concentration of 30% at 10 Mc. the radii of the rotating units are found to be 16.7, 16.6 and 16.1 Angstroms for V 1 1/2, V 15 and V 25 respectively.

Dipole Moments

A particularly convenient equation, which has been used by several workers (84)(85), for interpreting dielectric dispersion data at very high frequencies can be derived from the Debye theory.

$$\frac{\epsilon''}{\epsilon'} = \tan \delta = \frac{(\epsilon' + 2)^2}{\epsilon'} \cdot \frac{\omega \tau}{1 + \omega^2 \tau^2} \frac{4\pi^2 Nc}{27 kT} \quad 68$$

where  $\epsilon'$  is the dielectric constant of the solution, c is the concentration in moles/cc., and the other symbols have their usual significance.

When the absorption maximum is reached  $\omega\tau = 1$ , and

$\frac{\omega\tau}{1 + \omega^2\tau^2} = \frac{1}{2}$ . The dipole moment can thus be evaluated from the observed maxima of the dielectric loss curve and the corresponding values of the dielectric constant.

In the previous evaluation of the relaxation time from the maxima of the loss curves it was assumed that the experimental value obtained at varying temperature in this way was the same as that obtained at this temperature at varying frequency. Whiffen and Thomsen (84) have suggested that, since  $(\frac{\epsilon' + 2}{\epsilon'})^2$  is reasonably constant near the maximum, a plot of  $\frac{T \tan \delta}{\epsilon}$  versus  $T$  would give a plot whose maximum would have the value

$$\left(\frac{\epsilon' + 2}{\epsilon'}\right)^2 \cdot \frac{4\pi \cdot \mu^2 \cdot N \cdot \frac{1}{2}}{27k}$$

and thus  $\mu$  can be evaluated and the temperature effect compensated.

This type of plot was tried on the data for 15%, 30% and 40% V 15 in order to evaluate the dipole moment per monomer unit, and to test the method of evaluating the relaxation time. These data are shown in Table XXIV. Only values near the dispersion region have been recorded. The values of  $T'_{\max}$  were obtained from this plot and should be compared with the values of  $T_{\max}$  obtained directly from the maxima of the loss curves. The last column gives the calculated values of the dipole moment  $\mu$ .

Thus it can be seen that the correction for the temperature dependence of the relaxation time is not significant in the present work. The values of 0.91, 0.98 and  $1.26 \times 10^{-18}$  esu x cm (i.e. Debye units) for the dipole moment per monomer unit of polyvinyl acetate seem reasonable. The variation with concentration is a consequence of the

previously noted shift of the maxima to higher temperatures at higher concentrations, probably due to dipole hindrance. The values can be compared with the dipole moment of 1.67 for methyl acetate.

TABLE XXIV

Evaluation of Dipole Moment per Monomer Unit by Method of Whiffen and Thomsen for V 15 Gelva at 3 Mc.

Conc. gm/cc	T °A	ε''	ε'	tan δ	T tan δ °A	T' max °A	T max	μ Debye
40%	235	0.382	3.30	0.115	27.0			
	246	0.469	3.52	0.133	32.8			
	255	0.463	3.76	0.125	31.8			
	265	0.378	3.84	0.099	26.3	250	250	0.91
30%	234	0.340	3.23	0.107	24.0			
	241	0.403	3.38	0.119	28.7			
	251	0.408	3.56	0.115	28.8			
	257	0.374	3.64	0.103	26.4			
	272	0.249	3.70	0.067	18.3	247	246	0.98
15%	220	0.207	3.02	0.0685	15.1			
	231	0.260	3.13	0.0830	19.2			
	240	0.273	3.22	0.0845	20.3			
	251	0.236	3.30	0.0715	17.9	240	240	1.26

Equation 68 provides a method of evaluating the relaxation times at varying temperatures from measurements performed at one frequency over a range of temperatures. It can be seen from 68 that the ratio of the value of  $\tan \delta$  at a given temperature, to its maximum value is

$$\frac{\tan \delta}{\tan \delta_{max}} = \frac{\omega \tau}{1 + (\omega \tau)^2} \times 2 \quad \text{69}$$

where the  $\delta$ 's correspond to the same frequency.

Thus at any given temperature  $\tau$  can be evaluated by solving the above quadratic equation. The choice between the two possible

values for  $\tau$  is made on the basis of whether the given temperature is above or below the temperature of maximum absorption. The values of  $\tau$  obtained in this way are listed in Table XXV for data obtained from a single run on 30% V 15 at 3 Mc.

TABLE XXV  
Evaluation of  $\tau$  by Method of Whiffen and Thomsen  
for 30% V 15 at 3 Mc.

Temp. ( $^{\circ}$ A)	210	221	234	241	247	257	272	(298)
$\tau \times 10^{-8}$ (sec)	27.1	15.6	10.6	6.95	5.31	3.34	1.70	(0.53)

The extrapolated value of the relaxation time to 25 $^{\circ}$ C. on a log vs.  $1/T$  plot gives a relaxation time of  $5.3 \times 10^{-9}$  seconds.

Although this is a convenient method for converting incomplete data to yield relaxation times at various temperatures, it is not a particularly reliable one.

F. C. Frank (28) has discussed the relative merits of various methods of interpreting data on dielectric dispersion. He concluded that data obtained at varying frequency yield the most reliable values. Kauzmann (25) also supports the above statement.

Extrapolation of the plots of  $\log \tau$  vs.  $1/T$  for 30% gelva V 1 1/2, V 15 and V 25 all yield the value of  $(1.50 \pm .2) \times 10^{-9}$  secs for the relaxation time at 25.0 $^{\circ}$ C. Since this value is based on 9 independent runs, it is definitely more reliable than that obtained by extrapolation in Table XXV.

Frank has also suggested that the plot of  $\log \epsilon''$  vs. T is a good test for checking the accuracy of loss curves. The bell shaped

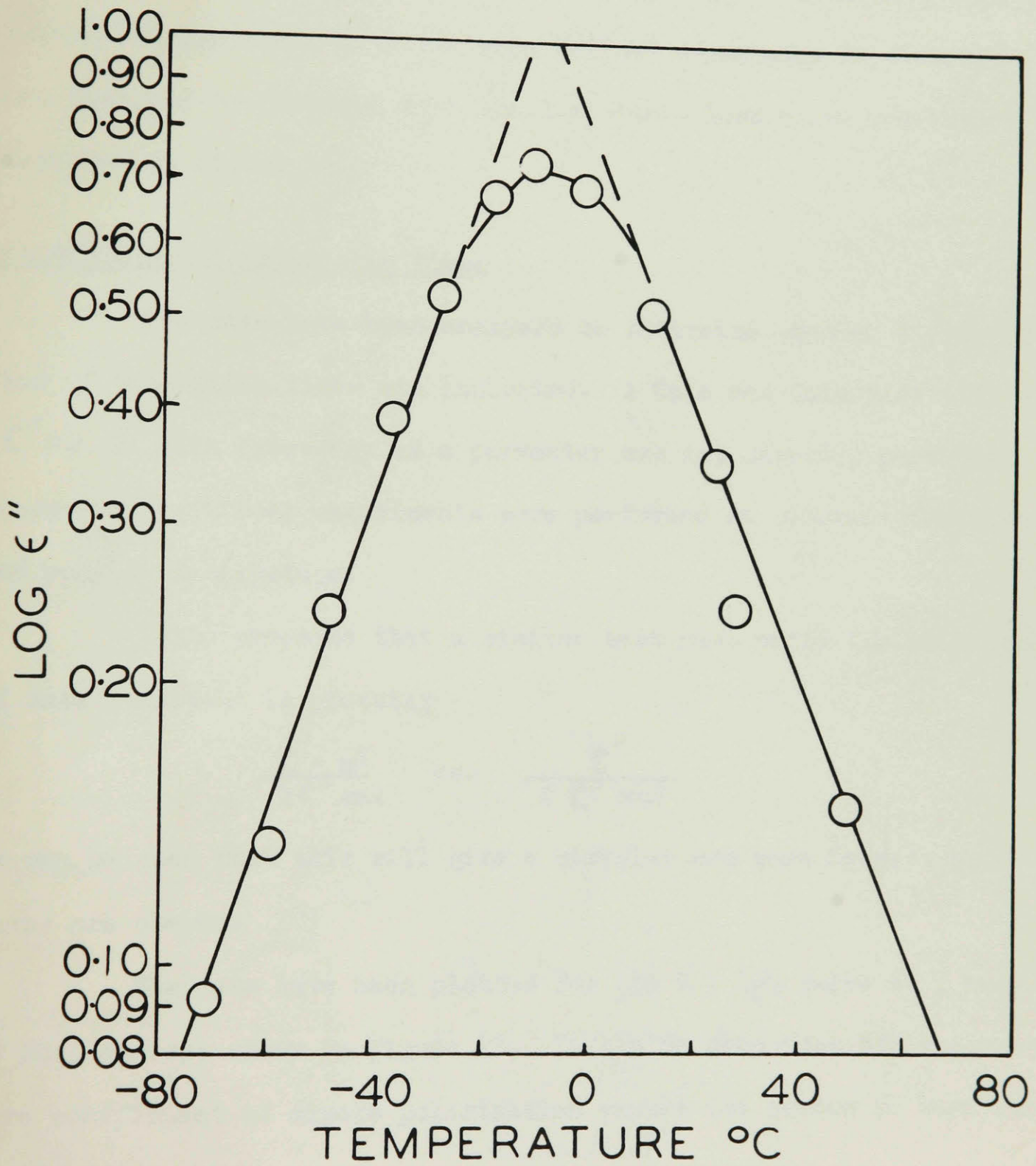


Figure 22: Logarithmic plot of dielectric loss against temperature for 60% V-1/2 gelva at 3 Mc.

loss curve should become a rectangular hyperbola whose asymptotes are straight lines with the slope  $\frac{d}{dT} \log \tilde{\tau}$ . The data for 60% V 1 1/2 at 3 Mc. have been plotted in this way in Figure 22. It is seen that a rectangular hyperbola with two well defined asymptotes is obtained. This plot may be compared with the dielectric loss curve previously presented in Figure 16.

### Distribution of Relaxation Times

The data have been analyzed to determine whether a distribution of relaxation times was indicated. A Cole and Cole plot (33) of  $\epsilon''$  vs.  $\epsilon'$  with frequency as a parameter was not directly possible, since the individual experiments were performed at constant frequency and varying temperature.

Fuoss proposed that a similar test plot valid for this type of data consisted in plotting

$$\frac{\epsilon' - n^2}{2 \epsilon''_{\max}} \quad \text{vs.} \quad \frac{\epsilon''}{2 \epsilon''_{\max}}$$

It can be seen that this will give a circular arc when Debye's equations are obeyed.

The data have been plotted for 40% V 1 1/2 gelva at 1 and 10 Mc., and are shown in Figure 23. It can be seen that the temperature coefficient of dipole polarization causes the curves to turn back on themselves.

A value of the Cole and Cole parameter  $\alpha$  as defined in diagram 3, Figure 1, could not be obtained with sufficient accuracy. Although an empirical correction for the temperature variation of the dipole polarization could have been applied, this was not done.

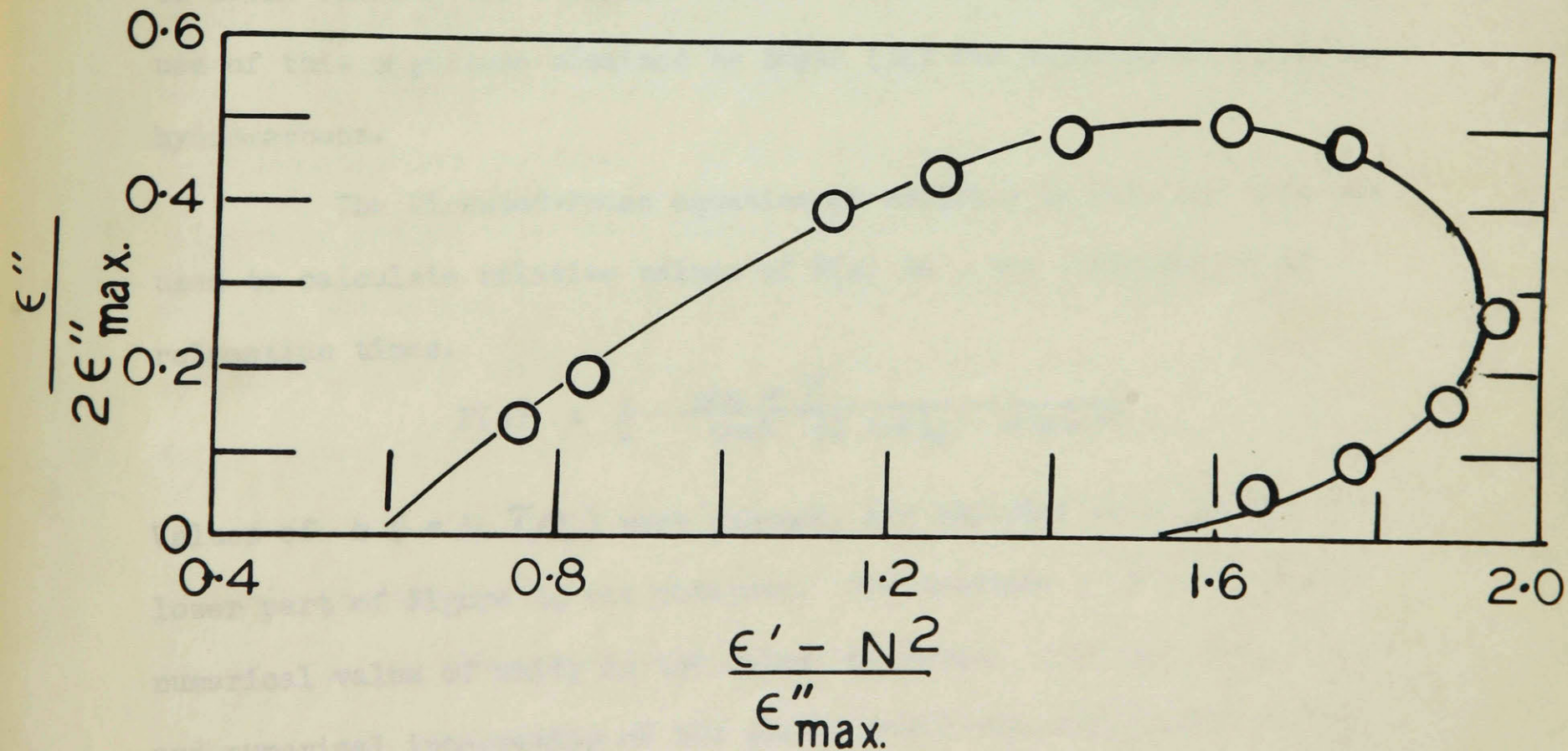
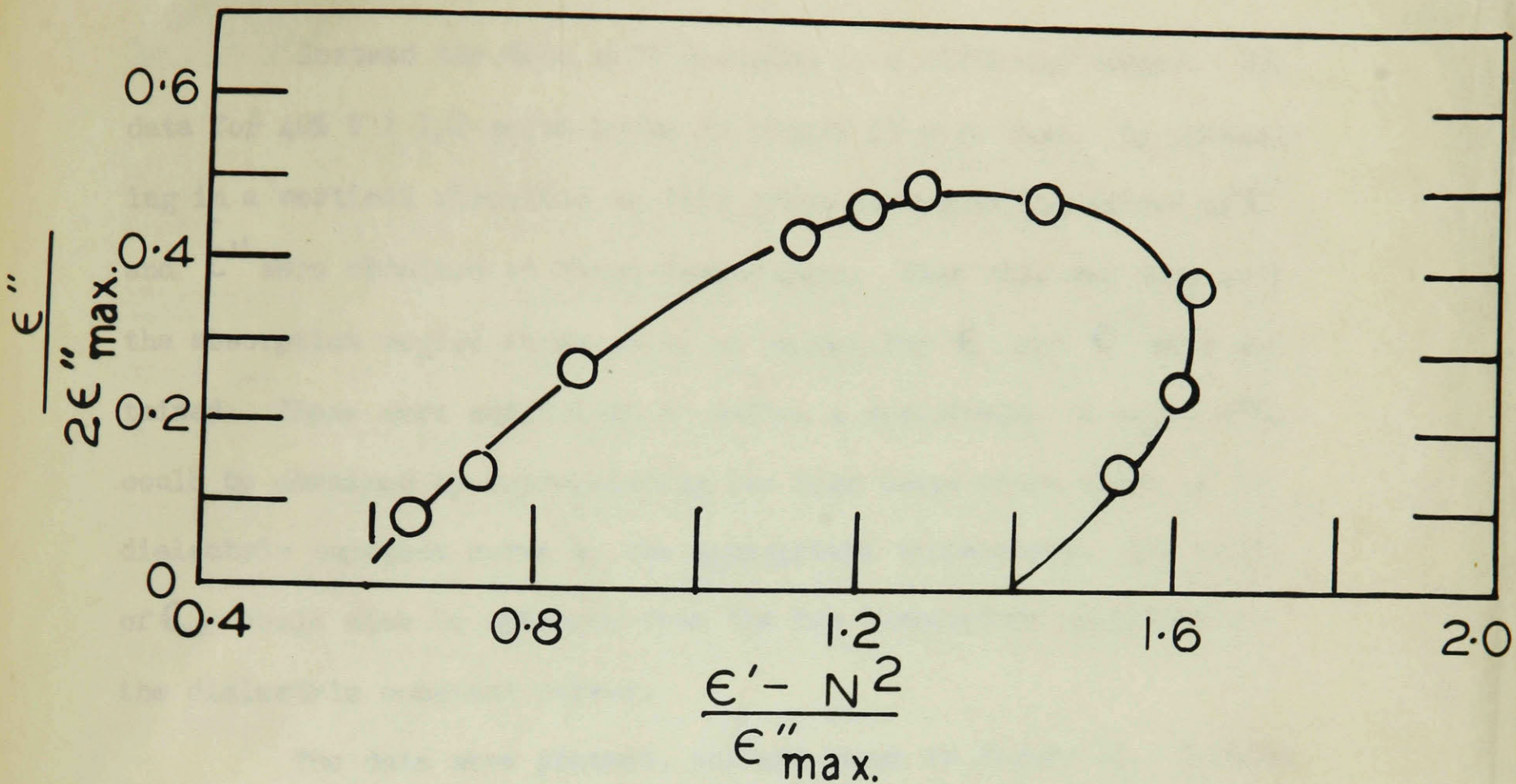


Figure 23: Modified Cole and Cole plot for 40% V-1 $\frac{1}{2}$  at 10 Mc. (top) and 1 Mc. (bottom)

Instead the data were analyzed in a different manner. The data for 40% V 1 1/2 gelva shown in Figure 18 were used. By proceeding in a vertical direction on this graph corresponding values of  $\epsilon'$  and  $\epsilon''$  were obtained at fixed temperature. When this was done near the absorption region three pairs of values for  $\epsilon'$  and  $\epsilon''$  were obtained. These were sufficient to define a semicircle. A value of  $\epsilon_0$  could be obtained by extrapolating the high temperature slope of the dielectric constant curve to the appropriate temperature. The value of  $\epsilon_\infty$  could also be obtained from the low temperature asymptote to the dielectric constant curves.

The data were plotted, and are shown in Figure 24. A value of 0.312 radians was obtained for  $\alpha$ . This can be compared with values of this magnitude obtained by Smyth (34) for chlorinated aliphatic hydrocarbons.

The Kirkwood-Fuoss equation as modified by Cole and Cole was used to calculate relative values of  $F(s) ds$ , the distribution of relaxation times.

$$F(s) = \frac{A \sin \alpha \pi}{2 \cosh (1 - \alpha)s - \cos \alpha \pi}$$

Values of  $s$  ( $= \ln \tau/\tau_0$ ) were assumed, and the plot shown in the lower part of Figure 24 was obtained. The constant A is given the numerical value of unity in the Coles' equation. This was done here, and numerical integration of the graph showed that approximately one-half the area is contained in a region where  $\ln \tau/\tau_0$  is between -1 and 1.

### Conclusions

The data showed good qualitative agreement with the Debye theory. At constant concentration and molecular weight the dielectric constant curves had common limiting values at temperatures above and below the dispersion region. The negative slope at temperatures above the dispersion region has been stated to be due to the temperature dependence of the dipole polarization. The dielectric loss curves were bell shaped and were symmetric about a central value of the temperature. A displacement of the maxima towards higher temperature with increasing frequency was found in agreement with theory.

A closer examination showed deviations from the behavior predicted for simple polar substances by the Debye theory. A displacement of the absorption maxima towards higher temperatures with increasing concentration was found. On the other hand, the positions of the absorption maxima were particularly insensitive to the effects of increasing the molecular weight of the solute. This indicated that the rotating unit was smaller than a whole molecule. Evaluation of the molar volume of the rotating units gave values of approximately 25,000 cc., corresponding to molecular weights of approximately 30,000. The approximate radius of the spherical unit of volume containing the rotating unit was evaluated as about 20 Angstroms.

The calculation of the entropy values by the theory of absolute reaction rates yielded values commonly found for some of the larger simple molecules. It is believed that this can be interpreted as indicating relative freedom for dipole rotation, especially when

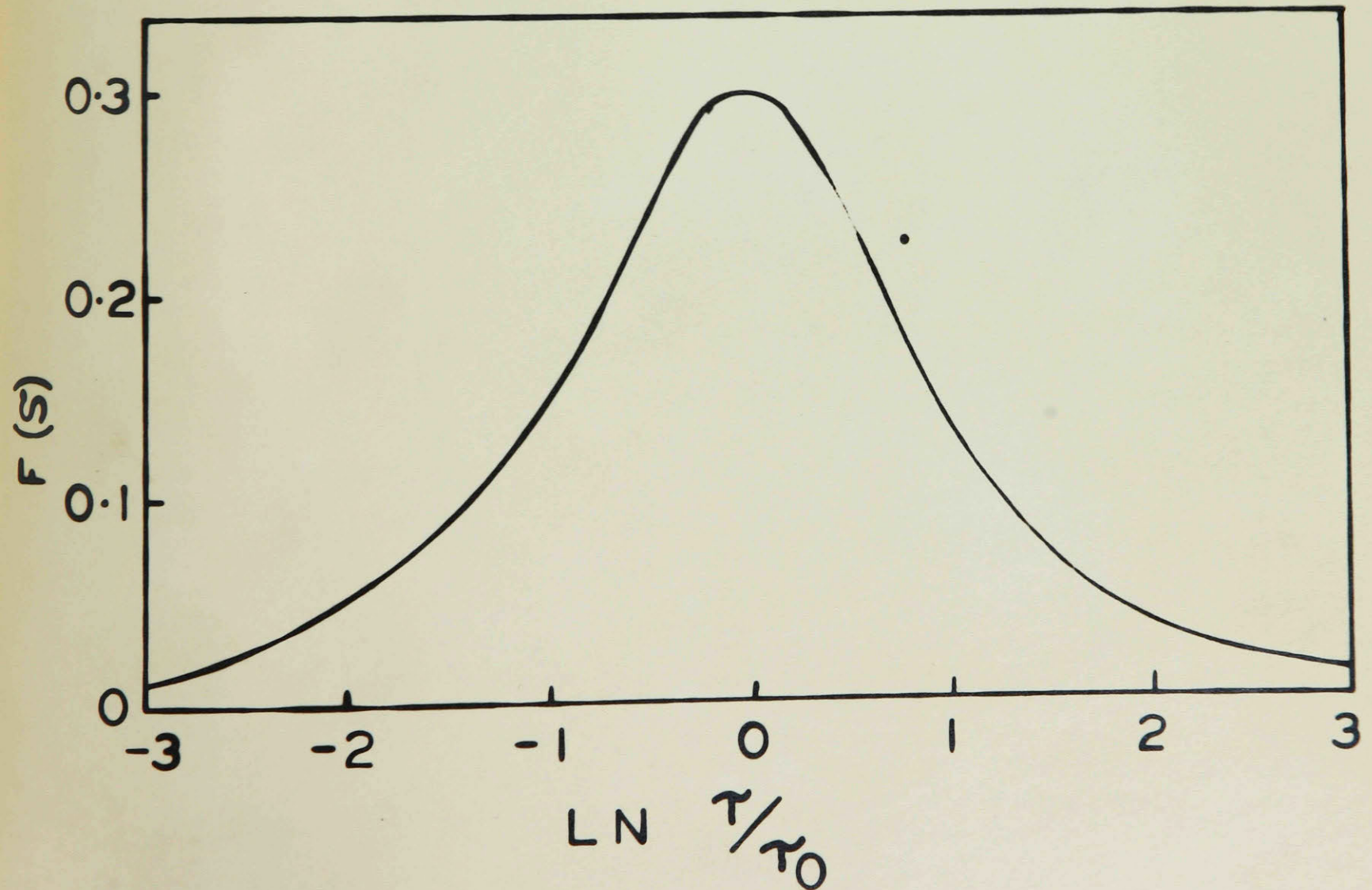
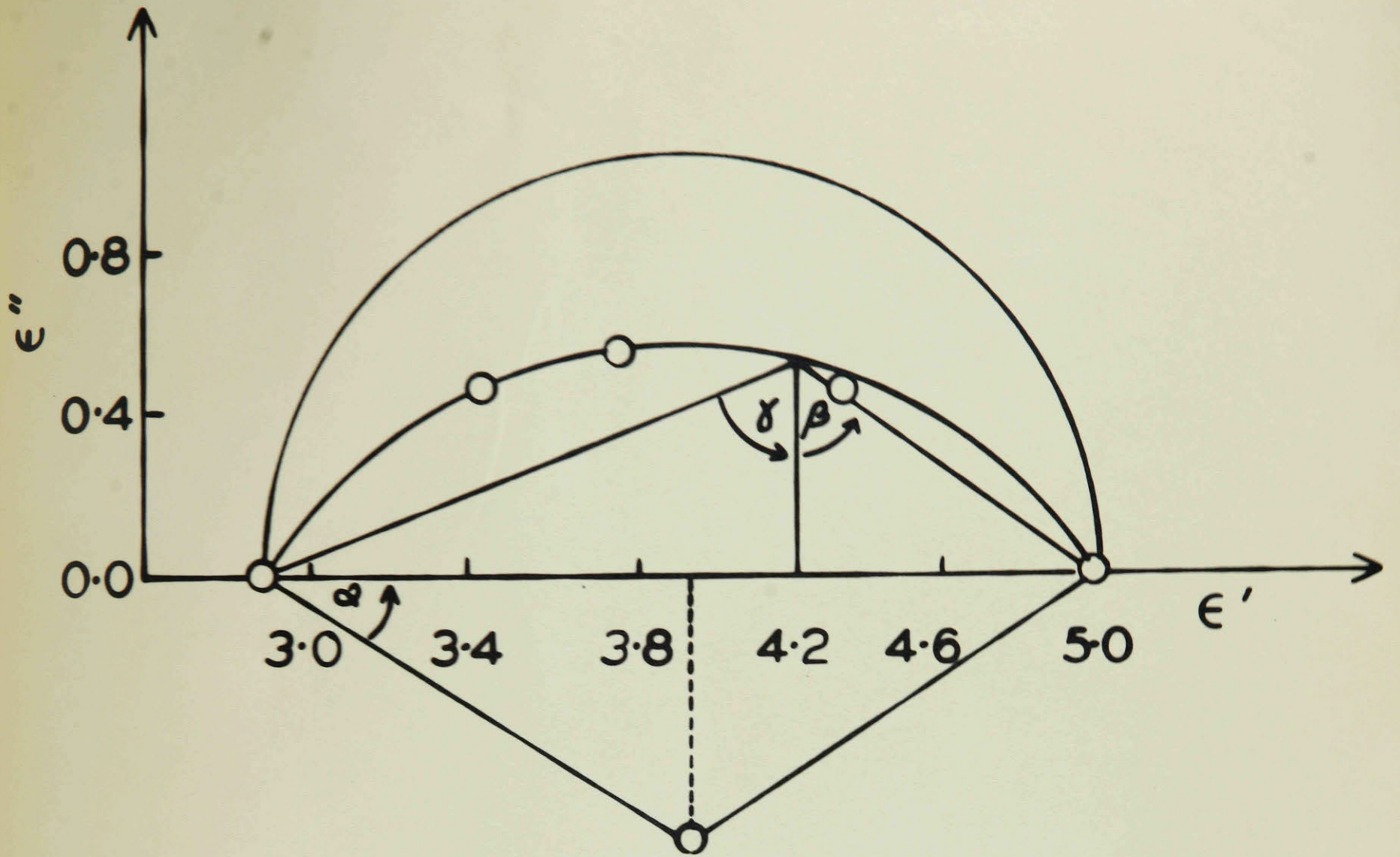


Figure 24: Cole and Cole plot for 40% V-1 $\frac{1}{2}$  (top)  
Distribution of relaxation times (bottom)

compared to the amorphous solid.

The dipole moment of a monomer unit was evaluated, and values of approximately 1 Debye unit were obtained.

The relaxation time was extrapolated to 25°C. for 30% V 1 1/2, V 15 and V 25, and was found to be  $1.5 \times 10^{-9}$  seconds.

A distribution of relaxation times was indicated by a Cole and Cole circular plot. The distribution was found to be relatively narrow, in sharp contrast to the wide distributions reported for solid polyvinyl chloride and other polymers (61). In many instances the ratios of the observed loss curves to those expected on the Debye theory were reported to be anywhere from 300 to 1, to 5,000,000 to 1 (25).

Although significant deviations from the Debye theory were found in the present work, there is every reason to believe that the experimental data are quite accurate. Error larger than 2% are not inherent in the measuring circuit employed in the present work. All the empirical tests tried and the general agreement of the experimental data support the belief that the data are quite accurate. It must be concluded that the present theory cannot be expected to yield better quantitative agreement than that found.

CLAIMS TO ORIGINAL WORK AND CONTRIBUTIONS TO KNOWLEDGE

PART I

1. Dielectric constants of solutions of macromolecules were measured at rates of shear from 1 to 20,000 sec<sup>-1</sup>.
2. (a) A decrease of dielectric constant with increasing rate of shear was found for solutions of polyvinyl acetate, cellulose acetate butyrate, polyvinyl formal and for carbon black suspensions.  
(b) An increase of dielectric constant under shear was found for solutions of ethyl cellulose in benzene.
3. A correlation between the conductance of gels of the aluminum soaps and rate of shear was found.

PART II

1. Dielectric dispersion data were obtained at frequencies of 1, 3, and 10 Mc. over the temperature range -80°C. to 60°C. for samples of three molecular weights of polyvinyl acetate in toluene.
2. The maxima of the dispersion curves were shifted by changes in frequency and concentration. Relaxation times were evaluated from these maxima, and interpretations of the theoretical significance of the data were given.
3. (a) Values of the free energy, enthalpy and entropy for dipole rotation were calculated.  
(b) Generally good agreement with the Debye theory was found.  
The size of the rotating unit was evaluated as approximately 20 Å

in radius, corresponding to a molecular weight of 30,000. The dipole moment per monomer unit was calculated to be 1 Debye.

4. Evidence of a distribution of relaxation times was found, and an empirical measure of the distribution was evaluated.

BIBLIOGRAPHY

1. Edsall, J.T., "Advances in Colloid Science" Vol. 1, Interscience, New York, (1942)
2. "First Report on Viscosity and Plasticity", Academy of Sciences, Amsterdam (1935)
3. "Second Report on Viscosity and Plasticity", Academy of Sciences, Amsterdam (1938)
4. Goodeve, C.F., Trans. Faraday Soc. 35, 342 (1939)
5. Scott Blair, G.W., "A Survey of General and Applied Rheology", Pitman & Sons, London, (1945)
6. Gray, V.R. and Alexander, E., J.Phys. and Coll. Chem. 53, 9 (1949)
7. Robinson, J.R., Proc. Roy. Soc. (London) (A)170, 519 (1939)
8. Page, L., Introduction to Theoretical Physics, Van Nostrand, New York (1935)
9. Clausius, R., "Die Mechanische Warmetheorie" Vol.II, Vieweg (1879)
10. Onsager, L., J. Am. Chem. Soc. 58, 1486 (1936)
11. Debye, P., Physik Zeits 36, 100 (1935)
12. Kirkwood, J.G., J. Chem. Phys. 7, 911 (1939)
13. Kirkwood, J.G., Trans. Faraday Soc. 42A, 7 (1946)
14. Frank, F.C., Trans. Faraday Soc. 42, 16 (1946)
15. Baueur, E. and Massignon, D., Trans. Faraday Soc. 42A, 12 (1946)
16. Frohlich, H., J. Inst. El. Eng. 91, 486 (1944)
17. Frohlich, H., Proc. Roy. Soc. A149, 1 (1935)
18. Glasstone, S., "Textbook of Physical Chemistry", Van Nostrand, New York (1940)
19. Williams, J.W. and Cady, L.C., Chem. Rev. 14, 171 (1934)
20. Debye, P., "Polar Molecules", Dover Publications, New York (1945)
22. Van Vleck, J.H., J. Phys. Chem. 5, 556 (1937)
23. ... and Eddv. C.R., J. Chem. Phys. 8, 424, 889 (1940)

24. Richards, R.B., Trans. Faraday Soc. 42A, 194 (1946)
25. Kauzmann, W., Rev. Mod. Phys. 14, 12 (1942)
26. Elliott, M.A. and Williams J. Am. Chem. Soc. 61, 718 (1939)
27. Debye, P. and Ramm Ann. Physik 28, 28 (1937)
28. Frank, F.C., Trans. Faraday Soc. 32, 1634 (1936)
29. Eyring, H., J. Chem. Phys. 4, 283 (1936)
30. Glasstone, S., Laidler, K.J. and Eyring, H., "The Theory of Absolute Reaction Rates", McGraw-Hill, New York (1939)
31. Powell, R.E. and Eyring, H., "Advances in Colloid Science", Vol. 1, Interscience, New York (1942)
32. Schallamach, A., Trans. Faraday Soc. 42, 180 (1946)
33. Cole, K.S. and Cole, R.H., J. Chem. Phys. 9, 341 (1941)
34. Smyth, C.P. and Lacquer, H.L., J. Am. Chem. Soc. 70, 4163 (1948)
35. Yager, W.A., Physics 7, 434 (1936)
36. Kirkwood, J.G. and Fuoss, R.M., J. Chem. Phys. 19, 329 (1941)
37. Kirkwood, J.G. and Fuoss, R.M., J. Am. Chem. Soc. 63, 385 (1941)
38. Einstein, A., Ann d. Physik IV 19, 289 (1906)
39. Boeder, P., Z. Physik 75, 258 (1932)
40. Kuhn, W., Z. Physik Chem. A 175, 1 (1935)
41. Jeffery, G.B., Proc. Roy. Soc. (London) A102, 161 (1923)
42. Brewster, D., Trans. Roy. Soc. (London) 106, 156 (1816)
43. Alfrey, T., "Mechanical Behavior of High Polymers" Vol. VI, Interscience, New York (1948)
44. Sheffer, H., Can. Jour. Res. (B) 26, 481 (1948)
45. Gray, V.R. and Alexander, A., J. Phys. and Coll. Chem. 52, 23 (1949)
46. Singh and Singh, Phil. Mag. 36, 622 (1945)
47. Voet, A., J. Phys. and Coll. Chem. 51, 1037 (1947)

48. Carter, W.C., Schneider, W.C., Magat, M. and Smyth, C.P., J. Am. Chem. Soc. 67, 959 (1945)
49. Fuoss, R.M., J. Am. Chem. Soc. 59, 1703 (1937)
50. Fuoss, R.M., J. Am. Chem. Soc. 60, 451 (1938)
51. Fuoss, R.M., J. Am. Chem. Soc. 60, 456 (1938)
52. Fuoss, R.M., J. Am. Chem. Soc. 61, 2329 (1939)
53. Fuoss, R.M., J. Am. Chem. Soc. 61, 2334 (1939)
54. Fuoss, R.M., J. Am. Chem. Soc. 63, 369 (1941)
55. Fuoss, R.M., J. Am. Chem. Soc. 63, 378 (1941)
56. Fuoss, R.M., J. Am. Chem. Soc. 63, 2401 (1941)
57. Fuoss, R.M., J. Am. Chem. Soc. 63, 2410 (1941)
58. Mead, D.J. and Fuoss, R.M., J. Am. Chem. Soc. 63, 2832 (1941)
59. Mead, D.J., Tichenor, R.L. and Fuoss, R.M., J. Am. Chem. Soc. 64, 283 (1942)
60. Mead, D.J. and Fuoss, R.M., J. Am. Chem. Soc. 64, 2389 (1942)
61. Davies, J.M., Miller, R.F. and Busse, W.F., J. Am. Chem. Soc. 63, 361 (1941)
62. Plessnert, W. and Richards, R.B., Trans. Faraday Soc. 42A, 206 (194)
63. Ferry, J.D. and Oncley, J.L., J. Am. Chem. Soc. 63, 272 (1941)
64. Oncley, J.L., Jensen, C.C. and Gross, P.M., J. Phys. and Coll. Chem. 53, 162 (1949)
65. Oncley, J.L., Ann. N.Y. Acad. Sci. 41, 121 (1941)
66. Oncley, J.L., Chem. Rev. 30, 433 (1942)
67. Morgan, S.O. and Yager, W.A., Ind. Eng. Chem. 32, 1519 (1940)
68. Moullin, E.B., Inst. El. Eng. 86, 113 (1940)
69. Hague, B., "A. C. Bridge Measurements", Pitman & Sons (1943)
70. Hollies, N.R.S., Thesis McGill U. April 1947

71. Lamson, H.W., Rev. Sc. Insts. 9, 272 (1938)
72. Taylor, G.I., Phil. Trans. Roy. Soc. (London) A223, 289 (1923)
73. Taylor, G.I., Proc. Roy. Soc. (London) A157, 546 (1936)
74. Smyth, C.P., "Dielectric Constant and Molecular Structure", Chemical Catalog Co. (1931)



McGILL UNIVERSITY LIBRARY

I x M



.1F9.1949

**UNACC.**